

## ABSTRACT

Title of Dissertation:           Generation of a CW Local Oscillator Signal Using a Stabilized Injection Locked Semiconductor Laser

Jonah Massih Pezeshki, Doctor of Philosophy, 2007

Dissertation directed by:      Professor Julius Goldhar  
Department of Electrical and Computer Engineering

In high speed-communications, it is desirable to be able to detect small signals while maintaining a low bit-error rate. Conventional receivers for high-speed fiber optic networks are Amplified Direct Detectors (ADDs) that use erbium-doped fiber amplifiers (EDFAs) before the detector to achieve a suitable sensitivity. In principle, a better method for obtaining the maximum possible signal to noise ratio is through the use of homodyne detection.

The major difficulty in implementing a homodyne detection system is the generation of a suitable local oscillator signal. This local oscillator signal must be at the same frequency as the received data signal, as well as be phase coherent with it. To accomplish this, a variety of synchronization techniques have been explored, including

Optical Phase-Lock Loops (OPLL), Optical Injection Locking (OIL) with both Fabry-Perot and DFB lasers, and an Optical Injection Phase-Lock Loop (OIPLL).

For this project I have implemented a method for regenerating a local oscillator from a portion of the received optical signal. This regenerated local oscillator is at the same frequency, and is phase coherent with, the received optical signal. In addition, we show that the injection locking process can be electronically stabilized by using the modulation transfer ratio of the slave laser as a monitor, given either a DFB or Fabry-Perot slave laser. We show that this stabilization technique maintains injection lock (given a locking range of  $\sim 1\text{GHz}$ ) for laser drift much greater than what is expected in a typical transmission system. In addition, we explore the quality of the output of the slave laser, and analyze its suitability as a local oscillator signal for a homodyne receiver.

GENERATION OF A CW LOCAL OSCILLATOR SIGNAL USING A STABILIZED  
INJECTION LOCKED SEMICONDUCTOR LASER

by

Jonah Massih Pezeshki

Dissertation submitted to the Faculty of the Graduate School of the  
University of Maryland, College Park in partial fulfillment  
of the requirements for the degree of  
Doctor of Philosophy  
2007

Advisory Committee:

Professor Julius Goldhar, Chair  
Assistant Professor Thomas E. Murphy  
Professor Mario Dagenais  
Doctor Marshall Saylor  
Professor Wendell T. Hill

## TABLE OF CONTENTS

Chapter 1 – Introduction .....	1
Optical Receivers .....	3
Direct Detection .....	4
Ideal Direct Detection of Amplitude Shift Key (DD-ASK) Transmissions.....	4
Non-Ideal DD-ASK .....	5
BER for ideal ADD for ASK Transmissions.....	7
Non-Ideal ADD for ASK Transmissions.....	9
Coherent Detection .....	11
Heterodyne Detection .....	11
Homodyne Detection .....	13
Polarization Effects.....	16
Overview of Project .....	17
Implementation of DD .....	17
Implementation of ADD .....	18
ADD Example.....	18
Implementation of a Heterodyne Receiver .....	20
Implementation of a Homodyne Receiver .....	20
Homodyne Receiver with an Amplified Local Oscillator .....	21
Homodyne Receiver with an Injection Locked Local Oscillator.....	24
Relative Merits.....	28
Chapter 2 – Passive Optical Filtering .....	29
Background .....	29
Feedback Control of Filter .....	31
Chapter 3 – Injection Locking a DFB Semiconductor Laser.....	34
Background .....	34
Rate Equation for the Photon Field.....	35
Rate equation for two level population dynamics.....	37
Phase Stability Range .....	38
Phase Shift of a Tracking Oscillator .....	39
Feedback Control of an Injection Locked DFB Semiconductor Slave Laser.....	40
Generation of a Feedback Signal .....	41
MTR as a Measure of Detuning.....	41
Solving for 1 <sup>st</sup> Order Perturbation on $r$ .....	44
Solving for 1 <sup>st</sup> Order Modulation Transfer Ratio of Locked Oscillator .....	45
Numerical Modeling.....	47
Experimental Verification of the Injection Locking Theory.....	50
Varying the Free-Running Frequency of the Slave Laser .....	53

Creating the Feedback Control System for the Injection Lock.....	54
Analog Feedback Control .....	55
Modeling the Analog Feedback Loop.....	59
Digital Feedback Control.....	60
Implementation of a Digital Feedback Loop .....	64
Chapter 4 – Injection Locking a Fabry-Perot Semiconductor Laser .....	68
Background.....	68
Modeling an Injection Locked Multi-Mode Slave Laser.....	68
Feedback Control of an Injection Locked Fabry-Perot Semiconductor Slave Laser.....	69
Generation of a Feedback Signal .....	69
Establishing a Relationship Between the Electric Fields of the Main and Unwanted Modes .....	71
Solving for the 1 <sup>st</sup> Order Perturbation on $r$ .....	72
Solving for the 1 <sup>st</sup> Order MTR of the Injection Locked Fabry-Perot Laser.....	72
Numerical Modeling .....	74
Experimentally Verifying the Injection Locking Theory .....	76
Varying the Free-Running Frequency of the Slave Laser .....	78
Modeling the Modulation Transfer Ratio of the Slave Laser .....	80
Suppressing the Unwanted Modes in the Slave Laser .....	81
Creating the Feedback System for the Injection Lock.....	83
Chapter 5 – Characterizing the Local Oscillator Signal .....	89
Characteristics of the Fabry-Perot Filter.....	89
Quality of the Injection Locked Fabry-Perot Laser .....	92
Noise on the Output of the Fabry-Perot Laser .....	93
Modulation Transfer Ratio of the Fabry-Perot Laser .....	98
Linewidth of the Fabry-Perot Laser.....	99
Phase Noise Generated by Amplitude Noise .....	104
Phase Coherence Between Injected Signal and Fabry-Perot Laser Output.....	111
Gain of the Fabry-Perot Laser.....	114
Parasitic Oscillations.....	115
Modulation Suppression as a Function of Modulation Frequency .....	118
Generating a Local Oscillator Signal.....	120
Chapter 6 – Design of Homodyne Receiver .....	122
Phase Locking.....	122
Background.....	122
Practical Feedback Systems.....	123
Future Work.....	131
Polarization Control.....	131
Layout of Receiver.....	132
Support for PSK Transmissions.....	133

Chapter 7 – Conclusions .....	137
Appendix A – MatLab Code for Plotting Results for DFB Injection Locking.....	138
MatLab Code for Ploting Magnitude and Phase of 1st Harmonic for various modulation frequencies .....	138
MatLab Code for Ploting Magnitude and Phase of 1st Harmonic for various injected powers.....	140
Matlab Function for solving for $e_0$ .....	142
Appendix B – Matlab Code for Plotting Results for Fabry-Perot Injection Locking.....	143
MatLab Code for Ploting Magnitude and Phase of 1st Harmonic for Various Injected Powers.....	143
Matlab Function for solving for $e_0$ .....	144
Appendix C – Matlab Code for Plotting Phase Modulation due to Amplitude Modulation on Input .....	145
MatLab Code for Ploting Phase Modulation of 1st Harmonic .....	145
Appendix D – Stamp Basic Code for the Microcontroller .....	146
References.....	150

## I. CHAPTER 1 - Introduction

In high speed-communications, it is critical to be able to detect the smallest possible signals while maintaining a low bit-error rate. This permits data transmission across longer distances without the aid of repeaters or optical amplifiers. This effectively lowers the cost, noise and potential delays of the optical communication network. Currently, the most popular method to achieve this is through the use of Amplified Direct Detection (ADD). However, it is possible to achieve greater sensitivity with the use of a homodyne receiver [1, 2].

The major difficulty in implementing a homodyne detection system is the generation of a suitable local oscillator signal. This local oscillator signal must be at the same frequency as the received data signal, as well as be phase coherent with it. To accomplish this, a variety of synchronization techniques have been explored, including Optical Phase-Lock Loops (OPLL) [1, 34, 35, 36, 37, 38], Optical Injection Locking (OIL) with both Fabry-Perot [42, 43, 44] and DFB [18, 45, 46] lasers, and an Optical Injection Phase-Lock Loop (OIPLL) [19].

Several studies demonstrate the effectiveness of OPLL for locking heterodyne [34, 35, 36] and homodyne [1, 37, 38] signals to within acceptable limits. However, previous work has also shown that, to minimize the laser phase noise (i.e. the variation in the phase difference between the two synchronized optical signals) the loop delay must be kept as small as possible [19]. For wideband lasers (i.e. laser linewidths  $>10\text{MHz}$ ), the maximum loop delay must be less than  $\sim 100\text{ps}$  (the exact value depends on the particular loop filter used in the OPLL), assuming a reliable operation time of 10 years (estimated time until a cycle-slip occurs) [19]. As such, OPLLs may not be physically

realizable with Commercial Off-The-Shelf (COTS) components for wideband lasers, and were not seriously considered for generating a local-oscillator signal in this experiment.

Alternatively, OIL provides a low-noise output signal that is phase coherent with the received signal [18, 19, 42, 43, 44, 45, 46]. However, OIL output becomes chaotic for large injected powers [39, 40]. Additionally, for small injection (i.e. the injected signal is  $\sim 30$ dB below the OIL output signal), OIL requires a slave laser whose optical frequency differs from the received optical signal by at most 1GHz, and as little as the linewidth of the received optical signal. As such, frequency drift (due to either glitches in the laser controller or environmental drifts) makes this method ineffective in real systems. OIPPL integrates an OPLL into OIL in order to overcome this limitation [19]. However, OIPLL has only been proven to work for low data-rate optical signals (10-100Mb/s). In addition, this method is intolerant to phase noise due to the thermal drift of the optical path length of the interferometer used in the OPPL.

Thus, I have explored a method for regenerating a local oscillator from a portion of the received optical signal that improves upon OIPLL to accommodate received signals with higher data rates. Specifically, a portion of the received signal will be optically pre-filtered, and used to injection lock a slave laser. When locked, the output of this slave laser will be at the same frequency and phase coherent with, the received optical signal. Thus it can be used as a suitable local oscillator signal.

In addition, we demonstrate that the injection locking process can be electronically stabilized by using the modulation transfer ratio of the slave laser as a monitor. Specifically, the modulation transfer ratio of an injected laser is at a minimum at the center of the locking range, and increases as the difference between the frequencies

of the injected and free-running signals increase. This holds true for both Fabry-Perot lasers and DFB lasers. This effect was also modeled with the use of the laser rate equations.

Both Distributed Feedback (DFB) lasers and Fabry-Perot lasers are tested for use as an appropriate slave laser for the local oscillator generator. In addition, stabilized injection locking utilizing the modulation transfer function of the slave laser was developed and tested for both laser types. For this, the effectiveness of both digital and analog feedback systems were explored. Finally, the quality of the local oscillator signal that is generated by the injection locked Fabry-Perot laser was explored.

## 1.1 Optical Receivers

Optical receiver sensitivity is effectively specified by the input optical power that is required to achieve a particular maximum bit-error rate. Specifically, if a certain bit-error rate is desired, this will determine the minimum received power that is necessary to obtain it at a given data rate and optical wavelength. Although receivers demand a greater power than this to overcome Johnson noise, dark noise, and detector inefficiency, it is not necessary to consider these additional terms when determining the physical limits.

For a given data rate, the bit-error rate is defined as the sum of the probability that an intended 1-bit is interpreted as a 0-bit and the probability that a 0-bit is interpreted as a 1-bit [3]. The bit-error rate of a fiber optic communication system depends on both the particular transmission scheme and the type of receiver used to detect the transmission.

### 1.1.1 Direct Detection

#### 1.1.1.1 Ideal Direct Detection of Amplitude Shift Key (DD-ASK) Transmissions

The most basic way of detecting and interpreting an incident optical signal is with a direct detection system. A direct detection system that is designed to decode ASK transmissions is depicted in Figure 1.01. The first component in a direct detection system may either be a reversed-biased photodiode or an Avalanche Photodiode (APD). This device effectively converts an incident optical signal into electrical current. The detector is then followed by a trans-impedance amplifier (often packaged with the detector), which amplifies the incident electrical current into a larger electrical voltage. This resulting voltage is then compared to an electrical threshold voltage, which determines if the incident signal is to be interpreted as a 0-bit or a 1-bit.

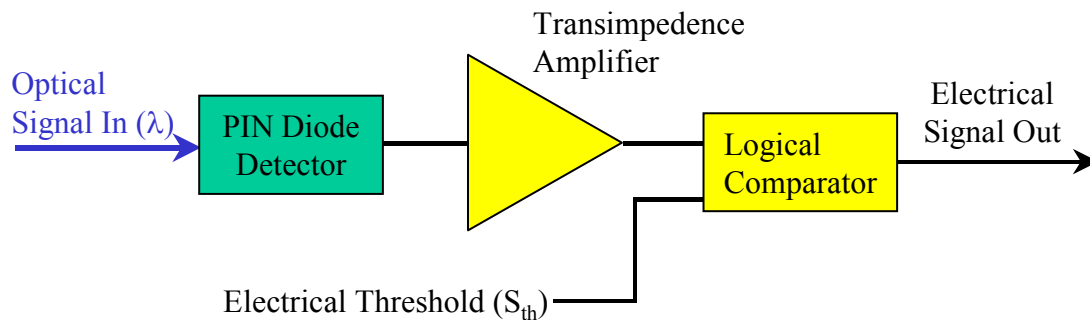


Figure 1.01 - Direct Detection System for ASK Transmissions

For an ideal detector and electronic amplifier, the thermal noise is considered to be negligible. As such, the noise on the detected signal can be attributed to shot noise. Shot noise is due to the inherent randomness in the arrival time of the individual photons, and thus can be modeled as a Poisson random variable. In general, the probability of a Poisson random variable of mean  $m$  being equal to  $k$  is [5]:

$$P[k] = \frac{m^k}{k!} e^{-m} \quad (1.01)$$

In this case, it is assumed that the bit-error rate is equal to the probability that zero photons ( $k=0$ ) are received for a 1-bit (it is assumed that the probability of a 0-bit being misinterpreted is zero). As such, if a bit-error rate of  $10^{-9}$  for example is desired, then the minimum number of photons/bit that are required for the direct detection of an ASK encoded transmission is:

$$m = -\ln(2 * 10^{-9}) \cong 20 \quad (1.02)$$

Thus, if a BER of  $10^{-9}$  is desired then 20 photons/mark are required for the direct detection of an ASK transmission, which translates to an average of 10 photons/bit.

Using the definition of photons per bit given above, the average power for a transmission can be found, given the number of photons/bit, the optical wavelength, and the data rate by:

$$P = \left( \frac{hc}{\lambda} \right) \left( \frac{\text{photons}}{\text{bit}} \right) \left( \frac{\text{bits}}{\text{sec}} \right) \quad (1.03)$$

Thus for an optical wavelength of 1550nm and a bit-rate of 10Gb/s, the average power that is required to obtain a BER of  $10^{-9}$  is approximately -49dBm.

#### 1.1.1.2 Non-Ideal DD-ASK

In a non-ideal direct detection system, Johnson and detector noise are normally represented as the Noise Equivalent Power (NEP) of the receiver. NEP is defined as the radiant power that produces a signal-to-noise ratio of unity at the output of a given optical receiver, given the data-rate, frequency, and effective noise bandwidth of the incident optical signal.

For systems where the NEP is normally greater than the shot noise, it may still be possible to achieve a shot noise limited, non-amplified direct detector. This would be accomplished by cryogenically cooling the detector and electronic amplifier so that the Johnson noise is an order of magnitude lower than the shot noise [4]. However, this technology is not currently available at a practical cost for deployment on a large scale optical network.

The BER for an equal probability of transmitting a 0-bit and a 1-bit can be calculated from:

$$BER_{ASK} = \frac{1}{2} \left[ \frac{1}{\sigma_1 \sqrt{2\pi}} \int_{-\infty}^{S_{th}} \exp\left(-\frac{(S_1 - x)^2}{2\sigma_1^2}\right) dx + \frac{1}{\sigma_0 \sqrt{2\pi}} \int_{S_{th}}^{\infty} \exp\left(-\frac{(S_0 - x)^2}{2\sigma_0^2}\right) dx \right] \quad (1.04)$$

where  $S_1$  is the electrical current after the detector that is due to an optical 1-bit,  $S_0$  is the current due to a 0-bit,  $\sigma_1$  is the noise (standard deviation of the signal) in the 1-bit,  $\sigma_0$  is the noise in the 0-bit, and  $S_{th}$  is the threshold level (in terms of electrical current) that is used to differentiate between a 0-bit and a 1-bit [5]. This equation can also be written in terms of the complimentary error function as:

$$BER_{ASK} = \frac{1}{4} \left[ \operatorname{erfc}\left(\frac{S_1 - S_{th}}{\sqrt{2}\sigma_1}\right) + \operatorname{erfc}\left(\frac{S_{th} - S_0}{\sqrt{2}\sigma_0}\right) \right] \quad (1.05)$$

For the ideal case, we assume an infinite S/N on the input of the detector and no optical signal during a 0-bit. Using (1.03), the signal current is:

$$S_1 = \frac{q\eta P_s \lambda}{hc} \quad (1.06)$$

Furthermore,  $\sigma_1$  is equal to a combination of Shot, dark and Johnson noise, while  $\sigma_0$  is equal to a combination of just dark and Johnson noise. Shot noise, also known as quantum noise, is due to the optical signal being quantized. In general, shot noise is

given by the product of quantity, current, and bandwidth:  $qIB$ . This is valid for any discrete quantity where  $q$  is the quantity,  $I$  is its current, and  $B$  is the bandwidth. In this case,  $q$  is electronic charge and  $I$  is the photoelectron conversion current. Optical shot noise current is described by [7] again using (1.06) to obtain the current:

$$\sigma_s = \sqrt{q \left( \frac{\eta q}{h\nu} \right) P_s B_e} = \sqrt{q S_1 B_e} \quad (1.07)$$

where  $\eta$  is the quantum efficiency of the detector,  $h$  is Planck's constant,  $P_s$  is the signal power,  $\nu$  is the frequency of the optical signal, and  $B_e$  is the noise bandwidth (which is assumed to be equal to twice the signal bandwidth). As such,  $\sigma_I$  is equal to  $(\sigma_s + \text{NEP})$ , while  $\sigma_0$  is simply equal to the NEP. Given this, the BER can be determined from (1.05) and (1.06).

#### 1.1.1.3 BER for ideal ADD for ASK Transmissions

Optical amplifiers may be added before the detector in cases where the NEP of the receiver is greater than the shot noise of the incident optical signal. This effectively increases the power of both the received optical signal and optical noise that is detected such that the shot noise is greater than the NEP, ensuring that shot noise will be the limiting noise on the system.

For the ideal direct detection of an amplified ASK encoded transmission, the receiver noise can be modeled as a Gaussian random variable with a 3dB degradation to the signal to noise ratio. This 3dB degradation is the direct result of the ASE generated by the optical amplifier [6, 13].

Thus, if it is assumed that there is an equal probability of transmitting a 0-bit and a 1-bit, then the bit-error rate is given by (1.05). If amplifier and thermal noise after the detector are considered to be negligible, the noise on the detected signal can be attributed to shot noise and a minimum 3dB noise figure ( $F_{3dB}$ ) due to ASE. Thus, from (1.07), the noise on the detected signal during a 1-bit is equal to:

$$\sigma_1 = F_{3dB} \sqrt{q \left( \frac{\eta q}{h \nu} \right) P_s B_e} = 2 \sqrt{q \left( \frac{\eta q}{h \nu} \right) P_s B_e} \quad (1.08)$$

In addition, the detected signal during a 1-bit can be expressed as:

$$S_{DI} = \left( \frac{\eta q}{h \nu} \right) P_I \quad (1.09)$$

where  $P_I$  is the optical power associated with a 1-bit.

For this system, the limiting noise during a 1-bit is shot noise that is due to the signal power. Additionally, since we are considering an ideal system, we assume that the power and noise during a 0-bit is negligible. The modulation is ASK, thus from (1.05) the bit-error rate can be expressed as:

$$BER_{ASK-D} = \frac{1}{4} \operatorname{erfc} \left( \frac{S_{DI} - S_{th}}{\sqrt{2} \sigma_{DI}} \right) \quad (1.10)$$

Also, since the noise during a 0-bit is assumed to be negligible, the threshold value ( $S_{th}$ ) is set close to zero. Thus the equation for the bit-error rate can be written as:

$$BER_{ASK-D} = \frac{1}{4} \operatorname{erfc} \left( \frac{1}{2} \sqrt{\frac{\eta P_I}{h \nu B_e}} \right) \quad (1.11)$$

In an ideal detector, the quantum efficiency is equal to 1 and the bandwidth is equal to the bit-rate. From this, the bit-error rate can be written as:

$$BER_{ASK-D} = \frac{1}{4} \operatorname{erfc}\left(\frac{\sqrt{N}}{2}\right) \quad (1.12)$$

where  $N$  is the number of photons per bit, which can also be expressed by the equation:

$$N = \left(\frac{P_l T_b}{h\nu}\right) = \left(\frac{P_l}{h\nu}\right) \left(\frac{1}{B_e}\right) \quad (1.13)$$

Given this, if a bit-error rate of  $10^{-9}$  is desired then the value of  $N$  can be numerically determined. From this numerical analysis it is found that 72 photons/bit are required for the pre-amplified direct detection of an ASK transmission, which is very close to the accepted value of 80 photons/bit [8]. If it is assumed that the optical wavelength is 1550nm and the bit-rate is 10Gb/s, the average power that is required to obtain a BER of  $10^{-9}$  is approximately -43.4dBm.

#### 1.1.1.4 Non-Ideal ADD for ASK Transmissions

The uncertainty principle dictates that the minimum degradation to the signal to noise ratio by a linear amplifier is 3dB. However, the actual value is greater in real amplifiers. This degradation, expressed as a Noise Figure, is typically in the range of 3dB-5dB for low-noise optical pre-amplifiers, and 6dB-8dB for power amplifiers.

Given incomplete population inversion of the optical amplifier, the equivalent noise power at the input to the optical amplifier is equal to:

$$P_N = h\nu BF \quad (1.14)$$

where  $B$  is the bandwidth of the optical amplifier,  $\nu$  is the optical frequency of the injected signal,  $F$  is the noise figure, and  $h$  is Plank' constant ( $\approx 6.626 \times 10^{-34}$  J\*s) [13].

The noise figure serves as a practical value to offset the degradation to the S/N ratio due

to internal loss within the amplifier and the less than full population inversion, and is derived experimentally from the measured noise power and gain. Thus, the S/N at the output of an optical amplifier is given by:

$$\frac{S_o}{N_o} = \frac{GS_i}{GN_i + NEP + P_{shot} + P_{ASE}} \quad (1.15)$$

where  $P_{shot}$  is the shot noise power, which produces a current of  $\sigma_s$  in an ideal detector.

Thus, if it is assumed that there is an equal probability of transmitting a 0-bit and a 1-bit, then the bit-error rate is given by (1.05). For the non-ideal case,  $\sigma_1$  is equal to a sum of Shot, dark, Johnson, ASE, and ASE-shot noise, while  $\sigma_0$  is equal to a sum of just dark, Johnson, ASE, and ASE-shot noise. The signal is given by (1.06), the signal shot noise is given by (1.07), the ASE-shot noise also given by (1.07); with the ASE power substituted for the signal power, the ASE power is given by (1.14), and the Johnson and dark noises are given by the NEP.

From (1.14), it can be seen that the ASE noise that is added by the optical amplifier is proportional to the bandwidth. An optical filter to limit the effective bandwidth at the output of the amplifier can reduce this noise, as long as this bandwidth is still greater than the data rate of the received optical signal. For example, if we assume a 10Gb/s transmission on a 1550nm optical carrier, then the input noise power that is added to the signal by the optical amplifier will be at least -59dBm. This value will be greater if the amplifier is not operating at full population inversion (effectively increasing the noise figure), or if the received data was transmitted at a higher data rate (requiring a filter with a larger bandwidth).

### 1.1.2 Coherent Detection

In a coherent detection system, the received optical signal is mixed with a more intense “local oscillator”. The electric fields of these two signals interfere with each other, provided that the two fields are in the same polarization state. Since detectors measure optical power (which is proportional to the square of the magnitude of the total electric field), the two signals are effectively mixed at the detector [9]. This signal is given by:

$$S_{coherent} = \left( \frac{\eta q}{h \nu} \right) \sqrt{2P_I P_{lo}} \cos(\omega_1 t - \omega_{lo} t + \phi_{lo}) \sin(\omega_m t) \quad (1.16)$$

where  $\omega_1$  is the signal frequency,  $\omega_{lo}$  is the local oscillator frequency,  $\omega_m$  is the modulation, and  $\phi_{lo}$  is the phase of the local oscillator signal relative to the received signal.

After the detector, the electrical signal is amplified by a trans-impedance amplifier. The signal from the trans-impedance amplifier is electronically filtered in order to limit the bandwidth of the detected signal to that of the data and noise. This effectively minimizes the noise on the electronic signal.

#### 1.1.2.1 Heterodyne Detection

When the frequency of the received optical signal is different from the local oscillator signal, then the coherent receiver is known as a heterodyne system (Figure 1.02). As seen from (1.16), for a heterodyne detection system  $S_{coherent}$  is proportional to:

$$S_{coherent} \sim \cos(\omega_1 t - \omega_{lo} t + \phi_{lo}) \sin(\omega_m t) \quad (1.17)$$

and that  $\phi_o$  is indeterminate. The difference between  $\omega_l$  and  $\omega_o$  is an intermediate frequency whose bandwidth must be at least twice the signal bandwidth. Thus, the bandwidth of the bandpass filter (Figure 1.02) is equal to the IF bandwidth. The magnitude of the detected signal can be expressed as:

$$S_{het1} = \left( \frac{\eta q}{h \nu} \right) \sqrt{2 P_1 P_{lo}} \quad (1.18)$$

Note that this power refers to the peak power, not the average power (the average power would be equal to  $S_{het1} / \sqrt{2}$ ). For ideal Heterodyne, we assume that the signal during a 0-bit is approximately zero and thus is ignored and that the dominant noise during both the 1-bit and 0-bit is shot noise due to the local oscillator.

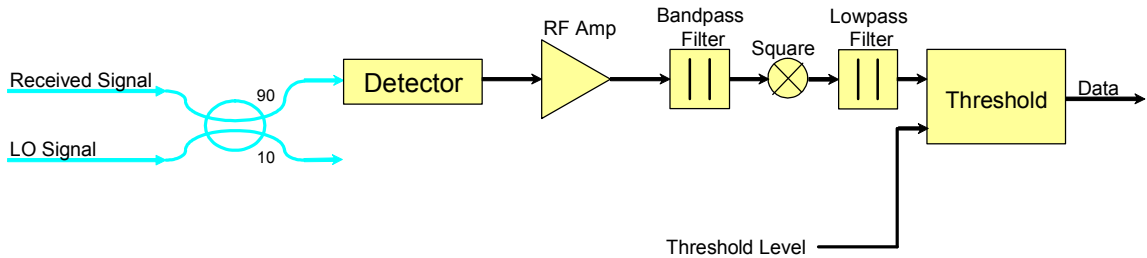


Figure 1.02 – Heterodyne Receiver for ASK Transmissions

The (shot) noise during both the 1-bit and 0-bit is equal to:

$$\sigma_{het} = \sqrt{q \left( \frac{\eta q}{h \nu} \right) P_{lo} B_{het}} \quad (1.19)$$

(Because the noise bandwidth, set by the bandpass filter, is equal to twice the signal base bandwidth). If an ASK transmission is incident upon the heterodyne receiver, then from (1.05), (1.18) and (1.19) the bit-error rate can be expressed as:

$$BER_{ASK-het} = \frac{1}{4} \left[ \operatorname{erfc} \left( \sqrt{\frac{\eta P_1}{h\nu B_e}} - \frac{S_{th}}{\sqrt{2q \left( \frac{\eta q}{h\nu} \right) P_{lo} B_e}} \right) + \operatorname{erfc} \left( \frac{S_{th}}{\sqrt{2q \left( \frac{\eta q}{h\nu} \right) P_{lo} B_e}} \right) \right]. \quad (1.20)$$

Using (1.13) and assuming that  $\eta=1$ , the BER can be written in terms of the number of photons per bit as:

$$BER_{ASK-het} = \frac{1}{4} \left[ \operatorname{erfc} \left( \sqrt{N} - \frac{S_{th}}{\sqrt{2q \left( \frac{\eta q}{h\nu} \right) P_{lo} B_e}} \right) + \operatorname{erfc} \left( \frac{S_{th}}{\sqrt{2q \left( \frac{\eta q}{h\nu} \right) P_{lo} B_e}} \right) \right] \quad (1.21)$$

If a bit-error rate of  $10^{-9}$  is desired, then a numerical analysis of this equation can be used to determine the appropriate values of  $S_{th}$  and  $N$ . From this, it was found that 72 photons per bit are required to obtain a  $10^{-9}$  bit-error rate with a heterodyne receiver. If it is assumed that the optical wavelength is 1550nm and the bit-rate is 10Gb/s, the average power that is required to obtain a BER of  $10^{-9}$  is approximately -43dBm.

#### 1.1.2.2 Homodyne Detection

A coherent receiver is known as a homodyne system when the frequency of the received optical signal is the same as that of the local oscillator signal (Figure 1.03). As seen from (1.16), for a homodyne detection system  $S_{coherent}$  is proportional to:

$$S_{coherent} \sim \cos(\phi_{lo}) \sin(\omega_m t) \quad (1.22)$$

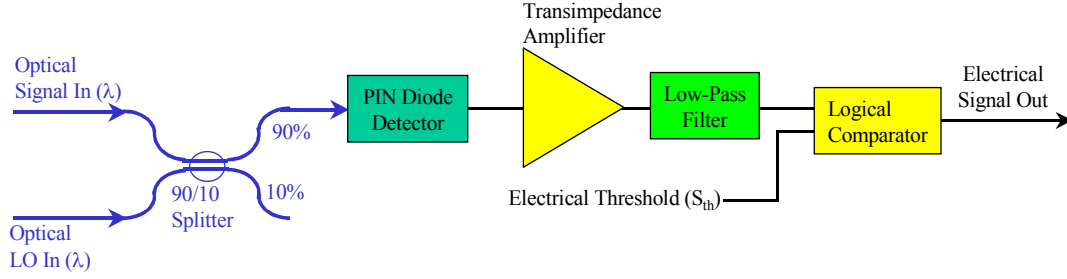


Figure 1.03 – Homodyne Receiver for ASK Transmissions

As opposed to heterodyne, where the difference between  $\omega_l$  and  $\omega_{lo}$  is at an intermediate frequency, the signal is now in the base-band. Thus, the bandwidth of the lowpass filter (Figure 1.03) is equal to the signal bandwidth. In addition,  $\phi_{lo}$  is now critical, and directly affects the magnitude of the detected signal. Specifically, this magnitude can be expressed as

$$S_{homol} = \left( \frac{\eta q}{h \nu} \right) \sqrt{2P_l P_{lo}} \cos(\phi_{lo}) \quad (1.23)$$

As such, the phase difference between the received and local oscillator signals must be equal to zero in order to maximize the output from the homodyne receiver. In this case, the signal from a homodyne receiver reduces to (1.18).

The signal during a 0-bit is approximately zero and thus is ignored. Thus, if the intensity of the local oscillator signal is strong enough such that the shot on the signal dominates the other noise sources in the system (Johnson noise, dark noise, etc), the (shot) noise during both the 1-bit and 0-bit is equal to:

$$\sigma_{homol} = \sqrt{\frac{1}{2} q \left( \frac{\eta q}{h \nu} \right) P_{lo} B_e} \quad (1.24)$$

Because the signal is at base-band, the filter bandwidth is equal to the signal bandwidth.

Note that this equation differs from (1.19) by a factor of  $\sqrt{2}$ . This difference is due to

the fact that the use of a homodyne detection system reduces the bandwidth of the detector from  $2B_e$  to  $B_e$  [10]. This is the origin of the homodyne 3dB advantage over heterodyne.

If an ASK transmission is incident upon the homodyne receiver, and we assume that the phase difference between the received and local oscillator signals is zero, then from (1.05), (1.18) and (1.24) the bit-error rate can be expressed as:

$$BER_{ASK-homo} = \frac{1}{4} \left[ \operatorname{erfc} \left( \sqrt{\frac{2\eta P_s}{h\nu B}} - \frac{S_{th}}{\sqrt{q \left( \frac{\eta q}{h\nu} \right) P_{lo} B_e}} \right) + \operatorname{erfc} \left( \frac{S_{th}}{\sqrt{q \left( \frac{\eta q}{h\nu} \right) P_{lo} B_e}} \right) \right] \quad (1.25)$$

which, when given (1.13) and the assumption that  $\eta=1$ , becomes:

$$BER_{ASK-homo} = \frac{1}{4} \left[ \operatorname{erfc} \left( \sqrt{2N} - \frac{S_{th}}{\sqrt{q \left( \frac{\eta q}{h\nu} \right) P_{lo} B_e}} \right) + \operatorname{erfc} \left( \frac{S_{th}}{\sqrt{q \left( \frac{\eta q}{h\nu} \right) P_{lo} B_e}} \right) \right] \quad (1.26)$$

As before, if a bit-error rate of  $10^{-9}$  is desired, then a numerical analysis of this equation can be used to determine the appropriate values of  $S_{th}$  and  $N$ . From this, it was found that 36 photons per bit are required to obtain a  $10^{-9}$  bit-error rate with a homodyne receiver. If it is assumed that the optical wavelength is 1550nm and the bit-rate is 10Gb/s, the average power that is required to obtain a BER of  $10^{-9}$  is approximately -46dBm.

To maximize the output of a homodyne receiver, the difference between the phases of the received and local oscillator signals must be minimized. The two ways to accomplish this are with either a phase diversity system, or a phase tracking system. In a phase diversity system, the received optical signal is first split by 50/50 splitter. At this

point, one half of the signal (one of the outputs of the splitter) is mixed with the local oscillator signal, while the other half is mixed with a local oscillator signal that has been phase shifted by  $90^\circ$ . These two signals are then detected separately and the outputs of the detectors are summed electronically [14]. Although this method effectively allows for a signal with an arbitrary phase to be detected with a homodyne receiver, the use of the 50/50 splitter decreases the final signal to noise ratio by 3dB, which in turn effectively doubles the photons/bit that are required for this detection method.

The alternative to a phase diversity system is a phase tracking system. In this, an electronic feedback loop is set up to compensate for any detected phase difference. This system does not decrease the signal to noise ratio by 3dB (as was the case for a phase diversity system). However, a phase tracking system will not effectively minimize the phase difference between the received and local oscillator signals if the phase drift of these two signals is faster than the response time of the feedback loop.

#### 1.1.2.3 Polarization Effects

In order to maximize the output signal for any coherent detection scheme, the polarization of the local oscillator signal must be aligned with the received signal. The two ways to accomplish this are with either a polarization diversity system, or a polarization tracking system. In a polarization diversity system, the received optical signal is first split by a polarizing beam splitter into two orthogonal polarization states. These two polarization states can then be separately detected. However, this effectively doubles the complexity of the receiver, since a separate coherent receiver must be assembled for each output of the beam splitter.

The alternative to a polarization diversity system is a polarization tracking system. In this, the received signal is transmitted through a polarization rotator, while an electronic feedback loop is used to maximize the output from the detector. This system adds significantly less optical path complexity to the overall receiver design. However, a polarization tracking system will be incapable of maximizing the output of the polarizer if the polarization drift of the received signal is faster than the response time of the feedback loop.

## 1.2 Overview of Project

In this section, DD, ADD, heterodyne, and homodyne detection will be discussed and their merits compared. The required number of photons/bit for each detection scheme are summarized in Table 1. From this, it can be seen that the most sensitive receiver is a non-amplified direct detector. However, such a system would need to be cooled to sub-zero temperatures [4]. The next two most practical methods for detecting a low intensity received optical signal are amplified direct detection and homodyne detection.

Receiver	Photons/Bit	Average Power (Bit Rate = 10Gb/s) [dBm]
Non-Amplified Direct Detection	20	-48.9
Pre-Amplified Direct Detection	72	-43.4
Heterodyne Detection	72	-43.4
Homodyne Detection	36	-46.4

Table 1 – Number of Photons per Bit that is Required for Various Detection Schemes

### 1.2.1 Implementation of DD

A direct detection system simply consists of a detector, and must exhibit low detector noise and high optical sensitivity. Direct detection can be employed if the

received signal is high power and low bandwidth or if the detector exhibits low Johnson and dark noise (e.g. Cryogenically-cooled PIN diodes). Currently, APDs are employed at moderate data rates, due to their high sensitivity. However, current APDs cannot detect data-rates higher than 3Gb/s. In addition, cryogenically cooling a PIN diode detector is not a practical solution for large optical networks.

### 1.2.2 Implementation of ADD

As was discussed in the previous section, an amplified direct detection system consists of a detector that is preceded by an optical amplifier (Figure 1.04). Although this appears to be an effective receiver design, there are two major problems. First, the ASE noise that is generated by the optical amplifier will decrease the effective S/N ratio of the detected signal. This in turn limits the minimum signal power that the detector is capable of receiving.

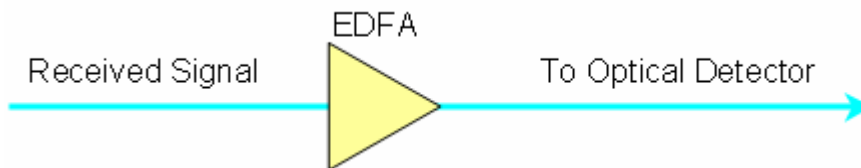


Figure 1.04 – Amplified Direct Receiver

#### 1.2.2.1 ADD Example

Earlier, we calculated that in order to obtain a BER of  $10^{-9}$ , we need an average signal strength of 36 photons/bit (assuming that the noise bandwidth is twice the signal bandwidth). Given a data rate of 10Gb/s and an optical wavelength of 1550nm, this translates to a signal power of approximately -46dBm. We assume that the amplified

optical signal is incident on a NewFocus detector (Model #1544), over a bandwidth of 10GHz. The NEP of this detector is approximately -24.8dBm. If we assume a threshold of  $\frac{1}{2}$  the signal strength and solve (1.05) for  $S_I$  (assuming  $S_0 = 0$  and  $\sigma_I = \sigma_0 = -24.8\text{dBm}$ ) we find that the peak signal required to obtain a BER of  $10^{-9}$  at the detector (given the Johnson noise) is -14dBm. This translates to an average power of -17dBm. Thus, given that the optical filter imposes at least a 3dB loss on the amplified signal, a gain of at least 29dB is required from the optical amplifier.

One parameter that must be addressed when designing an amplified receiver is the number of optical amplifiers that will be required to obtain a desired total gain. Any optical amplifier has a maximum allowable gain. This maximum gain is determined by the point at which the amplifier is saturated by both the amplified signal, and the ASE that is generated by the amplifier. Figures 1.05a and 1.05b show the maximum allowable gain from an EDFA (Figure 1.05a) [15] and an SOA (Figure 1.05b) [16], for various lengths of the amplifying medium. From this, it can be seen that, for a typical EDFA or SOA, the maximum gain that can be provided is 36dB or 34dB respectively [15, 16].

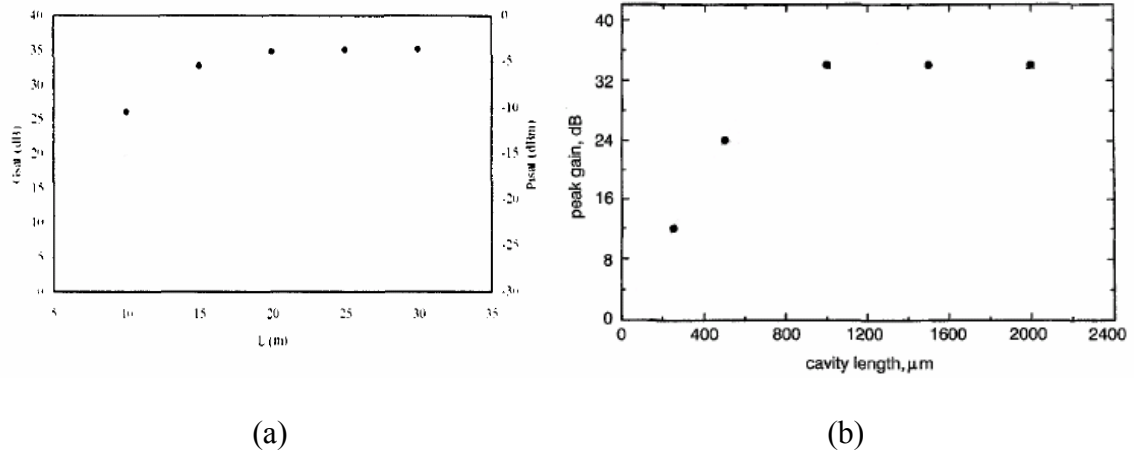


Figure 1.05 – Maximum Allowable Gain for an EDFA (a) [15] and an SOA (b) [16], for Various Lengths of the Amplifying Medium

However, losses within the system may require additional gain, which in turn may require the use of additional amplifiers.

### 1.2.3 Implementation of a Heterodyne Receiver

As with any coherent receiver, a heterodyne receiver mixes the received signal with a strong local oscillator signal. The benefit of this is that it makes shot noise the dominant noise, while shifting the frequency to an intermediate value, where RF technology can provide low-noise amplifiers and narrow filters. However, at current optical data-rates, optical filters are as narrow, and have comparable bandwidth characteristics as their RF counterparts.

Its advantage over homodyne detection is that it is phase insensitive (with a 3dB penalty). This receiver does not require a tight phase tracking feedback loop, but (in many cases) does require a frequency control feedback loop to keep the beat-note within the IF band-pass filter.

### 1.2.4 Implementation of a Homodyne Receiver

If we assume that the coherence length of the received optical signal is such that its linewidth is much less than the envelope of the optical data, then an effective alternative to a direct detection system is a homodyne receiver. From Table 1, it can be seen that a homodyne receiver is capable of higher sensitivities than an amplified direct detector. However, any homodyne receiver requires a local oscillator signal that is synchronized (phase coherent) with the received signal. Such a local oscillator signal can

be regenerated from a portion of the received signal. This will ensure that the local oscillator is at the same frequency, and is phase locked with, the received optical signal. There are three main methods that may be utilized to generate a local oscillator signal. First, a small portion of the received signal may be filtered and amplified for use as the local oscillator signal. Second, a small portion of the received signal may be injected into a slave laser, the output of which can be used as the local oscillator signal. Finally, an Optical Phase-Locked Loop (OPLL) may be used to force the frequency and phase of an independent laser to mimic the frequency and phase of the received signal.

There have been several studies work that demonstrate the effectiveness of OPLL for locking narrowband heterodyne [34, 35, 36] and homodyne [1, 37, 38] signals to within acceptable limits. However, previous work has also demonstrated that, in order to effectively lock two wideband homodyne signals together, the loop delay must become very small, typically less than 0.1ns for lasers with linewidths  $>10\text{MHz}$ , depending on the loop filter implemented in the setup [19]. As such, OPLLs may not be physically realizable with Commercial Off-The-Shelf (COTS) components and were not seriously considered for generating a local-oscillator signal in this experiment.

#### 1.2.4.1 Homodyne Receiver with an Amplified Local Oscillator

The most obvious approach to generate this local oscillator signal is to use a narrow Fabry-Perot pre-filter to strip the data from the diverted portion of the received optical signal. After this, the stripped signal can be amplified and re-filtered to remove the added ASE from the signal. The layout of this method is depicted in Figure 1.06.

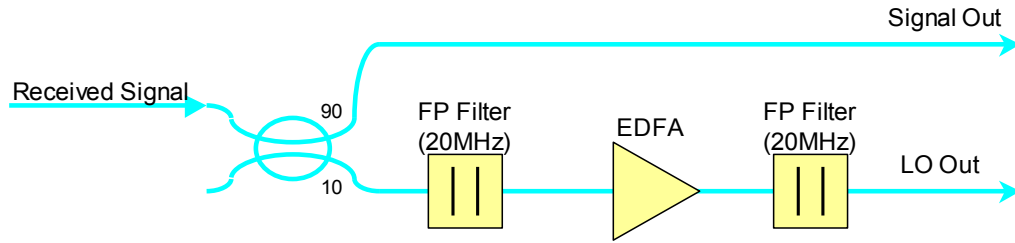


Figure 1.06 – LO Generator Utilizing an Optical Amplifier

The primary advantage of this method over an amplified direct detector is that, since only the local oscillator signal needs to be amplified, the ASE noise that is present on the detected signal can be reduced by limiting the bandwidth on the output of the optical amplifier. For the direct detector the minimum allowable bandwidth was 10GHz, limited by the data rate of the received optical signal. However, since only the local oscillator signal needs to be amplified in the case of a homodyne receiver, the bandwidth on the output of the optical amplifier can be limited to the linewidth of the carrier, typically less than 10MHz. This effectively reduces the magnitude of the ASE noise that is present on the detected signal by 30dB (compared to filtered ADD). It should be noted that this is lower than was predicted for the BER calculations in the previous section, since those were calculated assuming a bandwidth comparable to the data-rate.

However, there is a problem with this method. To demonstrate this by specific example, we first assume that the received signal is -43.4dBm (as in the example for the amplified direct detector to achieve a BER of  $10^{-9}$  at a data rate of 10Gb/s and an optical wavelength of 1550nm), and that 10% of the received signal is diverted for generating the local oscillator signal. Additionally, we assume that we are mixing the received and local oscillator signals in a detector whose equivalent input noise (due to Johnson noise) is approximately -24.8dBm as in the ADD example (Section 1.2.2.1). As previously

mentioned in section 1.2.1, this detector requires an average signal power of -17dBm to achieve the conditions assumed above. Since the detected signal from a coherent receiver is effectively the geometric average of the signal and local oscillator powers, the homodyne receiver requires a local oscillator power of approximately:

$$P_{lo} = \frac{P^2}{P_1} = 2 \times (-17\text{dBm}) - (-43\text{dBm}) = -9\text{dBm} \quad (1.27)$$

to reach the shot noise limit. Given this, it follows that a total gain of 44dB is required from the system. Since this system already incorporates two Fabry-Perot filters, whose minimum loss is 3dB per filter, the total gain that is required from the optical amplifier is 50dB.

However, and as was discussed in section 1.2.1, the maximum gain that a typical optical amplifier can provide is approximately 35dB. Thus, multiple amplifiers are required. As such, we must adopt the configuration that is depicted in Figure 1.07. In this, the diverted portion of the received optical signal is pre-filtered and amplified, just as in the previous case. However, after this the signal is then re-filtered and diverted into a second optical amplifier. The purpose of this is to remove the ASE that is outside the bandwidth of the filter before re-amplifying the signal. This will prevent the second amplifier from saturating, increasing the overall signal gain. After the second amplifier, the remaining ASE is removed from the local oscillator signal by a third optical filter.

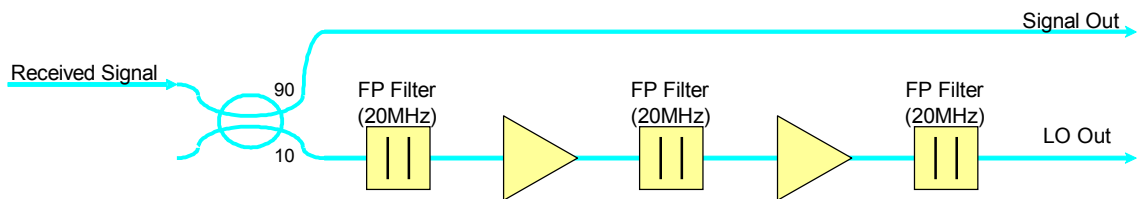


Figure 1.07 – LO Generator Utilizing Multiple Optical Amplifiers

The drawback to this method is that it is even more expensive than the amplified direct detector. This is due to the need for multiple optical amplifiers and narrow-band Fabry-Perot filters. As such, a different, less costly method for generating a local oscillator signal is desired.

#### 1.2.4.2 Homodyne Receiver with an Injection Locked Local Oscillator

A local oscillator generator, similar to the one discussed in the previous section, may be obtained by placing an amplifying medium within a cavity. In this case, instead of passing through multiple optical amplifiers, the received optical signal will make multiple passes through a single amplifying medium. This process is known as "Regenerative Amplification" [11]. In fact, unless there is an isolator on each side of the gain media in the previous design, regenerative amplification will occur in that design as well. In general, a regenerative amplifier provides high-gain for a received signal (relative to the single-pass gain) over a narrow bandwidth. If the gain of the amplifying medium within the regenerative amplifier is greater than or equal to the cavity loss, the regenerative amplifier will self-oscillate. Amplifier chains without isolators are prone to runaway self lasing. When no input signal is provided, the regenerative amplifier will be seeded by the noise generated by the amplifying medium. This noise-seeded optical regenerative amplifier (the case in which the ratio of gain to loss is greater than 1) is a laser oscillator. Such a laser will emit a coherent signal whose center frequency is the point at which the in-band (as determined by the optical path length of the cavity) gain of the amplifying medium is at a maximum.

Let us assume that a laser is injected with a low-intensity optical signal (as opposed to noise generated by the amplifying medium within the cavity) that is detuned from the center frequency of the cavity by a small amount. If this injected signal is weak enough, it can circulate within the cavity and be regeneratively amplified by the laser medium. As such, this injected signal will be amplified, independent of any other signals currently oscillating within the cavity.

Given both an injected optical frequency that is close to the free-running frequency of the oscillator and a sufficiently intense injected signal, the amplified injected signal will approach the free-running oscillation intensity of the laser cavity. Once this occurs, the injected signal will steal enough of the available gain from the amplifying medium so that the free-running signal is effectively suppressed. At this point, the injected laser (commonly known as the "slave laser") will emit a signal that is at the same frequency as the injected signal, but at the intensity of the free-running signal.

The ability for these injection locked lasers to produce local oscillator signals has been previously explored [18, 19, 20]. Since this method is based on regenerative amplification, it is similar to the "amplifier-filter chain" method described in the previous section. However, this method is significantly less expensive since it only requires a single slave laser.

Although injection locking is an effective means to generate a local oscillator signal, there may be additional concerns that must be addressed, depending on the intensity of the injected signal. Previous research has shown that the output of the slave laser becomes non-linear for high-powered injection [39, 40]. The cause of this non-linearity can be attributed to both the suppression of free-running oscillation due to light

injection in the slave laser, and to the change of the active layer index due to the high intensity of the injected signal [40]. To avoid this issue, we ensure that the injected signal is approximately 20-30dB lower than the output of the slave laser. However, the locking range of the slave laser will be <1GHz given this condition. As such, a feedback loop will be required to maintain the injection lock.

The methodology that we use to generate a local oscillator signal is based on the approach described in [19]. In [19], a DFB laser is injection locked with a portion of the received signal. An optical phase-locked loop is then used to maintain the injection lock (required to compensate for the narrow locking range, as described in the previous paragraph). However, this method has only been proven to work for low data-rate optical signals (10-100Mb/s).

In my implementation, depicted in Figure 1.08, a 90/10 splitter is used to divert a portion of the received optical signal into a narrow Fabry-Perot bandpass filter. The purpose of this filter is to average over the modulation on the received signal. The injection locking process will suppress the incident modulation by 10-30dB (depending on the intensity of the injected signal and the properties of the slave laser used). If the injected signal is On-Off Keyed (OOK), then the resulting local oscillator will still have a 0.1%-10% modulation on it at the data frequencies. Without the input filter, this high-frequency residual modulation may interfere with the received data, effectively increasing the BER of the receiver.

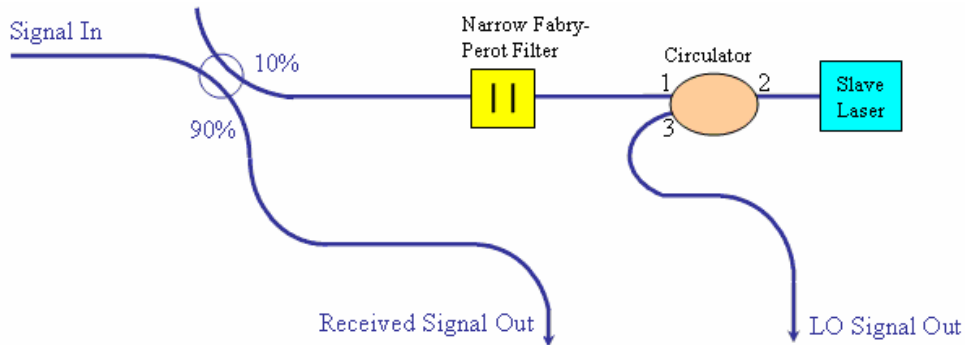


Figure 1.08 – Layout of Local Oscillator Generator

The filtered signal is then used to injection lock a slave laser. The output of the slave laser is a CW signal at the frequency of the received optical signal. In addition, it is expected (and will be shown) that this CW signal is also phase coherent with the received optical signal [21]. This regenerated CW signal can then be used as the local oscillator for a homodyne receiver.

From this, I will demonstrate that a suitable local oscillator for a high-speed homodyne receiver can be generated using either a DFB or a Fabry-Perot slave laser that is injected with a portion of the received optical signal. In addition, I will show that the injection locking process can be stabilized by monitoring the modulation transfer ratio of the slave laser. Specifically, the modulation transfer ratio of an injected laser is at a minimum at the center of the locking range, and increases as the difference between the frequencies of the injected and free-running signals increase. This effect will be shown in both Fabry-Perot lasers and DFB lasers. I will also show that this effect can be modeled with the 1<sup>st</sup> order approximations of the laser rate equations.

The suitability of both Distributed Feedback (DFB) lasers (Chapter 3) and Fabry-Perot lasers (Chapter 4) will be discussed for use as an appropriate slave laser for the local oscillator generator. In addition, a novel method for stabilizing the detuning within the injection lock that utilizes the modulation transfer function of the slave laser will be discussed for both slave laser types. Finally, in Chapter 5, the quality of the local oscillator signal that is generated by the injection locked Fabry-Perot laser will be explored.

#### 1.2.5 Relative Merits

The advantage of DD is that it has the highest inherent sensitivity (as seen on Table 1). However, DD is also impractical at high data-rates, due to the unavailability of high-frequency APDs, and the impracticality of cryogenically-cooling PIN diode detectors. Also, in most cases, a DD will not be shot noise limited.

The next most sensitive detection system is the homodyne receiver. Due to this, it is the detection method that is currently being considered for this project. In addition to being a sensitive method of detection this method is shot noise limited. Unlike ADD and heterodyne, the homodyne signal is in the base-band. This allows for a low-pass filter to limit the noise bandwidth that is equal to the signal bandwidth. The disadvantage of this method is that it requires a phase tracked local oscillator signal.

Heterodyne detection is not being considered as a viable alternative to ADD, since both methods require a filter that is twice the signal bandwidth, and because a heterodyne receiver is much more complex than an ADD while offering no increase to measurement sensitivity.

## II. CHAPTER 2 – Passive Optical Filtering

### 2.1 Background

As previously mentioned, an optical pre-filter will be placed at the input of the slave laser. The purpose of this pre-filter is to average over the modulation on the received signal. This will effectively reduce the residual modulation on the final local oscillator signal beyond what could be obtained by the slave laser alone.

A Fabry-Perot filter was chosen for use as the pre-filter, due to its availability (other filter types, such as microrings, would also serve as suitable pre-filters). A Fabry-Perot filter, illustrated in Figure 2.01, is a resonant optical cavity. If an optical signal is incident normal to one facet of this cavity, the ratio of the transmitted signal ( $I_t$ ) to the incident signal ( $I_0$ ) can be expressed as [22]:

$$\frac{I_t}{I_0} = \frac{(1-R)^2}{(1-R)^2 + 4R \sin^2(\delta/2)} \quad (2.01)$$

where  $R$  is the power reflectance of each facet of the optical cavity, and  $\delta$  is the phase difference between successive round trips of the optical signal within the cavity. From (2.01), it can be seen that the transmission ratio is equal to one when  $\delta=0$ . This occurs when the frequency of the light is approximately

$$\nu_f = \frac{mc_0}{2nl} \quad (2.02)$$

where  $n$  is the index of refraction of the optical cavity,  $l$  is the length of the optical cavity,  $c_0$  is the speed of light, and  $m$  is a positive integer.

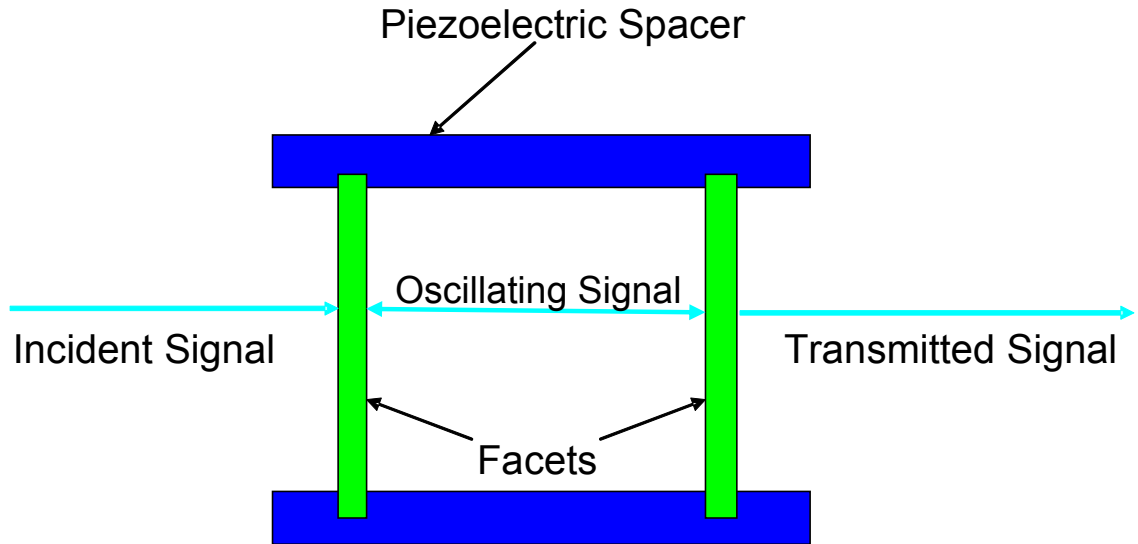


Figure 2.01 – Fabry-Perot Filter with Piezoelectric Spacer

The phase difference between successive round trips can be expressed as approximately

$$\delta = \frac{4\pi ml(\nu - \nu_m)}{c_0} \quad (2.03)$$

where  $\nu$  is the optical frequency of the incident signal. If the optical frequency of the received signal is close to the center frequency of the filter (the phase difference between successive round trips is small), then this equation can be rewritten as

$$\frac{I_t}{I_0} = \frac{1}{1 + \frac{F^2 \delta^2}{\pi^2}} \quad (2.04)$$

where  $F$  is the finesse of the filter, and is defined as

$$F = \frac{\pi\sqrt{R}}{1 - R} \quad (2.05)$$

The bandwidth of this filter is defined by the FWHM of the Lorentzian function, (2.04).

Thus, from (2.03) and (2.04), the bandwidth of the optical filter is

$$\Delta \nu_f = \frac{c_0}{4nlF} \quad (2.06)$$

From (2.02), it can be seen that the center frequency of the filter can be varied by adjusting the optical path length ( $nl$ ) of the cavity. This is done by varying the spacing by using a piezoelectric spacer (Figure 2.01). The size of this spacer varies due to a voltage that is applied across it. Thus, the center wavelength of this filter can be adjusted by changing the applied voltage via a filter controller. It should be noted that the change in the optical path length is assumed to be much smaller than the overall length of the cavity. This is so we can neglect the effect of adjusting the optical path length on the bandwidth of the filter.

## 2.2 Feedback Control of Filter

Due to laser drift (which typically does not exceed a drift rate of 0.1Hz over a range of not more than 0.2nm over the laser lifetime [33]), as well as thermal drift of the fiber as well as of the filter itself (whose drift rate is typically sub-kHz), it is necessary to have a feedback system that controls the center frequency of the filter. Specifically, the feedback system is required to lock one of the modes of the Fabry-Perot filter to the incident optical signal in order to obtain maximum transmission.

If the voltage applied by the filter controller is harmonically dithered, the center frequency of the filter is also dithered. Thus, the magnitude of the amplitude modulation at the dither frequency will be proportional to the derivative of the (Lorentzian) transfer function of the filter.

Given this, an amplitude locking loop, as shown in Figure 2.02, can be created. This system starts by detecting a small portion of the output of the dithered filter. The output of the detector is then used as the input to a lock-in amplifier whose reference is the frequency at which the filter is dithered. The real component output (X) of the lock-in amplifier is effectively the derivative of the transfer function of the filter, depicted in Figure 2.03. From this figure, it can be seen that the derivative is nearly linear in the region where  $|\nu - \nu_m| < 10\text{MHz}$ . This is the range in which the feedback loop will be able to maintain the filter lock. It should be noted that a feedback loop that utilizes a lock-in amplifier is not the only suitable feedback control method. Since the feedback signal is simply the intensity of the detector output, any feedback system that monitors (and maximizes) the signal from the detector is acceptable. A lock-in amplifier is only needed for a feedback loop if a phase-sensitive measurement is required.

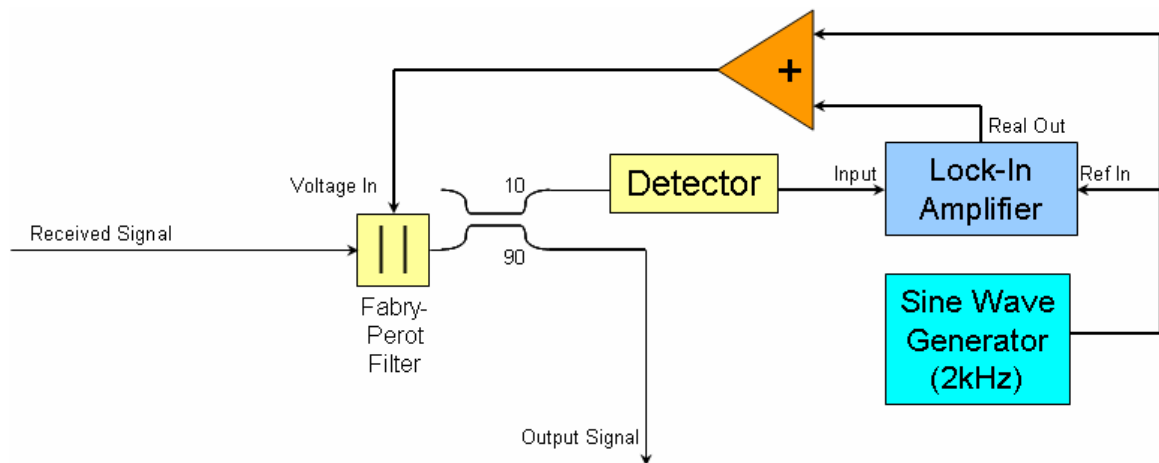


Figure 2.02 – Example of Feedback System for a Fabry-Perot Optical Bandpass Filter

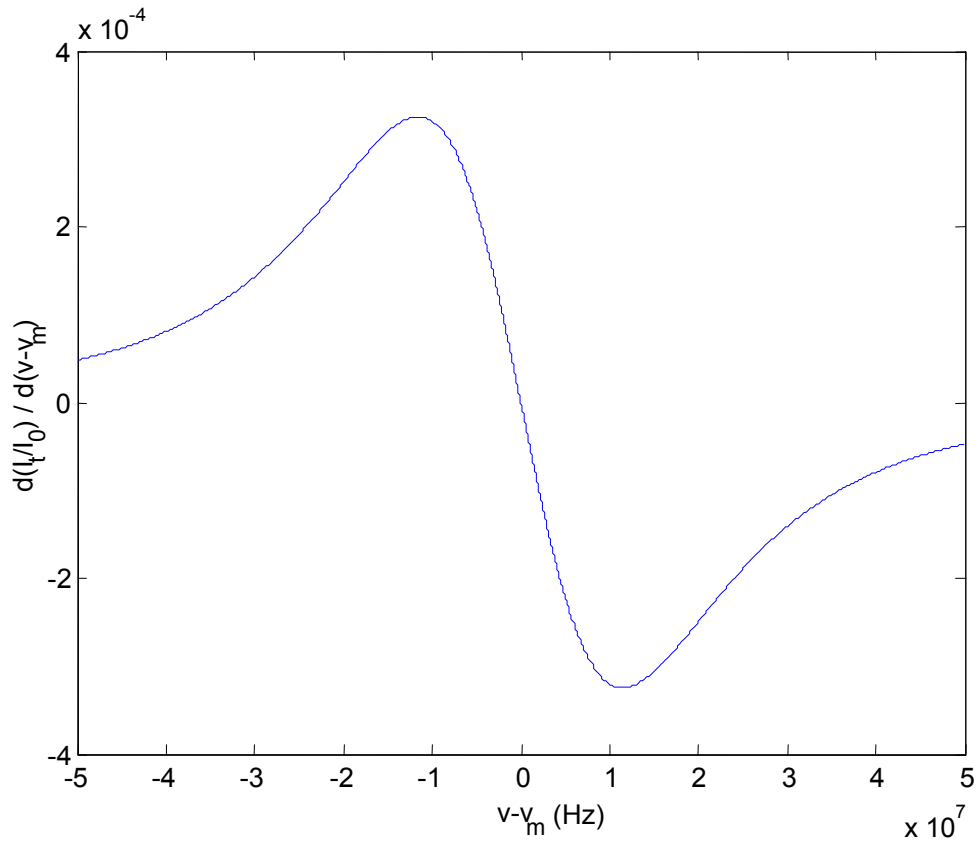


Figure 2.03 – Derivative of Transfer Function of Fabry-Perot Filter

For this feedback system, a 2kHz dither (chosen to be at least 10x faster than the drift rate of the filter) was added to the output of the lock-in amplifier and applied to the piezoelectric controller of the filter. In addition, the lock-in amplifier was set to have a 300ms integration time across a 6dB/octave low-pass filter.

In order to test the feedback loop, the output from the detector was monitored over a period of 10 seconds, while the filter bias was randomly varied. From this, it was observed that the feedback loop successfully adjusted a mode of the Fabry-Perot laser so that it was approximately equal to the center frequency of the received optical signal.

### III. CHAPTER 3 – Injection Locking a DFB Semiconductor Laser

#### Laser

#### 3.1 Background

“Injection Locking” is the process of injecting a weak seeding optical signal into a more powerful free-running oscillator, in order to lock the frequency of the free-running oscillator to approximately the same frequency as the seed. The output of the locked oscillator will then be coherent (in frequency and phase) with the injected signal.

We assume that the particular laser that is being injection locked is a Distributed Feedback (DFB) laser. A DFB laser is fabricated such that a periodic grating is etched close to the active region of the laser, throughout much of the gain region (Figure 3.01) [23]. Since only wavelengths that match the grating spacing will oscillate within the laser structure, unwanted modes will be effectively suppressed in a DFB laser.

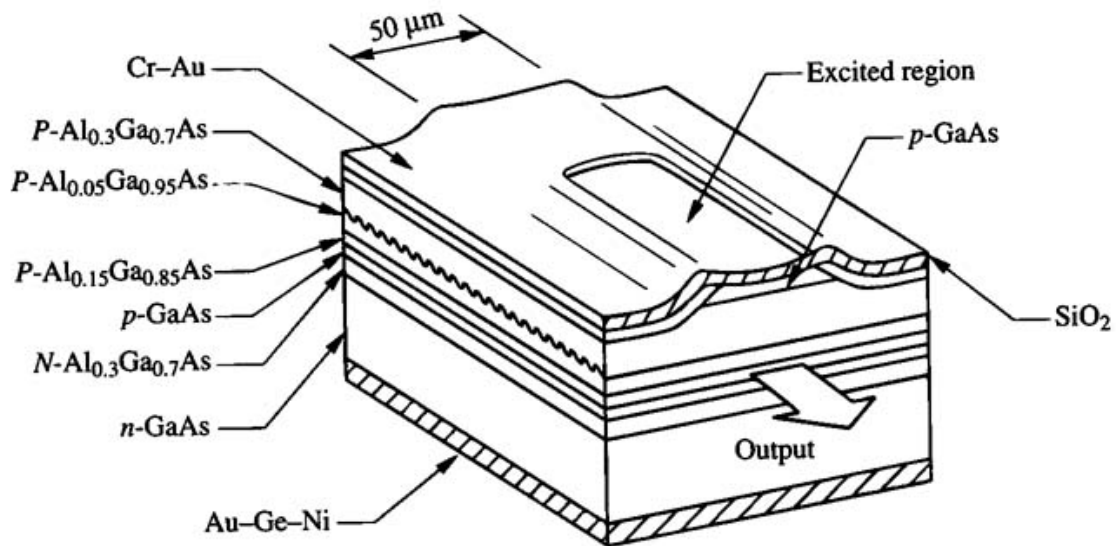


Figure 3.01 – Structure of a GaAlAs Double Heterojunction DFB Laser [23]

To model this system, we assume that the laser can be approximated as an effective two-level system, consisting of a ground state and an excited state for the gain medium. This medium excitation dynamic is modeled as a simplified rate equation which ignores non-radiative excitation. Furthermore, the excitation of the photon field can be described by a rate equation.

### 3.1.1 Rate Equation for the Photon Field

For the purposes of developing an injection locking theory for a DFB semiconductor laser it will be assumed that the free-running oscillator is operating in single-mode, and the optical frequency of the injected signal is close to the frequency of the free-running oscillator.

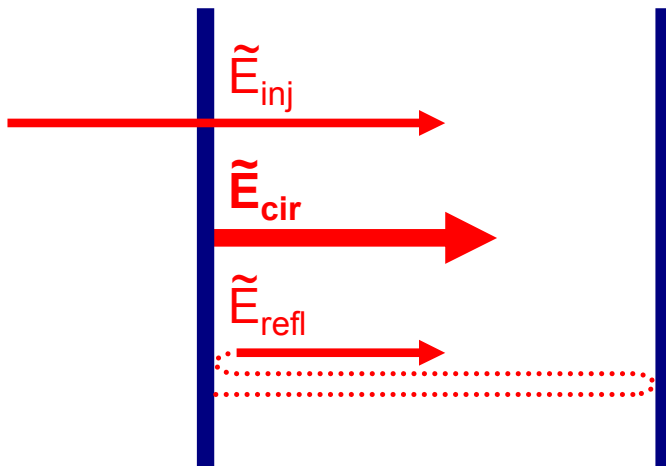


Figure 3.02 – Phasor Picture of Laser Cavity

To further explore the behavior of this system, we use the phasor picture depicted in Figure 3.02. In this,  $\tilde{E}_{cir}$  represents the total phasor amplitude of the optical wave that is circulating within the cavity.  $\tilde{E}_{cir}$  is comprised of both the portion of the circulating

field that is reflected off of the left mirror ( $\tilde{E}_{refl}$ ) and the injected field ( $\tilde{E}_{inj}$ ). As such,

$\tilde{E}_{cir}$  can be expressed as

$$\tilde{E}_{cir} \equiv \tilde{E}_{refl} + \tilde{E}_{inj} \quad (3.01)$$

In addition,  $\tilde{E}_{refl}$  can be expressed as:

$$\tilde{E}_{refl} = \left[ \tilde{E}_{cir}(t - T_{RT}) \right] e^{\delta_m - \delta_c - jT_{RT}(\omega_1 - \omega_0)} \quad (3.02)$$

where  $T_{RT}$  is the round-trip transit time,  $\delta_m$  is the round-trip gain of the cavity,  $\delta_c$  is the roundtrip loss of the cavity, and  $\omega_1$  and  $\omega_0$  are the frequencies of the injected electric field and the electric field inside the slave laser (respectively). From these two equations, the total field at the first mirror can be expressed as:

$$\tilde{E}_{cir} - \left[ \tilde{E}_{cir}(t - T_{RT}) \right] e^{\delta_m - \delta_c - jT_{RT}(\omega_1 - \omega_0)} = \tilde{E}_{inj} \quad (3.03)$$

If we assume that  $T_{RT}$  is small, then we can use a 1<sup>st</sup> order time series expansion of the time-delay and exponential terms of the equation to rewrite it as:

$$\frac{d\tilde{E}_{cir}}{dt} - \frac{\delta_m - \delta_c}{T_{RT}} \tilde{E}_{cir} + j(\omega_1 - \omega_0) \tilde{E}_{cir} = \frac{\tilde{E}_{inj}}{T_{RT}} \quad (3.04)$$

If we define the single-pass carrier lifetime ( $\tau_c$ ) and the unsaturated gain to loss ratio ( $r$ ) as:

$$\tau_c \equiv \frac{T_{RT}}{2\delta_c} \quad (3.05)$$

$$r = r_1 + jr_2 = \frac{\delta_m}{\delta_c} \quad (3.06)$$

then (3.04) can be written as:

$$\frac{d\tilde{E}_{cir}}{dt} - \frac{r_1 - 1}{2\tau_c} \tilde{E}_{cir} - j \frac{r_2}{2\tau_c} \tilde{E}_{cir} + j(\omega_1 - \omega_0) \tilde{E}_{cir} = \frac{\tilde{E}_{inj}}{T_{RT}} \quad (3.07)$$

Note that  $r$  has been defined as a complex value in (3.06). The real portion of  $r$  represents the unsaturated gain-to-loss ratio, while the imaginary portion represents the phase shift that occurs at the edge of the laser cavity. Given this, (3.07) can be separated into amplitude and phase components by expressing  $\tilde{E}_{cir}$  and  $\tilde{E}_{inj}$  as:

$$\tilde{E}_{cir} = E e^{j\phi_0} \quad (3.08)$$

$$\tilde{E}_{inj} = E_1 e^{j\phi_1} \quad (3.09)$$

where  $E$  and  $E_1$  are the magnitudes of the circulating and injected fields, and  $\phi$  and  $\phi_1$  are the phases of the circulating and injected fields, respectively. Given this, we can express the change in the amplitude of the circulating electric field as:

$$\frac{dE}{dt} - \frac{r_1 - 1}{2\tau_c} E = \gamma_e E_1 \cos \phi \quad (3.10)$$

and the change in the phase of the circulating field as:

$$\frac{d\phi}{dt} - \frac{r_2}{2\tau_c} + (\omega_1 - \omega_0) = \frac{\gamma_e E_1}{E} \sin \phi \quad (3.11)$$

where  $\phi$  is the phase difference between the injected electric field and the electric field inside the slave laser ( $\phi = \phi_1 - \phi_0$ ),  $\gamma_e$  is the photon loss rate due to external coupling ( $\gamma_e = 1/T_{RT}$ )

### 3.1.2 Rate equation for two level population dynamics

To determine the change in the unsaturated gain, we assume that the laser is operating in a state of near-full population inversion. In this case, the rate equation for

the excited energy level of the laser ( $N_2$ ) can be expressed as (ignoring non-radiative de-excitation):

$$\frac{dN_2}{dt} = \rho - \frac{N_2}{T_1} - \frac{E^2}{I_{sat}} \Delta N_2 \quad (3.12)$$

where  $\rho$  is the pump rate,  $T_1$  is the cavity lifetime, and  $I_{sat}$  is the saturation intensity. In this equation,  $-N_2/T_1$  represents the change in the excited energy level of the laser due to spontaneous emission, and  $-(E^2/I_{sat})\Delta N_2$  represents the change due to stimulated emission. If we assume a two-level system with full population inversion, then the overall gain of the cavity can be expressed as:

$$\delta_m = 2\sigma L \Delta N_2 \quad (3.13)$$

where  $L$  and  $\sigma$  are the is the length and stimulated emission cross-section of the cavity, respectively. Since  $\delta_m$  is proportional to  $N_2$  and  $\delta_c$  is independent of  $N_2$ , then from (3.06) the unsaturated gain to loss ratio ( $r$ ) is also proportional to  $N_2$ . Given (3.12), this allows  $r$  to be expressed as:

$$\frac{dr}{dt} = \rho - r \frac{1}{T_1} \left( 1 + \frac{E^2}{I_{sat}} \right) \quad (3.14)$$

Equations (3.10), (3.11), and (3.14) can be used to approximately describe the behavior of the injection locked DFB laser.

### 3.1.3 Phase Stability Range

The steady-phase solution of (3.11) can be used to solve for the detuning of the injected optical signal with respect to the optical signal generated by the locked oscillator [50]:

$$\Delta\omega = \omega_1 - \omega_0 = \gamma_e \sqrt{\frac{P_1}{P_0}} (\sin \phi - \alpha_\phi \cos \phi) \quad (3.15)$$

where  $\alpha_\phi$  is a phase factor whose value is comprised slow thermal refractive effects and the linewidth enhancement factor due to high-frequency electronic effects, and  $P_I$  and  $P_0$  are the injected and slave laser output powers, respectively ( $P_I = E_{I0}^2$ ,  $P_0 = E_0^2$ ).

Since these effects have opposite effects on the laser, the value of  $\alpha_\phi$  is less than the linewidth enhancement factor of the laser. Experimentally, it was found that  $\alpha_\phi$  is negligible for our DFB laser and  $\sim 2$  for the Fabry-Perot laser.

As the injected signal is detuned, the output of the slave oscillator remains at the frequency of the injected signal, but the phase difference between the signals varies over a range of  $-\pi/2$  to  $\pi/2$  [50]. From (3.15) and this phase limitation, the detuning must be within the range [50]:

$$-\gamma_e \sqrt{\frac{P_1}{P_0}} < \Delta\omega < \gamma_e \sqrt{\frac{P_1}{P_0}} \sqrt{1 + \alpha_\phi^2} \quad (3.16)$$

in order to maintain injection lock.

#### 3.1.4 Phase Shift of a Tracking Oscillator

The steady-phase solution of (3.11) can also be used to solve for the phase difference between the injected optical signal and the optical signal generated by the locked oscillator. For cases where the value of  $\alpha_\phi$  is negligible, this phase difference can be expressed as:

$$\phi = \sin^{-1} \left( \frac{E}{\gamma_e E_1} (\omega_1 - \omega_0) \right) \quad (3.17)$$

As the injected signal is detuned, the output of the slave oscillator remains at the frequency of the injected signal, but the phase difference between the signals varies over a range of  $-\pi/2$  to  $\pi/2$ .

### 3.2 Feedback Control of an Injection Locked DFB Semiconductor Slave Laser

In order for the regenerated local oscillator to lock in frequency with the received optical signal, the difference between the frequency of the received optical signal and the free-running frequency of the slave laser must be within a narrow range (i.e. the locking range). However, due to thermal drift, the free-running frequency of the slave laser will vary (given a stable laser controller, this typically does not exceed a drift rate of 0.1Hz over a range of not more than 0.2nm over the laser lifetime [33], although circuit glitches may cause a temporary, rapid "drift"). In order to compensate for this drift, as well as for the normal frequency drift that is associated with the received optical signal (due to environmental drift, whose drift rate is typically sub-kHz), a feedback system to match these two frequencies is required.

In order to create this feedback system, a method of determining the difference between the free-running frequency of the slave laser and the frequency of the received optical signal is required. As previously mentioned, when the difference between these two frequencies is within the locking range, the frequency of the output of the slave laser is equal to the frequency of the received optical signal. Thus, there is no obvious, simple, direct way of determining this difference. From (3.17), we see that the detuning can be indirectly measured by monitoring the phase difference between the injected signal and

slave laser output (assuming that  $\alpha_\phi$  is negligible). However, since a coherent receiver is essentially an interferometer, this phase difference can be due to either detuning, or to drift in the interferometer arms. Thus, a new method for monitoring the detuning is required.

### 3.2.1 Generation of a Feedback Signal

In order to determine a new method for generating an appropriate feedback signal, we must first delve deeper into the theory of injection locking. Once we do this, we will find that if an amplitude modulated signal is injected into the slave laser, the resulting transmission ratio can be used to determine the difference between the free-running frequency of the slave laser and the frequency of the received optical signal.

#### 3.2.1.1 MTR as a Measure of Detuning

We shall show that the Modulation Transfer Ratio (MTR) is a good way to measure detuning. For this, MTR is defined as the ratio of the output and input modulation indices, where the modulation index is defined as the ratio of the modulation on a given signal to its CW power. This will be defined below as  $(\Delta E_0/E_0)/(\Delta E_1/E_1)$ . To calculate the MTR as a function of detuning, we must first assume that a small perturbation is applied to  $E_1$ ,  $E$ ,  $r$ , and  $\phi$ . From this, we can express  $E_1$ ,  $E$ ,  $r$  and  $\phi$  as:

$$E_1 = E_{10} + \Delta E_1 \quad (3.18)$$

$$E = E_0 + \Delta E \quad (3.19)$$

$$r_1 = r_{10} + \Delta r_1 \quad (3.20)$$

$$r_2 = r_{20} + \Delta r_2 \quad (3.21)$$

$$\phi = \phi_0 + \Delta\phi \quad (3.22)$$

Substituting  $E_1$ ,  $E$ ,  $r$ , and  $\phi$  into (3.11):

$$\frac{d\phi_0}{dt} + \frac{d\Delta\phi}{dt} - \frac{r_2}{2\tau_c} - \frac{\Delta r_2}{2\tau_c} + (\omega_1 - \omega_0) = \frac{\gamma_e (E_{10} + \Delta E_1)}{E_0 + \Delta E} \sin(\phi_0 + \Delta\phi) \quad (3.23)$$

Expanding the sine term:

$$\left[ \frac{d\phi_0}{dt} - \frac{r_2}{2\tau_c} + (\omega_1 - \omega_0) \right] + \frac{d\Delta\phi}{dt} - \frac{\Delta r_2}{2\tau_c} = \frac{\gamma_e (E_{10} + \Delta E_1)}{E_0 + \Delta E} [\sin \phi_0 \cos \Delta\phi + \cos \phi_0 \sin \Delta\phi] \quad (3.24)$$

If we assume that  $\Delta\phi$  and  $\Delta E$  are very small, we can take the first order approximations of the trigonometric terms and of the denominator of the right side of the equation:

$$\begin{aligned} & \left[ \frac{d\phi_0}{dt} - \frac{r_2}{2\tau_c} + (\omega_1 - \omega_0) \right] + \frac{d\Delta\phi}{dt} - \frac{\Delta r_2}{2\tau_c} \\ &= \frac{\gamma_e}{E_0} (E_{10} + \Delta E_1) \left( 1 - \frac{\Delta E}{E_0} \right) (\sin \phi_0 + \Delta\phi \cos \phi_0) \end{aligned} \quad (3.25)$$

Expanding the right side of the equation:

$$\begin{aligned} & \left[ \frac{d\phi_0}{dt} - \frac{r_2}{2\tau_c} + (\omega_1 - \omega_0) \right] + \frac{d\Delta\phi}{dt} - \frac{\Delta r_2}{2\tau_c} \\ &= \frac{\gamma_e}{E_0} \left[ E_{10} \sin \phi_0 + E_{10} \Delta\phi \cos \phi_0 + \Delta E_1 \sin \phi_0 + \Delta E_1 \Delta\phi \cos \phi_0 \right. \\ & \quad \left. - \frac{E_{10} \Delta E}{E_0} \sin \phi_0 - \frac{E_{10} \Delta E}{E_0} \Delta\phi \cos \phi_0 - \frac{\Delta E \Delta E_1}{E_0} \sin \phi_0 - \frac{\Delta E \Delta E_1}{E_0} \Delta\phi \cos \phi_0 \right] \end{aligned} \quad (3.26)$$

Regrouping in order of powers of  $\Delta\phi$  and using (3.11) to simplify this equation:

$$\begin{aligned} & \frac{d\Delta\phi}{dt} - \frac{\Delta r_2}{2\tau_c} \\ &= \frac{\gamma_e}{E_0} \left[ E_{10} \Delta\phi \cos \phi_0 + \Delta E_1 \sin \phi_0 + \Delta E_1 \Delta\phi \cos \phi_0 \right. \\ & \quad \left. - \frac{E_{10} \Delta E}{E_0} \sin \phi_0 - \frac{E_{10} \Delta E}{E_0} \Delta\phi \cos \phi_0 - \frac{\Delta E \Delta E_1}{E_0} \sin \phi_0 - \frac{\Delta E \Delta E_1}{E_0} \Delta\phi \cos \phi_0 \right] \end{aligned} \quad (3.27)$$

Dropping the higher order terms and letting  $\alpha_\phi = \Delta r_2 / \Delta r_1$ :

$$\frac{d\Delta\phi}{dt} - \alpha_\phi \frac{\Delta r_1}{2\tau_c} = \frac{\gamma_e}{E_0} \left[ E_{10} \Delta\phi \cos \phi_0 + \Delta E_1 \sin \phi_0 - \frac{E_{10} \Delta E}{E_0} \sin \phi_0 \right] \quad (3.28)$$

Similarly, from (3.10) and (3.18-3.22):

$$\frac{dE_0}{dt} + \frac{d\Delta E}{dt} - \frac{r_{10} + \Delta r_1 - 1}{2\tau_c} (E_0 + \Delta E) = \gamma_e (E_{10} + \Delta E_1) \cos(\phi_0 + \Delta\phi) \quad (3.29)$$

Following the method for deriving (3.28), we get:

$$\frac{d\Delta E}{dt} - \frac{\Delta r_1}{2\tau_c} E_0 - \frac{r_{10} - 1}{2\tau_c} \Delta E = \gamma_e (\Delta E_1 \cos \phi_0 - E_{10} \Delta\phi \sin \phi_0) \quad (3.30)$$

Additionally, from the real part of (3.14) and (3.19-3.21):

$$\frac{dr_{10}}{dt} + \frac{d\Delta r_1}{dt} = P - (r_{10} + \Delta r_1) \frac{1}{T_1} \left( 1 + \frac{(E_0 + \Delta E)^2}{I_{sat}} \right) \quad (3.31)$$

Once again following the method for deriving (3.28), we get:

$$\frac{d\Delta r_1}{dt} = -\frac{1}{T_1} \left( \Delta r_1 + \frac{2E_0 \Delta E r_{10} + E_0^2 \Delta r_1}{I_{sat}} \right) \quad (3.32)$$

Equations (3.28), (3.30), and (3.32) describe a set of linearized equations that are approximately equivalent to equations (3.11), (3.12), and (3.14) to the 1<sup>st</sup> order. Given these equations, and the assumption of a harmonic driving force, we shall derive an expression for the MTR, correct to the first order. Thus, if a harmonically modulated signal is injected into a free-running oscillator, the perturbation on its electric field can be given as:

$$\Delta E_1 = A e^{j\Omega t} \quad (3.33)$$

where  $A$  and  $\Omega$  are the magnitude and frequency of this perturbation, respectively. From this, it can be assumed that resulting perturbation on  $E$ ,  $\phi$ , and  $r_l$  is of the form:

$$\Delta E = B e^{j\Omega t} \quad (3.34)$$

$$\Delta\phi = Ce^{j\Omega t} \quad (3.35)$$

$$\Delta r_1 = De^{j\Omega t} \quad (3.36)$$

where  $B$ ,  $C$ , and  $D$  are the magnitudes of the 1<sup>st</sup> order component of the perturbation on  $E$ ,  $\phi$ , and  $r_1$  respectively. Note that the MTR is simply  $(B/A)*(E_1/E)$ .

Substituting the results from (3.34-3.36) into (3.28), (3.30), and (3.32) results in the following three equations:

$$j\Omega D = -\frac{1}{T_1} \left( D + \frac{2E_0 B r_{10} + E_0^2 D}{I_{sat}} \right) \quad (3.37)$$

$$j\Omega C - \frac{\alpha_\phi}{2\tau_c} \frac{D}{B} = \frac{\gamma_e}{E_0} \left[ CE_{10} \cos \phi_0 + A \sin \phi_0 - B \frac{E_{10}}{E_0} \sin \phi_0 \right] \quad (3.38)$$

$$j\Omega B - B \frac{E_0 \frac{D}{B} + r_{10} - 1}{2\tau_c} = \gamma_e (-CE_{10} \sin \phi_0 + A \cos \phi_0) \quad (3.39)$$

### 3.2.1.1.1 Solving for 1<sup>st</sup> Order Perturbation on $r$

If we solve for  $D$  using (3.37), we get:

$$D = -\frac{2E_0 B r_{10}}{T_1 I_{sat} \left( j\Omega + \frac{1}{T_1} + \frac{E_0^2}{T_1 I_{sat}} \right)} \quad (3.40)$$

This equation can then be rewritten as:

$$\frac{D}{B} = -\frac{2r_{10} E_0}{T_1 I_{sat} \left( j\Omega + \frac{1}{T_1} + \frac{E_0^2}{T_1 I_{sat}} \right)} \quad (3.41)$$

### 3.2.1.1.2 Solving for 1<sup>st</sup> Order Modulation Transfer Ratio of Locked Oscillator

If we solve for  $C$  using equation (3.38), we get:

$$C = \frac{A \sin \phi_0 - B \frac{E_{10}}{E_0} \sin \phi_0 + \frac{\alpha_\phi E_0}{2\tau_c \gamma_e} \frac{D}{B} B}{j \frac{E_0}{\gamma_e} \Omega - E_{10} \cos \phi_0} \quad (3.42)$$

Additionally, solving (3.39) for  $C$  results in:

$$C = \frac{A \gamma_e \cos \phi_0 + \left( \frac{E_0 \frac{D}{B} + r_{10} - 1}{2\tau_c} - j\Omega \right) B}{\gamma_e E_{10} \sin \phi_0} \quad (3.43)$$

Equating (3.42) and (3.43) gives us:

$$\frac{A \sin \phi_0 - B \frac{E_{10}}{E_0} \sin \phi_0 + \frac{\alpha_\phi E_0}{2\tau_c \gamma_e} \frac{D}{B} B}{j \frac{E_0}{\gamma_e} \Omega - E_{10} \cos \phi_0} = \frac{A \gamma_e \cos \phi_0 + \left( \frac{E_0 \frac{D}{B} + r_{10} - 1}{2\tau_c} - j\Omega \right) B}{\gamma_e E_{10} \sin \phi_0} \quad (3.44)$$

Rearranging this equation results in:

$$B = \frac{\frac{\gamma_e \cos \phi_0}{\gamma_e E_{10} \sin \phi_0} - \frac{\sin \phi_0}{j \frac{E_0}{\gamma_e} \Omega - E_{10} \cos \phi_0}}{\frac{\alpha_\phi E_0}{2\tau_c \gamma_e} \frac{D}{B} - \frac{E_{10}}{E_0} \sin \phi_0 - \frac{E_0 \frac{D}{B} + r_{10} - 1}{2\tau_c} - j\Omega} A \quad (3.45)$$

$$\frac{\gamma_e \cos \phi_0}{\gamma_e E_{10} \sin \phi_0} - \frac{\sin \phi_0}{j \frac{E_0}{\gamma_e} \Omega - E_{10} \cos \phi_0} = \frac{\frac{\alpha_\phi E_0}{2\tau_c \gamma_e} \frac{D}{B} - \frac{E_{10}}{E_0} \sin \phi_0 - \frac{E_0 \frac{D}{B} + r_{10} - 1}{2\tau_c} - j\Omega}{\frac{j \frac{E_0}{\gamma_e} \Omega - E_{10} \cos \phi_0}{\gamma_e E_{10} \sin \phi_0}}$$

which can be further rearranged to:

$$B = \frac{jE_0\Omega \cos \phi_0 - \gamma_e E_{10}}{\frac{E_0}{2\tau_c} \frac{D}{B} E_{10} \cos \phi_0 + \frac{E_0}{2\tau_c} \frac{D}{B} E_{10} \alpha_\phi \sin \phi_0 - \frac{E_{10}^2}{E_0} \gamma_e \sin^2 \phi_0 + \frac{r_{10}-1}{2\tau_c} E_{10} \cos \phi_0} A \quad (3.46)$$

$$- \Omega^2 \frac{E_0}{\gamma_e} - j\Omega \left( \frac{r_{10}-1}{2\tau_c \gamma_e} E_0 + \frac{E_0^2}{2\tau_c \gamma_e} \frac{D}{B} + E_{10} \cos \phi_0 \right)$$

Then, if we make the substitution in (3.41), we get:

$$B = \frac{jE_0\Omega \cos \phi_0 - \gamma_e E_{10}}{-\frac{E_0 E_{10}}{\tau_c} \frac{r_{10} E_0}{T_1 I_{sat}} \left( \cos \phi_0 + \alpha_\phi \sin \phi_0 \right)} A$$

$$- \frac{E_{10}^2}{E_0} \gamma_e \sin^2 \phi_0 + \frac{r_{10}-1}{2\tau_c} E_{10} \cos \phi_0$$

$$- \Omega^2 \frac{E_0}{\gamma_e} - j\Omega \left( \frac{r_{10}-1}{\tau_c \gamma_e} E_0 - \frac{r_{10} E_0}{T_1 I_{sat}} \frac{E_0^2}{2\tau_c \gamma_e} + E_{10} \cos \phi_0 \right) \quad (3.47)$$

which can be further simplified with the steady-state solution of (3.10):

$$B = \frac{1 - j \frac{\Omega}{\gamma_e} \sqrt{\frac{P_0}{P_1}} \cos \phi_0}{\frac{r_{10}}{\tau_c \gamma_e} \frac{P_0}{(j\Omega T_1 I_{sat} + I_{sat} + P_0)} (\cos \phi_0 + \alpha_\phi \sin \phi_0) + \sqrt{\frac{P_1}{P_0}}}$$

$$+ \left( \frac{\Omega}{\gamma_e} \right)^2 \sqrt{\frac{P_0}{P_1}} + \frac{j\Omega}{\gamma_e} \sqrt{\frac{P_0}{P_1}} \left( \frac{r_{10}-1}{2\tau_c \gamma_e} - \frac{r_{10} P_0}{\tau_c \gamma_e (j\Omega T_1 I_{sat} + I_{sat} + P_0)} + \cos \phi_0 \right)$$

From this, the 1<sup>st</sup> order MTR can be stated as:

$$MTR = \frac{B}{A} \times \frac{E_1}{E} = \frac{1 - j \frac{\Omega}{\gamma_e} \sqrt{\frac{P_0}{P_1}} \cos \phi_0}{1 + \frac{r_{10}}{\tau_c \gamma_e} \frac{P_0}{(j\Omega T_1 I_{sat} + I_{sat} + P_0)} \sqrt{\frac{P_0}{P_1}} (\cos \phi_0 + \alpha_\phi \sin \phi_0) + \left( \frac{\Omega}{\gamma_e} \right)^2 \frac{P_0}{P_1} + \frac{j\Omega}{\gamma_e} \frac{P_0}{P_1} \left( \frac{r_{10} - 1}{2\tau_c \gamma_e} - \frac{r_{10} P_0}{\tau_c \gamma_e (j\Omega T_1 I_{sat} + I_{sat} + P_0)} + \cos \phi_0 \right)} \quad (3.48)$$

If it can be assumed that  $\gamma_e \gg \Omega$  (typically  $\gamma_e \sim 10^{11}$ ) and that the modulation frequency is sufficiently low so that  $T_1 \Omega \ll 1$  (typically true for modulation frequencies below 10MHz), (3.48) can be simplified:

$$MTR = \frac{1}{1 + \frac{r_{10}}{\tau_c \gamma_e} \left( \frac{P_0}{I_{sat} + P_0} \right) \sqrt{\frac{P_0}{P_1}} (\cos \phi_0 + \alpha_\phi \sin \phi_0)} \quad (3.49)$$

which can be further simplified with (3.15):

$$MTR = \frac{1}{1 + \frac{r_{10}}{\tau_c \gamma_e} \left( \frac{P_0}{I_{sat} + P_0} \right) \sqrt{\frac{P_0}{P_1}} \sqrt{\left(1 + \alpha_\phi^2\right) - \left(\frac{\Delta\omega}{\gamma_e}\right)^2} - \left(\frac{\Delta\omega}{\gamma_e}\right)^2 \frac{P_0}{P_1}} \quad (3.50)$$

Also, for the case of a DFB semiconductor laser, it was experimentally found that the value of  $\alpha_\phi \approx 0$ . As such, the MTR for the DFB semiconductor laser can be further simplified to:

$$MTR_{DFB} = \frac{1}{1 + \frac{r_{10}}{\tau_c \gamma_e} \left( \frac{P_0}{I_{sat} + P_0} \right) \sqrt{\frac{P_0}{P_1}} \sqrt{1 - \left(\frac{\Delta\omega}{\gamma_e}\right)^2} - \left(\frac{\Delta\omega}{\gamma_e}\right)^2 \frac{P_0}{P_1}} \quad (3.51)$$

### 3.2.1.1.3 Numerical Modeling

Given the equation for MTR, we numerically simulate the behavior of this system and present the results graphically. For this, we assume typical constraining values.

Specifically, we assume that the effective saturation intensity of the slave laser is 0dBm, the perturbation on the injected intensity is 10%, the unsaturated cavity gain to loss ratio ( $r$  when  $E=0$ ) is 2, the cavity lifetime ( $\tau_c$ ) is 150ps, the carrier lifetime ( $T_1$ ) is 1ns, the photon loss rate ( $\gamma_e$ ) is  $8*10^9 \text{ s}^{-1}$ , the pump rate ( $\rho$ ) is equal to  $2*10^9 \text{ s}^{-1}$ , and the phase factor ( $\alpha_\phi$ ) is equal to 0 (experimentally determined).

Additionally, in order to perform these simulations, values for  $E_0$  and  $r_l$  must be determined from the steady state solutions of (3.10) and (3.14). The steady state solution of (3.14), after some rearrangement, results in:

$$\frac{r_0 - 1}{2\tau_c} E_0 = \frac{-\frac{E_0^3}{I_{sat}} + (\rho T_1 - 1)E_0}{2\tau_c \left(1 + \frac{E_0^2}{I_{sat}}\right)} \quad (3.52)$$

Substituting this into the steady state solution of (3.10) results in:

$$\frac{E_0^3}{I_{sat}} - \frac{2\tau_c \gamma_e E_{10} \cos \phi_0}{I_{sat}} E_0^2 + (1 - \rho T_1)E_0 - 2\tau_c \gamma_e E_{10} \cos \phi_0 = 0 \quad (3.53)$$

From (3.53),  $E_0$  can be solved numerically.  $r_0$  is determined by (3.14) using the numerical value obtained for  $E_0$ :

$$r_0 = \frac{\rho T_1}{1 + \frac{E_0^2}{I_{sat}}} \quad (3.54)$$

Figure 3.03 depicts:

$$MTR(\omega_1 - \omega) = \left( \frac{|B|}{E_0} / \frac{|A|}{E_1} \right)^2 \quad (3.55)$$

over the locking range of the slave laser. This ratio was plotted for various modulation frequencies ( $\Omega$ ). From this figure, a distinctive ‘‘U’’ shape can be seen over the locking

range. Additionally, it should be noted that when this “U” shape was plotted at various modulation frequencies (below 10MHz), all of the curves were found to be graphically indistinguishable from each other. This indicates that, as was predicted by (3.51), the MTR of the slave laser is weakly dependant of the modulation frequency.

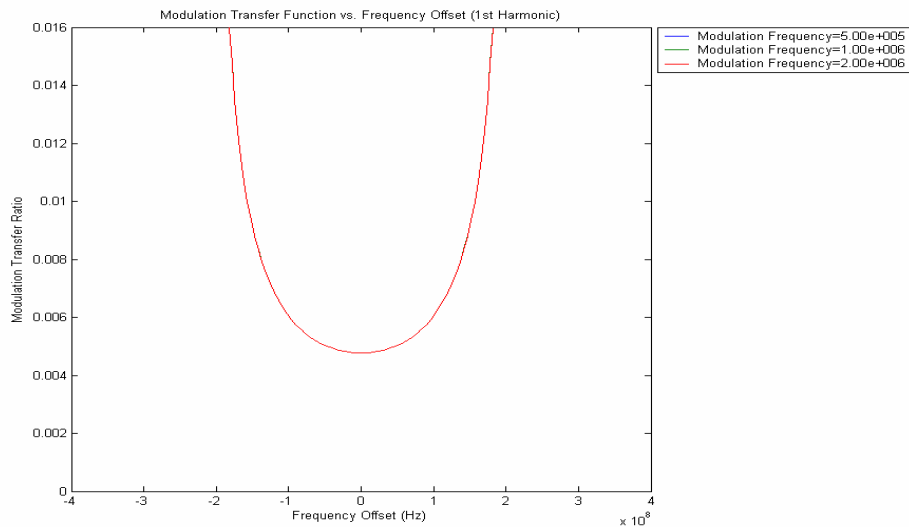


Figure 3.03 – 1<sup>st</sup> Order Modulation Transfer Ratio vs. Frequency Offset (At Various Modulation Frequencies [Hz])

Figure 3.04 depicts this ratio for various injected intensities. As can be seen from this figure, although the minimum of the “U” shape is less than one (indicating a suppression of the modulation of the injected signal) it does not go to zero. Instead, this minimum value is approximately proportional to the intensity of the injected master signal (at low modulation frequencies).

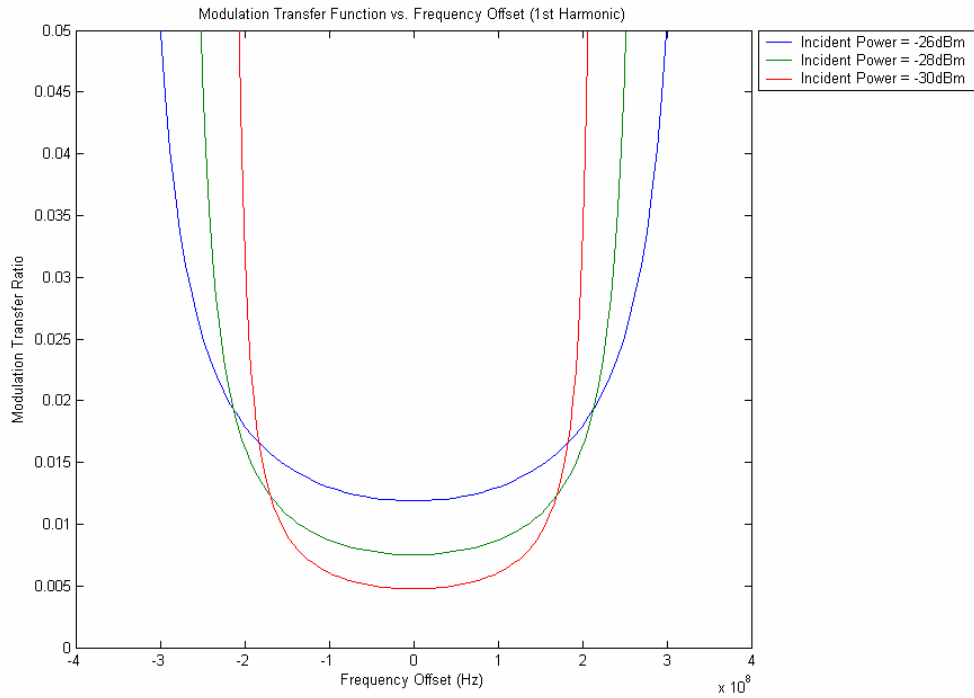


Figure 3.04 – 1<sup>st</sup> Order Modulation Transfer Ratio vs. Frequency Offset (At Various Injected Powers)

#### 3.2.1.1.4 Experimental Verification of the Injection Locking Theory

Figure 3.05 depicts the experimental setup used to monitor the magnitude of modulation on the optical signal that is emitted from the slave laser. In this setup, a CW signal from a tunable laser is externally modulated via a Mach-Zehnder Interferometer, the modulation depth of which is ~7% (chosen to model the modulation suppression due to an optical pre-filter). This provides the signal to which the slave laser will be locked. The DC bias of the external modulator is adjusted so that no detectable higher order harmonics are present on the output (2<sup>nd</sup> harmonic is <50dBm). The signal is directed into the slave laser via a circulator, and the circulator redirects the signal from the slave laser to an optical detector.

The signal generated by the detector is lock-in amplified and referenced to the modulator's drive signal. The lock-in amplifier filter was integrated over 0.3ms by a 24dB/octave low-pass filter. The amplitude of the amplified signal is then recorded by an oscilloscope. In order to detect the change in the magnitude of the modulated signal over the entire locking range, the free running frequency of the slave laser is sinusoidally swept across the locking range at a frequency of 20Hz. This is accomplished by modulating the current source of the slave laser.

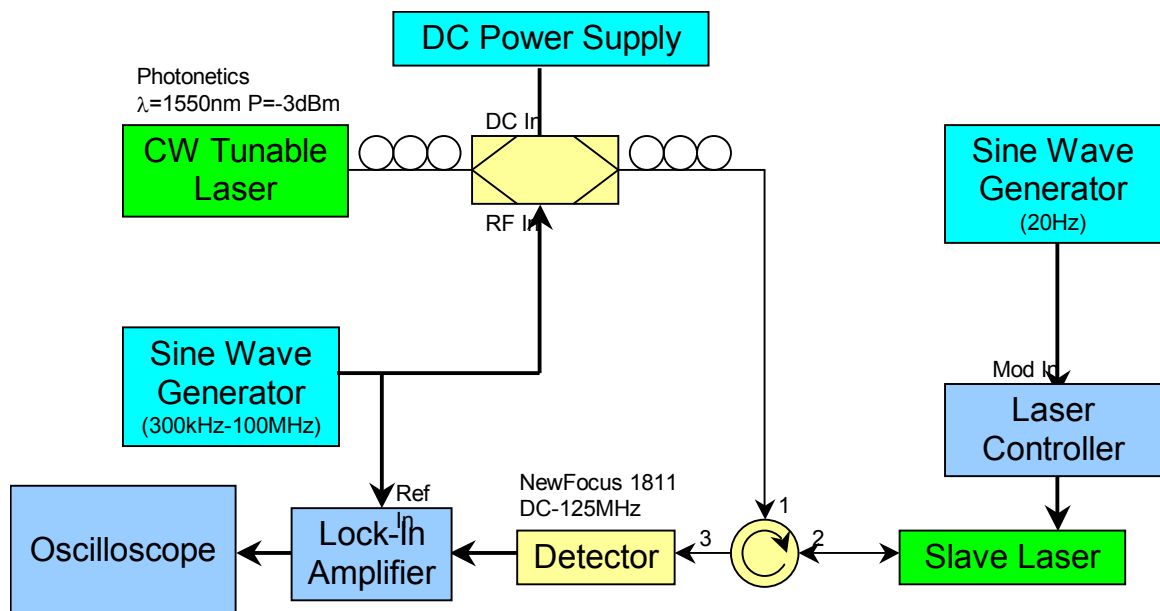


Figure 3.05 – Layout of Injection Locking Experiment

Figures 3.06 and 3.07 depict the change in the magnitude of the modulation out over the locking range, as seen on the oscilloscope following the lock-in amplifier. From this, it can be seen that the lock-in amplifier/oscilloscope combination shows the same behavior as was predicted by the theory. It should be noted that the curvature of the “U” shape remains fairly constant for modulation frequencies below 5MHz.

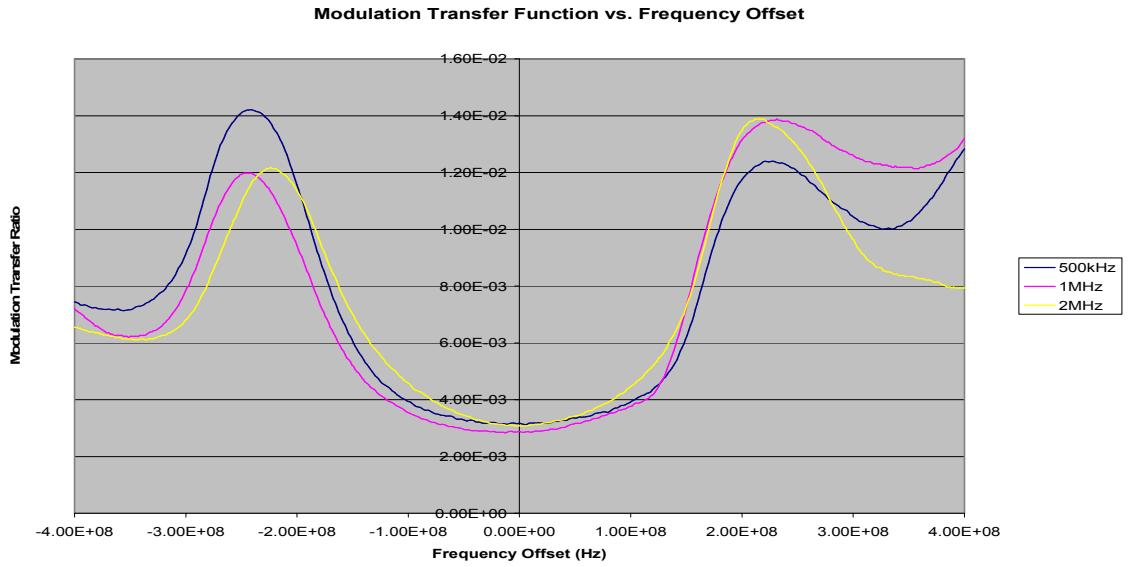


Figure 3.06 – 1<sup>st</sup> Order Modulation Transfer Ratio vs. Frequency Offset (At Various Modulation Frequencies)

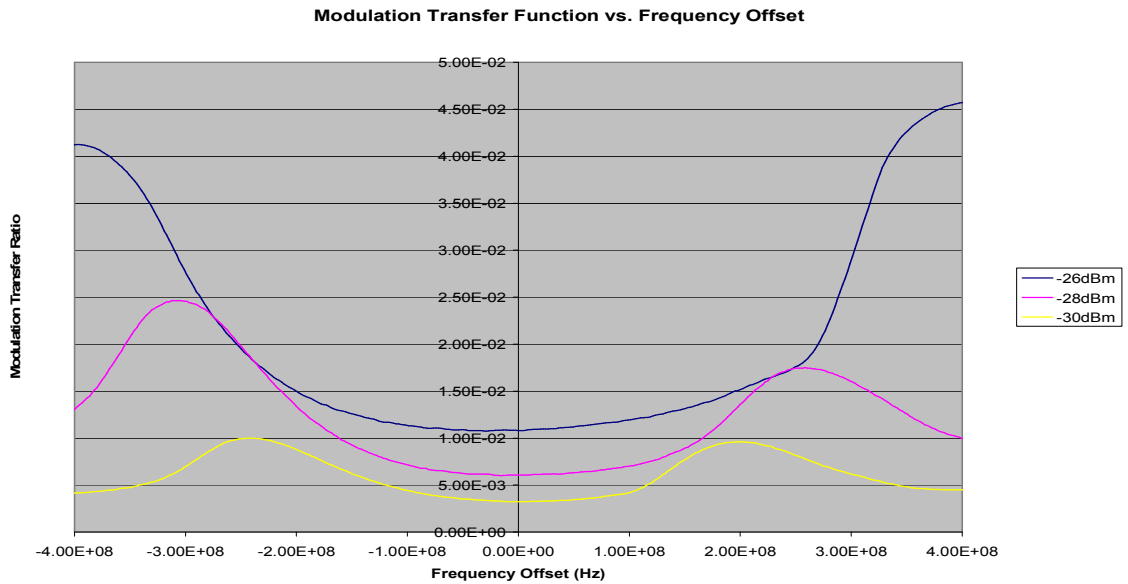


Figure 3.07 – 1<sup>st</sup> Order Modulation Transfer Ratio vs. Frequency Offset (At Various Injected Powers)

### 3.2.2 Varying the Free-Running Frequency of the Slave Laser

Before the MTR's dependence on detuning can be utilized by a feedback loop, a method for adjusting the free-running frequency of the slave laser is required. This frequency adjustment can be done in one of two ways. First, adjusting the temperature of the slave laser will affect the length of the optical cavity, due to thermal expansion. However, since the peltier cooler that is used to control the temperature is coupled to the slave-laser casing, the entire package needs to achieve thermal equilibrium before the free-running frequency of the slave laser can stabilize. Since the package has a huge heat capacity, changing the free-running frequency of the slave laser in this way is a slow process. This effectively limits the frequency at which the free-running frequency of the slave laser can be dithered.

The other way to adjust the free-running frequency of the slave laser is to change its drive current. As the drive current of the slave laser increases, the free electron concentration also increases. Since the index of refraction of a material is dependant on its free electron concentration [25], changing the free electron concentration of the laser medium effectively changes its optical path length, thereby changing the free-running frequency of the of the slave laser. This is a much faster process than varying the temperature, since its speed is only limited by the rate at which carriers can be generated. However, changing the drive current of the slave laser will also change the output power of the slave laser. This may not be desired, since the locking range is proportional to the square root of the ratio of the slave laser intensity to the intensity of the received optical signal. Thus, if the free-running frequency of the slave laser is dithered by modulating the drive current of the slave laser, the amplitude of this modulation must be kept small

enough to ensure that the change in the output power of the slave laser is much smaller than this output power.

### 3.2.3 Creating the Feedback Control System for the Injection Lock

As shown in Sections 3.2.1.1.3 and 3.2.1.1.4, the modulation transfer ratio of a laser that is locked to a modulated optical signal is essentially “U” shaped. If the free-running frequency of the slave laser is then dithered by modulating its drive current, then similar to the filter feedback loop presented in 2.2, the amplitude of the modulation on the output from the slave laser at the dither frequency will be proportional to the derivative of the “U” shape (depicted in Figure 3.08).

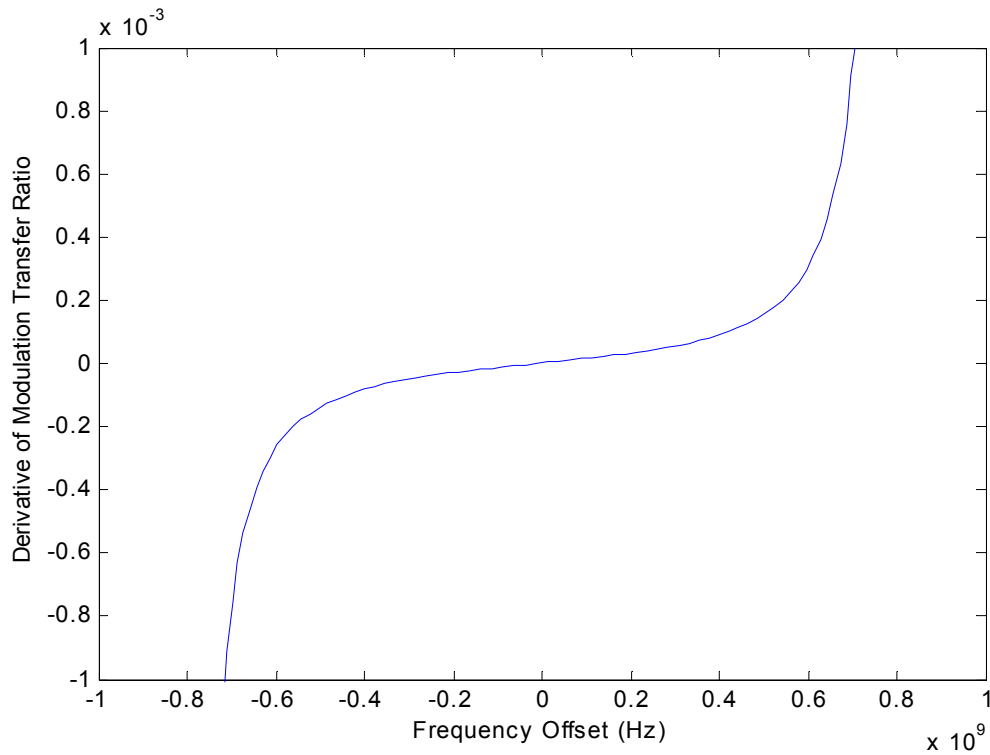


Figure 3.08 - Derivative of “U”-shape

### 3.2.3.1 Analog feedback control

The simplest feedback control loop is an analog control loop, depicted in Figure 3.09. For this, the received optical signal is modulated (with a modulation depth of  $M$ , typically  $\sim 0.1$ ), and injected into the slave laser. If we allow the modulation transfer ratio of the slave laser to be defined by  $F(\nu)$  (where  $\nu(t)$  is the total detuning at a given time  $t$ ), then the modulation intensity on the output of the slave laser will be  $P_{out}MF(\nu)$ , where  $P_{out}$  is the output of the slave laser (typically  $\sim 1\text{mW}$ ). This signal is then detected (the product of the detector sensitivity and any associated transimpedance gain,  $D$ , is  $\sim 2 \cdot 10^4$  V/W) and diverted to lock-in amplifier #1. The output of lock-in amplifier #1 is the magnitude of the modulation on the input signal, multiplied by a constant gain  $g_1$  (typically 30-40dB). As such, the output of lock-in amplifier #1, denoted as  $y(t)$  can be expressed as:

$$y(t) = g_1 \cdot P_{out} \cdot M \cdot D \cdot F(\nu) \quad (3.56)$$

The output of lock-in amplifier #1 is diverted to lock-in amplifier #2, whose output (denoted as  $x(t)$ ) can be expressed as:

$$x(t) = g_2 \int_{-\infty}^t e^{-\frac{(t-\tau)}{T}} y(\tau) \sin(\Omega_d(\tau - \tau_{lo})) d\tau \quad (3.57)$$

where  $g_2$  is the gain of lock-in amplifier #2 (typically 40-60dB),  $T_i$  is the integration time of lock-in amplifier #2, and  $\tau_{lo}$  is a delay set by the lock-in amplifier to match the phase of the modulation on the input.

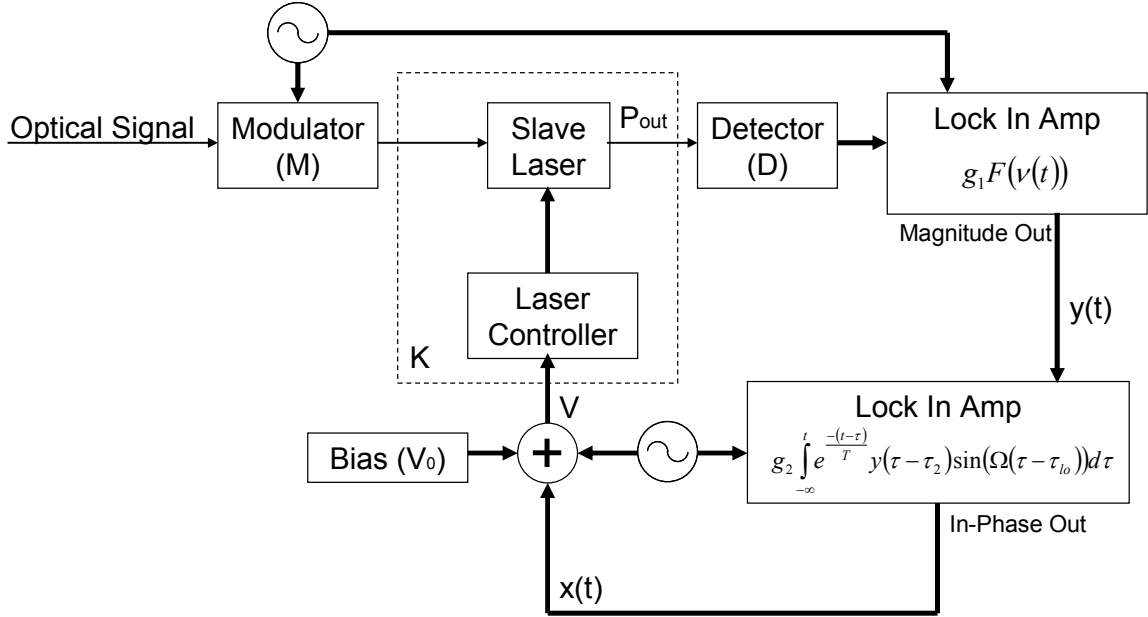


Figure 3.09 – Layout of Analog Feedback Loop

The output of lock-in amplifier #2 is added to both a bias voltage and dither signal, and this combined signal is used to drive the slave laser. For the purposes of modeling this system, the effect of the components within the dashed box in Figure 3.09 are treated as a constant  $K$  [41] (whose value is experimentally found to be  $\sim 10^9$  Hz/V).

As such,  $\nu(t)$  can be defined as:

$$\nu(t) = \nu_0(t) + a \sin(\Omega_d t) - Kx(t - \tau_0) \quad (3.58)$$

where  $\nu_0$  is the detuning due to the drift of the laser,  $a$  is the detuning due to the dither, and  $\tau_0$  is the loop delay. Combining (3.56) and (3.58) results in:

$$\begin{aligned} \nu(t) - \nu_0(t) - a \sin(\Omega_d t) &= -Kx(t - \tau_3) \\ &= -K \cdot g_2 \int_{-\infty}^{t-\tau_3} e^{-\frac{-(t-\tau-\tau_3)}{T}} y(\tau - \tau_2) \sin(\Omega_d (\tau - \tau_{lo})) d\tau \end{aligned} \quad (3.59)$$

If we then combine (3.57) and (3.59), assume  $\nu_0(t) \gg a$ , and define  $g = g_1 g_2$  (overall gain due to lock-in amplifiers), we get:

$$v(t) - v_0(t) = -K \cdot g \int_{-\infty}^{t-\tau_0} e^{\frac{-(t-\tau-\tau_0)}{T}} P_{out} \cdot M \cdot D \cdot F(v(\tau)) \sin(\Omega_d(\tau - \tau_{lo})) d\tau \quad (3.60)$$

If we assume that  $v_0$  and  $x$  vary slow compared to the dither period and  $\tau_{lo}$  is set equal to zero:

$$v(t) - v_0(t) = -\frac{P_{out} \cdot M \cdot D \cdot K \cdot g \cdot a}{2} \int_{-\infty}^{t-\tau_0} e^{\frac{-(t-\tau-\tau_0)}{T}} F'(v(\tau)) d\tau \quad (3.61)$$

For a small  $\Delta t$ , and assuming that  $v_0(t)$  is nearly constant over a time  $T_l$  ( $T_l \gg \tau_0 \gg \Delta t$ ):

$$\begin{aligned} \frac{dv}{dt} - \frac{dv_0}{dt} &= \frac{(v(t) - v_0(t)) - (v(t - \Delta t) - v_0(t - \Delta t))}{\Delta t} \\ &= -\frac{P_{out} \cdot M \cdot D \cdot K \cdot g \cdot a}{2\Delta t} \int_{-\infty}^{t-\tau_0} e^{\frac{-(t-\tau-\tau_0)}{T}} F'(v(\tau)) d\tau \\ &\quad + \frac{P_{out} \cdot M \cdot D \cdot K \cdot g \cdot a}{2\Delta t} \int_{-\infty}^{t-\tau_0-\Delta t} e^{\frac{-(t-\Delta t-\tau-\tau_0)}{T}} F'(v(\tau)) d\tau \end{aligned} \quad (3.62)$$

$$\begin{aligned} \frac{dv}{dt} - \frac{dv_0}{dt} &= -\frac{P_{out} \cdot M \cdot D \cdot K \cdot g \cdot a}{2\Delta t} \int_{-\infty}^{t-\tau_0} e^{\frac{-(t-\tau-\tau_0)}{T}} F'(v(\tau)) d\tau \\ &\quad + \frac{P_{out} \cdot M \cdot D \cdot K \cdot g \cdot a}{2\Delta t} e^{\frac{\Delta t}{T}} \int_{-\infty}^{t-\tau_0-\Delta t} e^{\frac{-(t-\tau-\tau_0)}{T}} F'(v(\tau)) d\tau \end{aligned} \quad (3.63)$$

$$\begin{aligned} \frac{dv}{dt} - \frac{dv_0}{dt} &= -\frac{P_{out} \cdot M \cdot D \cdot K \cdot g \cdot a}{2\Delta t} \int_{-\infty}^{t-\tau_0} e^{\frac{-(t-\tau-\tau_0)}{T}} F'(v(\tau)) d\tau \\ &\quad + \frac{P_{out} \cdot M \cdot D \cdot K \cdot g \cdot a}{2\Delta t} e^{\frac{\Delta t}{T}} \int_{-\infty}^{t-\tau_0} e^{\frac{-(t-\tau-\tau_0)}{T}} F'(v(\tau)) d\tau \\ &\quad - \frac{P_{out} \cdot M \cdot D \cdot K \cdot g \cdot a}{2\Delta t} e^{\frac{\Delta t}{T}} \int_{t-\tau_3-\Delta t}^{t-\tau_0} e^{\frac{-(t-\tau-\tau_0)}{T}} F'(v(\tau)) d\tau \end{aligned} \quad (3.64)$$

$$\begin{aligned} \frac{dv}{dt} - \frac{dv_0}{dt} &= -\frac{P_{out} \cdot M \cdot D \cdot K \cdot g \cdot a}{2\Delta t} \left( 1 - e^{\frac{\Delta t}{T}} \right) \int_{-\infty}^{t-\tau_0} e^{\frac{-(t-\tau-\tau_0)}{T}} F'(v(\tau)) d\tau \\ &\quad - \frac{P_{out} \cdot M \cdot D \cdot K \cdot g \cdot a}{2\Delta t} e^{\frac{\Delta t}{T}} \left( \int_{t-\tau_3-\Delta t}^{t-\tau_0} e^{\frac{-(t-\tau-\tau_0)}{T}} F'(v(\tau)) d\tau \right) \end{aligned} \quad (3.65)$$

$$\begin{aligned} \frac{dv}{dt} - \frac{dv_0}{dt} &= -\frac{1}{\Delta t} \left(1 - e^{-\frac{\Delta t}{T}}\right) \frac{P_{out} \cdot M \cdot D \cdot K \cdot g \cdot a}{2} \int_{-\infty}^{t-\tau_0} e^{-\frac{(t-\tau-\tau_0)}{T}} F'(v(\tau)) d\tau \\ &\quad - \frac{P_{out} \cdot M \cdot D \cdot K \cdot g \cdot a}{2} e^{-\frac{\Delta t}{T}} F'(v(t-\tau_0)) \end{aligned} \quad (3.66)$$

Substituting with (3.61):

$$\begin{aligned} \frac{dv}{dt} - \frac{dv_0}{dt} \\ = \frac{1}{\Delta t} \left(1 - e^{-\frac{\Delta t}{T}}\right) \cdot (v(t) - v_0(t)) - \frac{P_{out} \cdot M \cdot D \cdot K \cdot g \cdot a}{2} e^{-\frac{\Delta t}{T}} F'(v(t-\tau_0)) \end{aligned} \quad (3.67)$$

Expanding the exponentials to the 1<sup>st</sup> order:

$$\begin{aligned} \frac{dv}{dt} - \frac{dv_0}{dt} &= \frac{1}{\Delta t} \left(1 - \left(1 + \frac{\Delta t}{T}\right)\right) \cdot (v(t) - v_0(t)) \\ &\quad - \frac{P_{out} \cdot M \cdot D \cdot K \cdot g \cdot a}{2} \left(1 + \frac{\Delta t}{T}\right) F'(v(t-\tau_0)) \end{aligned} \quad (3.68)$$

Let  $G = P_{out}MDKga/2$ :

$$\frac{dv}{dt} - \frac{dv_0}{dt} + \frac{1}{T}(v(t) - v_0(t)) = -G \left(1 + \frac{\Delta t}{T}\right) (F'(v(t-\tau_0))) \quad (3.69)$$

If  $\tau_0$  is small, then:

$$\begin{aligned} \frac{d^2v}{dt^2} - \frac{d^2v_0}{dt^2} + \frac{1}{T} \left( \frac{dv}{dt} - \frac{dv_0}{dt} \right) &= \\ -\frac{1}{\tau_0} \left( G \left(1 + \frac{\Delta t}{T}\right) (F'(v(t))) - G \left(1 + \frac{\Delta t}{T}\right) (F'(v(t-\tau_0))) \right) \end{aligned} \quad (3.70)$$

Combining (3.69) and (3.70):

$$\begin{aligned} \frac{d^2v}{dt^2} - \frac{d^2v_0}{dt^2} + \left( \frac{1}{T} + \frac{1}{\tau_0} \right) \left( \frac{dv}{dt} - \frac{dv_0}{dt} \right) + \frac{1}{\tau_0 T} (v(t) - v_0(t)) &= \\ -\frac{1}{\tau_0} \left( G \left(1 + \frac{\Delta t}{T}\right) (F'(v(t))) \right) \end{aligned} \quad (3.71)$$

As  $\Delta t \rightarrow 0$ , and assuming  $T \gg \tau_0$ :

$$\tau_0 \left( \frac{d^2 v}{dt^2} - \frac{d^2 v_0}{dt^2} \right) + \left( \frac{dv}{dt} - \frac{dv_0}{dt} \right) + \frac{1}{T} (v(t) - v_0(t)) = -G \cdot F'(v(t)) \quad (3.72)$$

### 3.2.3.1.1 Modeling the Analog Feedback Loop

To model the behavior of the analog feedback loop we must first observe that equation (3.51) may be approximated by the inverse of a second order polynomial, i.e.:

$$F(v) \approx \frac{1}{Av^2 + Bv + C} \quad (3.73)$$

Thus, (3.72) can be expressed as:

$$\frac{d^2 v}{dt^2} - \frac{d^2 v_0}{dt^2} + \frac{1}{\tau_0} \left( \frac{dv}{dt} - \frac{dv_0}{dt} \right) + \frac{v - v_0}{T\tau_0} = \frac{G}{\tau_0} \left( \frac{2Av + B}{(Av^2 + Bv + C)^2} \right) \quad (3.74)$$

If we then define z(t), such that:

$$z = \frac{dv}{dt} \quad (3.75)$$

(3.74) can be expressed by a set of two first order equations:

$$\frac{dz}{dt} = - \left( \frac{z}{\tau_0} + \frac{v}{T\tau_0} \right) + \left( \frac{d^2 v_0}{dt^2} + \frac{1}{\tau_0} \frac{dv_0}{dt} + \frac{v_0}{T\tau_0} \right) + \frac{G}{\tau_0} \left( \frac{2Av + B}{(Av^2 + Bv + C)^2} \right) \quad (3.76)$$

$$\frac{dv}{dt} = z \quad (3.77)$$

This set of equations can be solved in MatLab, given an assumed function for  $v_0$ .

To test the effectiveness of the analog feedback system, we first assume that the free-running frequency of the slave laser is drifting at a constant rate (i.e.  $d^2 v_0/dt^2=0$ ,  $dv_0/dt=\text{constant}$ ). Given this, we can determine the detuning of the injection lock over time. The detuning over time of the slave laser is depicted in Figure 3.10, given various

drift rates and for  $g=70\text{dB}$  and  $g=100\text{dB}$  (the typical range for  $g$ ). From these plots, it can be seen that the analog feedback loop can only maintain the detuning to within 10MHz given drift rates of less than 40MHz/ms. As such, analog feedback is only appropriate for systems that are very stable. However, if drift rates  $>40\text{MHz/ms}$  are expected, either due to thermal instability in the slave laser or electrical glitches in the laser controller, an improved feedback control system is required.

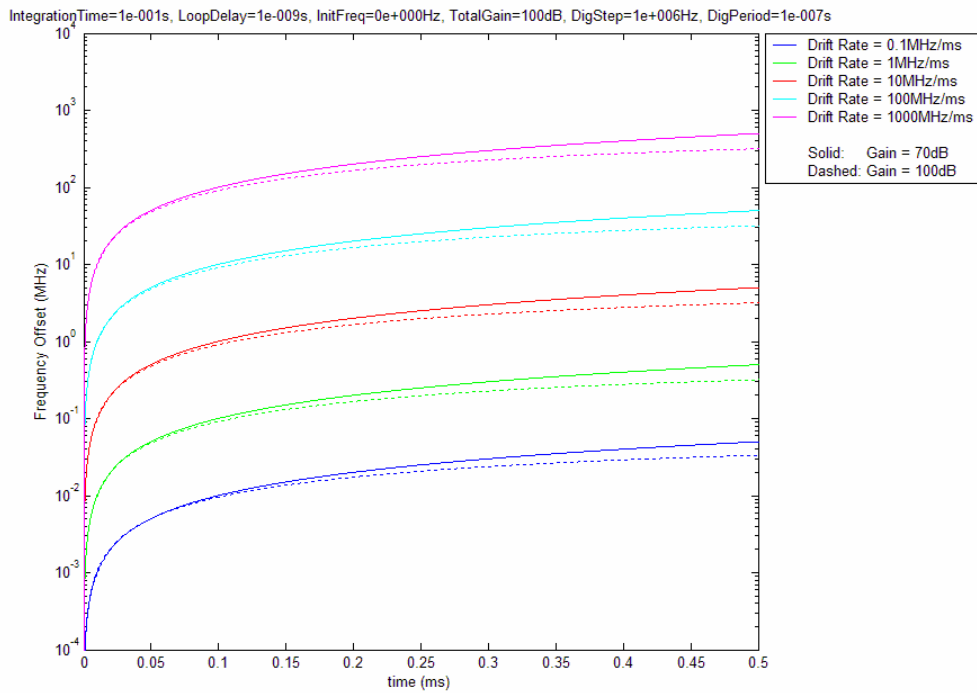


Figure 3.10 – Simulated Performance of Analog Feedback

### 3.2.3.2 Digital feedback control

To improve the analog feedback system, we implement a digital feedback system, as depicted in Figure 3.11. This feedback system is similar to the analog feedback system, except that the output of lock-in amplifier #2 is used by a digital control circuit to set the digital bias to the slave laser. This digital control circuit consists of a threshold

circuit, which controls a counter circuit. The output of the counter circuit is used by a D/A converter, whose output is used to bias the slave laser.

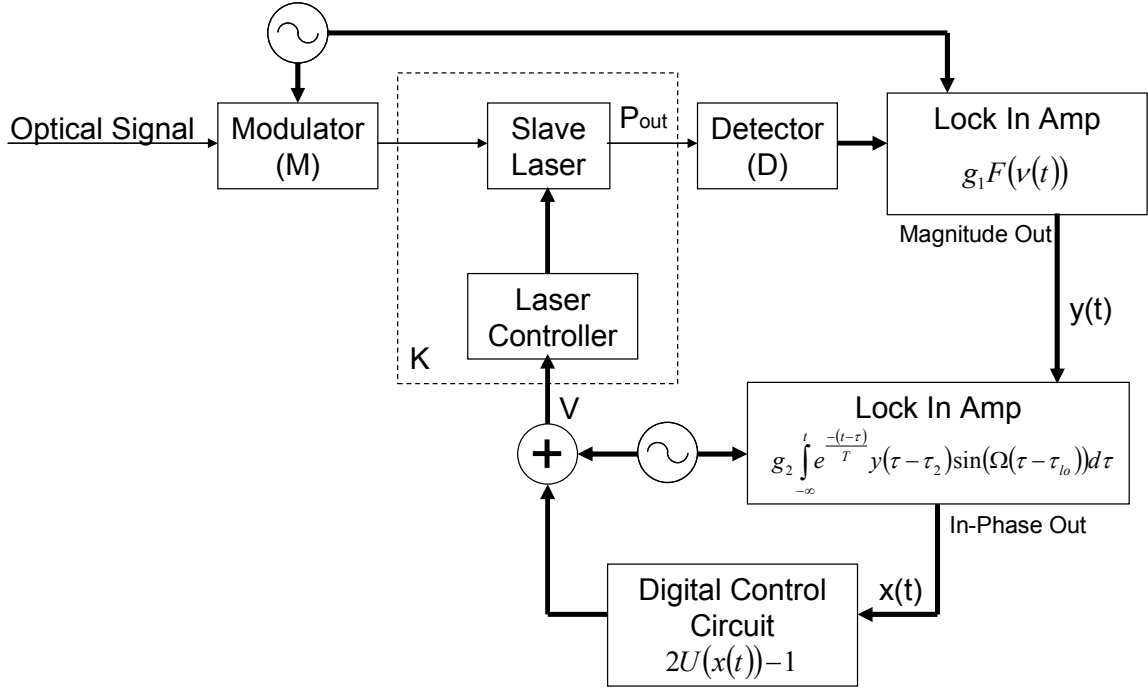


Figure 3.11 – Layout of Digital Feedback Loop

With the addition of the digital control circuit, detuning over time can be expressed as (assuming small  $a$ ):

$$v(t + \Delta t_s) - v_0(t + \Delta t_s) = v(t) - v_0(t) - \Delta v_s (2U(x(t - \tau_0)) - 1) \quad (3.78)$$

where  $\Delta t_s$  is the clock period of the digital circuit (typically 100ns),  $\Delta v_s$  is the step size of the digital offset applied by the circuit (typically 1MHz), and  $U(x)$  is a step function that returns 0 if  $x \leq 0$  and 1 if  $x > 0$ . From (6), this becomes:

$$v(t + \Delta t_s) - v_0(t + \Delta t_s) = v(t) - v_0(t) - \Delta v_s \left( 2U \left( G \int_{-\infty}^t e^{-\frac{(t-\tau)}{T}} F'(v(\tau - \tau_0)) d\tau \right) - 1 \right) \quad (3.79)$$

The output of the digital circuit is constant over a range of  $m\Delta t_s < t < (m+1)\Delta t_s$ , such that 'm' is an integer. If we then let  $t=n\Delta t_s$ , then (3.79) can be expressed as:

$$\begin{aligned} & \nu(t + \Delta t_s) - \nu_0(t + \Delta t_s) \approx \\ & \nu(t) - \nu_0(t) - \Delta \nu_s \left( 2U \left( G \cdot \sum_{k=-\infty}^n \int_{\Delta t_s(k-1)}^{\Delta t_s k} e^{-\frac{(n\Delta t_s - \tau)}{T}} F'(\nu(\tau - \tau_0)) d\tau \right) - 1 \right) \end{aligned} \quad (3.80)$$

If we let  $\Delta t_s \gg \tau_0$  (typically  $T/10 < \Delta t_s < T$  and  $T \gg \tau_0$ ), we can express this as a discrete function:

$$\nu[n+1] \approx \nu[n] + (\nu_0[n+1] - \nu_0[n]) - \Delta \nu_s \left( 2U \left( G \cdot \sum_{k=-\infty}^n \int_{\Delta t_s(k-1)}^{\Delta t_s k} e^{-\frac{(n\Delta t_s - \tau)}{T}} F'(\nu[k]) d\tau \right) - 1 \right) \quad (3.81)$$

$$\begin{aligned} & \nu[n+1] \approx \\ & \nu[n] + (\nu_0[n+1] - \nu_0[n]) - \Delta \nu_s \left( 2U \left( G \cdot T \left( 1 - e^{-\frac{\Delta t_s}{T}} \right) \cdot \sum_{k=-\infty}^n F'(\nu[k]) e^{\frac{\Delta t_s(k-n)}{T}} \right) - 1 \right) \end{aligned} \quad (3.82)$$

Since  $U(x)$  is a step function, (3.82) can be simplified to:

$$\nu[n+1] \approx \nu[n] + (\nu_0[n+1] - \nu_0[n]) - \Delta \nu_s \left( 2U \left( \sum_{k=-\infty}^n F'(\nu[k]) e^{\frac{\Delta t_s(k-n)}{T}} \right) - 1 \right) \quad (3.83)$$

If  $\Delta t_s$  is small, or if the frequency drift is linear (i.e.  $d\nu_0/dt$  is constant), (3.83) can also be expressed as:

$$\nu[n+1] \approx \nu[n] + \Delta t_s \frac{d\nu_0}{dt} - \Delta \nu_s \left( 2U \left( \sum_{k=-\infty}^n F'(\nu[k]) e^{\frac{\Delta t_s(k-n)}{T}} \right) - 1 \right) \quad (3.84)$$

To test the effectiveness of the digital feedback system, we first assume that the free-running frequency of the slave laser is drifting at a constant rate (i.e.  $d^2\nu_0/dt^2=0$ ,  $d\nu_0/dt=\text{constant}$ ). Given this, we can determine the detuning of the injection lock over time. The detuning over time of the slave laser is depicted in Figure 3.12 for both the

analog and digital feedback loops. The analog feedback loops were tested for drift rates ranging from 0.1MHz/ms to 1GHz/ms. The digital feedback loop was tested at 1GHz/ms, since the digital feedback loop is equally effective for all drift rates that do not exceed  $\Delta v_d/\Delta t_d$ . From this figure, it is apparent that the digital feedback system is capable of maintaining the detuning to within the digital step size (i.e. 1MHz).

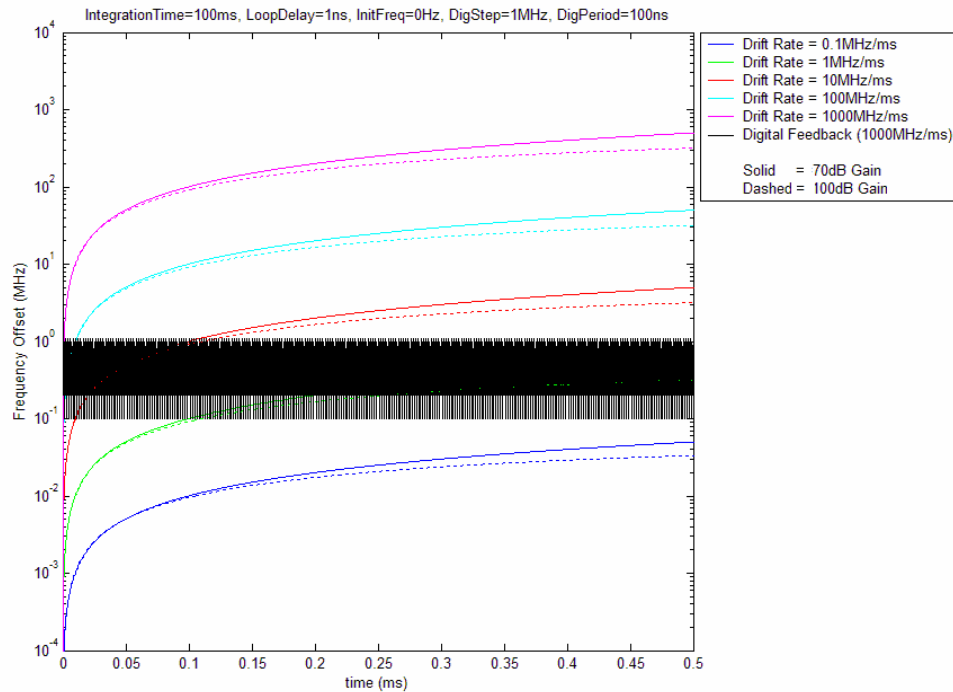


Figure 3.12 – Comparison of Performance for Analog and Digital Feedback

The advantage of the digital feedback loop is its ability to track large drift rates. In addition, the effectiveness of the digital feedback loop is independent on the overall gain of the feedback loop (due to lock-in amplifier gains and other amplifiers). However, this benefit comes at the cost of time added complexity to the feedback system (although the overall design is simple, and can be assembled with COTS components). Also, the digital feedback loop will always maintain detuning to within the digital step size, with a

mean error of  $\Delta\nu_s/2$ . As such, an analog feedback system may be a more effective solution if large drift rates are not expected. However, the error of the digital feedback system may also be improved by using a variable step size, in which the value of  $\Delta\nu_s$  is automatically decreased as detuning decreases. This improved digital feedback system will be explored in more detail for future projects.

### 3.2.3.3 Implementation of a Digital Feedback Loop

Since we use COTS components for the implementation of this LO generator, it may be susceptible to both thermal instability or electrical glitches. As such, the feedback system explored for this experiment is the digital feedback loop, as depicted in Figure 3.13. Similar to the setup depicted in Figure 3.05, a modulated CW signal (approximately a 5% modulation depth at a frequency of 1MHz) is directed into the slave laser via a circulator. A 50Hz sinusoid is applied to the bias port of the slave laser controller that effectively tunes the free-running frequency of the slave laser over  $\sim 10\%$  of the locking range.

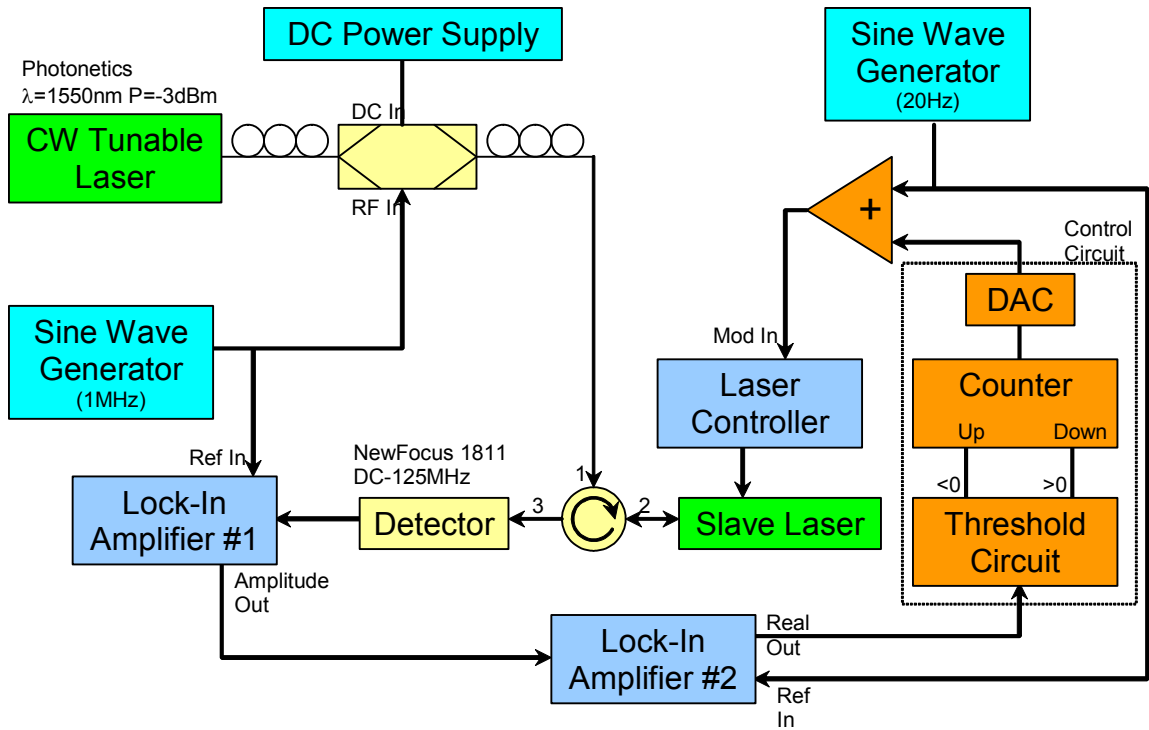


Figure 3.13 –Layout of Automated Injection Lock

A second lock-in amplifier operated as a saturating comparator and a digital level crossing counter are added to implement non-linear feedback. This second lock-in amplifier, whose reference signal is the 50Hz sinusoid that was used to modulate the free-running frequency of the slave laser, integrates the signal over 1.0s across a 6dB/octave band-pass filter, and is set to maximum sensitivity ( $300\text{nV}_{\text{rms}}$ ). Thus, instead of producing the derivative of the “U”-shape, the in-phase output of this lock-in amplifier will be a large, positive (negative) voltage when the difference between the free-running frequency of the slave laser and the frequency of the master laser is positive (negative). This signal is then directed to the control circuit (a similar circuit is depicted in Figure 6.06), which utilizes a binary counter to keep track of the offset that it applies to the laser controller. The counter will be incremented (decremented) if the input from the 2<sup>nd</sup> lock-

in amplifier is greater (less) than zero volts. The output of this counter is then converted to an analog voltage, via a D/A converter. This analog voltage is then added to the bias port of the slave laser controller.

In order to test the stability of the feedback loop, the output from Lock-In Amplifier #1 was monitored over a period of 5 minutes. The output from this lock-in amplifier is a function of frequency difference between the received optical signal and the free-running frequency of the slave laser, and thus is a good indicator of the effectiveness of the feedback loop.

The DFB laser used in this experiment is thermally unstable. As such, it's free-running frequency will randomly drift in and out of the locking range. Thus, the unlocked output of Lock-In Amplifier #1 over the course of 5 minutes will look like what is depicted in Figure 3.14. Figure 3.15 shows this same output, with the feedback loop activated. From this, it can be seen that the feedback loop successfully adjusts the free-running frequency of the slave laser so that it is consistently within the locking range.

### Output of Lock-In Amp #1 Without Feedback

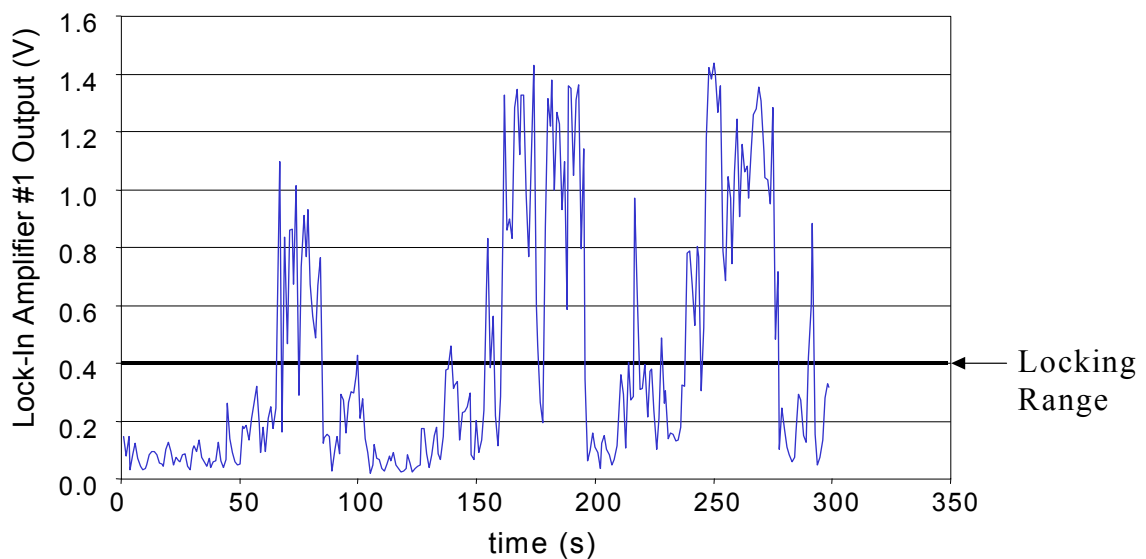


Figure 3.14 – Output of Lock-In Amplifier #1 Without Feedback

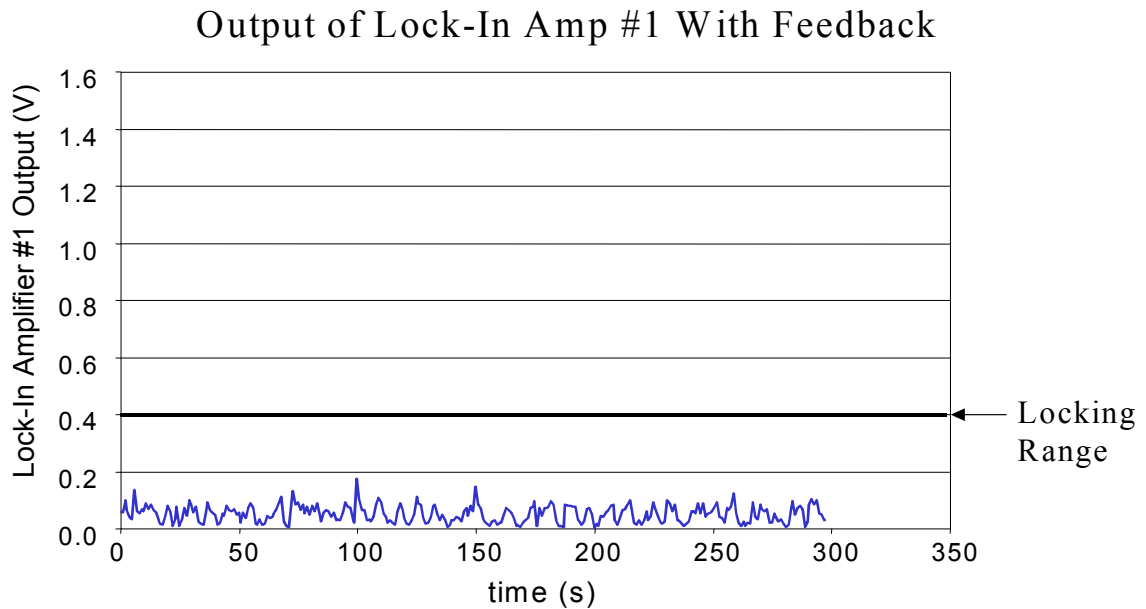


Figure 3.15 – Output of Lock-In Amplifier #1 With Feedback

From this it was found that, for a -31dBm injected signal with a modulation frequency of 1MHz, the difference between the free-running frequency of the slave laser and the frequency of the master laser was maintained within  $\sim 40\%$  of the full locking range. As a result, the phase difference between the injected signal and the output of the slave laser was approximately  $\pm 22^\circ$  (calculated by monitoring the output voltage from the first lock-in amplifier and assuming a one-sided locking range of  $90^\circ$ ). This also translates to a modulation depth ratio that ranges from  $\sim 3.75 \cdot 10^{-5}$  to  $\sim 9.38 \cdot 10^{-4}$ . Since this phase variation is slow (verified later in Section 5.2.2.5 as sub kHz), it can be compensated for with a phase lock loop.

## IV. CHAPTER 4 – Injection Locking a Fabry-Perot

### Semiconductor Laser

#### 4.1 Background

An alternative to using a DFB semiconductor laser for the slave laser is to use a Fabry-Perot laser. A Fabry-Perot laser differs from a DFB laser in that a Fabry-Perot laser can have multiple modes oscillating within the cavity [23, 26].

There are two distinct advantages for using a Fabry-Perot semiconductor laser, as opposed to a DFB, as the slave laser. First, a Fabry-Perot laser is capable of accommodating a much larger range of master laser wavelengths than a DFB laser. Second, Fabry-Perot lasers generally are much simpler to fabricate than DFB lasers, and therefore much cheaper to produce. The tuning range of a DFB laser is limited by the range of the Bragg-grating reflectors, typically only 2nm. Whereas, a Fabry-Perot laser can be injection locked to any frequency that is within the gain region of the laser (typical width is 5-10nm), as long as it is tuned close to one of its modes.

#### 4.2 Modeling an Injection Locked Multi-Mode Slave Laser

When modeling the behavior for an injection locked DFB semiconductor laser, it was assumed that only one laser mode was allowed to oscillate within the cavity. However, in the case of a Fabry-Perot semiconductor laser, this is no longer always the case. Therefore, the multi-mode system can be described by the following four rate equations:

$$\frac{d\phi}{dt} - \frac{r_2}{2\tau_c} + (\omega_1 - \omega_0) = \frac{\gamma_e E_1}{E} \sin \phi \quad (4.01)$$

$$\frac{dE}{dt} - \frac{r_1 - 1}{2\tau_c} E = \gamma_e E_1 \cos \phi \quad (4.02)$$

$$\frac{dE_L}{dt} - \frac{r_1 - 1}{2\tau_c} E_L = \gamma_e E_{L1} \quad (4.03)$$

$$\frac{dr_1}{dt} = \rho - r_1 \frac{1}{T_1} \left( 1 + \frac{I}{I_{sat}} \right) = \rho - r_1 \frac{1}{T_1} \left( 1 + \frac{E^2 + E_L^2}{I_{sat}} \right). \quad (4.04)$$

Three of these equations have been adopted from Chapter 3, and (4.03) has been added to describe the unwanted modes.  $E_L$  is the amplitude of the combined electric fields of the unwanted modes and  $E_{L1}$  is the injected electric field due to ASE (either from the slave laser, or from an external EDFA). Otherwise (4.03) is identical to (4.02) in form.

Since the equation for (4.01) is the same as (3.11), the previously derived equation describing the locking range, (3.16), is the same for the case of a multi-mode slave laser. Also, equation (3.17) still accurately describes the behavior of the phase difference between the injected signal and the optical signal generated by the locked oscillator as the injected signal is tuned across the locking range.

## 4.3 Feedback Control of an Injection Locked Fabry-Perot Semiconductor Slave Laser

### 4.3.1 Generation of a Feedback Signal

As was the case for the DFB laser, the modulation transfer characteristic for the Fabry-Perot laser can be used as a feedback control signal.

In order to determine the modulation transfer function for a multi-mode slave laser, we introduce a small perturbation onto  $E_I$ ,  $E$ ,  $E_{L1}$ ,  $E_L$ ,  $r$ , and  $\phi$ . Following the

method used in Section 3.2.1.1,  $E_I$ ,  $E$ ,  $r$ , and  $\phi$  are still represented by (3.18-3.22), and

$E_{L1}$ ,  $E_L$ , can be expressed as:

$$E_{L1} = E_{L10} + \Delta E_{L1} \quad (4.05)$$

$$E_L = E_{L0} + \Delta E_L \quad (4.06)$$

Since equations for  $E_I$ ,  $E$ ,  $r$ , and  $\phi$  remain unchanged, then  $d\Delta\phi/dt$  is described by (3.28), and the regenerated field ( $d\Delta E/dt$ ), is described by (3.30). Additionally, (4.03) yields to the first order, after simplification:

$$\frac{d\Delta E_L}{dt} - \frac{\Delta r E_{L0} + \Delta E_L r_{10} - \Delta E_L}{2\tau_c} = \gamma_e \Delta E_{L1} \quad (4.07)$$

Also, from (4.04), the equation for  $d\Delta r/dt$  has become:

$$\frac{d\Delta r_1}{dt} = -\frac{1}{T_1} \left( \Delta r_1 + \frac{(2E_0 \Delta E r_{10} + E_0^2 \Delta r_1 + 2E_{L0} \Delta E_L r_{10} + E_{L0}^2 \Delta r_1)}{I_{sat}} \right) \quad (4.08)$$

A harmonically modulated signal is injected into the free-running Fabry-Perot oscillator. As such, one can assume that the perturbation on its electric field can be given as:

$$\Delta E_1 = A e^{j\Omega t} \quad (4.09)$$

where  $A$  and  $\Omega$  are the magnitude and frequency of the driving perturbation, respectively.

From this, it can be assumed that resulting perturbation on  $E$ ,  $\phi$ , and  $r$  is the same was defined in (3.34-3.36), and the perturbation on  $E_L$  is of the form:

$$\Delta E_L = B_L e^{j\Omega t} \quad (4.10)$$

where  $B_L$  is the magnitude of the 1<sup>st</sup> order component of the perturbation on  $E_L$ .

Additionally, it is assumed that there is no perturbation on the ASE ( $\Delta E_{L1}=0$ ).

Thus, the equivalent set of equations for  $D$ ,  $C$ ,  $B$ , and  $B_L$  are:

$$j\Omega D = -\frac{1}{T_1} \left( D + \frac{(2E_0 r_{10} B + 2E_{L0} r_{10} B_L + E_0^2 D + E_{L0}^2 D)}{I_{sat}} \right) \quad (4.11)$$

$$j\Omega C - \frac{\alpha_\phi}{2\tau_c} \frac{D}{B} = \frac{\gamma_e}{E_0} \left[ CE_{10} \cos \phi_0 + A \sin \phi_0 - B \frac{E_{10}}{E_0} \sin \phi_0 \right] \quad (4.12)$$

$$j\Omega B - B \frac{E_0 \frac{D}{B} + r_{10} - 1}{2\tau_c} = \gamma_e (-CE_{10} \sin \phi_0 + A \cos \phi_0) \quad (4.13)$$

$$j\Omega B_L - \frac{DE_{L0} + B_L r_{10} - B_L}{2\tau_c} = 0 \quad (4.14)$$

The equation for  $D$  differs from (3.37) in that it is now a function of  $B_L$  and  $E_{L0}$ , as well as of  $B$  and  $E_0$ . The equations for  $B$  and  $C$  remain unchanged from (3.39) and (3.38), respectively.

#### 4.3.1.1 Establishing a Relationship Between the Electric Fields of the Main and Unwanted Modes

If we solve for the steady-state solutions of (4.02) and (4.03), we get:

$$-\frac{r_{10} - 1}{2\tau_c \gamma_e} = \frac{E_{10} \cos \phi_0}{E_0} \quad (4.15)$$

$$-\frac{r_{10} - 1}{2\tau_c \gamma_e} = \frac{E_{L10}}{E_{L0}} \quad (4.16)$$

These two equations can then be combined to yield:

$$E_{L0} = \frac{E_0 E_{L10}}{E_{10} \cos \phi_0} \quad (4.17)$$

#### 4.3.1.2 Solving for the 1<sup>st</sup> Order Perturbation on $r$

If we solve for  $B_L$  using (4.14), we get:

$$B_L = \frac{DE_{L0}}{1 - r_0 + j2\Omega\tau_c} \quad (4.18)$$

This equation can be written as:

$$2E_{L0}r_0B_L = \frac{2E_{L0}^2r_0D}{1 - r_0 + j2\Omega\tau_c} \quad (4.19)$$

If we then substitute this equation into (4.11), we get:

$$j\Omega D = -\frac{1}{T_1 I_{sat}} \left( DI_{sat} + 2E_0r_0B + \frac{2E_{L0}^2r_0D}{1 - r_0 + j2\Omega\tau_c} + E_0^2D + E_{L0}^2D \right) \quad (4.20)$$

which can be re-written as:

$$\frac{D}{B} = -\frac{2E_0r_0}{\left( j\Omega T_1 I_{sat} + I_{sat} + \frac{2E_{L0}^2r_0}{1 - r_0 + j2\Omega\tau_c} + E_0^2 + E_{L0}^2 \right)} \quad (4.21)$$

Note that when the amplitude of the electric fields of the unwanted modes ( $E_{L0}$ ) is equal to zero, this equation reduces to (3.41).

#### 4.3.1.3 Solving for the 1<sup>st</sup> Order MTR of the Injection Locked Fabry-Perot Laser

As before, we can determine the expression for MTR by substituting the expression for  $D/B$  into (3.46):

$$\begin{aligned}
MTR = \frac{B}{A} \times \frac{E_1}{E} = & \frac{1 - j \frac{\Omega}{\gamma_e} \sqrt{\frac{P_0}{P_1}} \cos \phi_0}{1 + \frac{r_{10}}{\tau_c \gamma_e} \frac{P_0}{\left( \frac{j\Omega T_1 I_{sat} + I_{sat}}{1 - r_0 + j2\Omega \tau_c} + \frac{2E_{L0}^2 r_0}{1 - r_0 + j2\Omega \tau_c} + E_0^2 + E_{L0}^2 \right)}} \sqrt{\frac{P_0}{P_1}} (\cos \phi_0 + \alpha_\phi \sin \phi_0) \\
& + \left( \frac{\Omega}{\gamma_e} \right)^2 \frac{P_0}{P_1} \\
& + \frac{j\Omega}{\gamma_e} \frac{P_0}{P_1} \left( \frac{r_{10} - 1}{2\tau_c \gamma_e} - \frac{r_{10} P_0}{\tau_c \gamma_e \left( \frac{j\Omega T_1 I_{sat} + I_{sat}}{1 - r_0 + j2\Omega \tau_c} + \frac{2E_{L0}^2 r_0}{1 - r_0 + j2\Omega \tau_c} + E_0^2 + E_{L0}^2 \right)} + \cos \phi_0 \right) \quad (4.22)
\end{aligned}$$

If it can be assumed that  $\gamma_e \gg \Omega$  (typically  $\gamma_e \sim 10^{11}$ ) and that the modulation frequency is sufficiently low so that  $T_1 \Omega \ll 1$  (typically true for modulation frequencies below 10MHz), (4.22) can be simplified:

$$MTR = \frac{1}{1 + \frac{r_{10}}{\tau_c \gamma_e} \frac{P_0}{\left( I_{sat} + \frac{2E_{L0}^2 r_0}{1 - r_0 + j2\Omega \tau_c} + E_0^2 + E_{L0}^2 \right)}} \sqrt{\frac{P_0}{P_1}} (\cos \phi_0 + \alpha_\phi \sin \phi_0) \quad (4.23)$$

In addition, if the slave laser is strongly locked, the effect from the unwanted modes becomes negligible. For this case, (4.23) can be restated as:

$$MTR = \frac{1}{1 + \frac{r_{10}}{\tau_c \gamma_e} \frac{P_0}{(I_{sat} + P_0)}} \sqrt{\frac{P_0}{P_1}} (\cos \phi_0 + \alpha_\phi \sin \phi_0) \quad (4.24)$$

which can be simplified with the use of (3.15):

$$MTR = \frac{1}{1 + \frac{r_{10}}{\tau_c \gamma_e} \left( \frac{P_0}{I_{sat} + P_0} \right) \sqrt{\frac{P_0}{P_1}} \sqrt{(1 + \alpha_\phi^2) - \left( \frac{\Delta\omega}{\gamma_e} \right)^2} \frac{P_0}{P_1}} \quad (4.25)$$

#### 4.3.1.4 Numerical Modeling

Given the equation for MTR, we numerically simulate the behavior of this system and present the results graphically, the code for which is presented in Appendix B. As constraining values, we assume that the effective saturation intensity of the slave laser is 10dBm, the perturbation on the injected intensity is 10%, the unsaturated cavity gain to loss ratio ( $r$  when  $E=0$ ) is 2, the cavity lifetime ( $\tau_c$ ) is 110ps, the carrier lifetime ( $T_l$ ) is 1ns, the photon loss rate ( $\gamma_e$ ) is  $1 \cdot 10^{10} \text{ s}^{-1}$ , and the pump rate ( $\rho$ ) is  $2 \cdot 10^9 \text{ s}^{-1}$ . The values for  $E_0$ ,  $E_{L0}$ , and  $r$  are determined from (4.02-4.04). In addition, it was experimentally found that the unwanted modes were sufficiently suppressed for us to assume that  $E_{L0} \approx 0$ , and that  $\alpha_\phi \approx 2$  for our Fabry-Perot slave laser.

Figure 4.01 depicts the MTR of the Fabry-Perot slave laser (over the locking range), plotted for various modulation frequencies ( $\Omega$ ). This figure depicts a limited "U"-shaped MTR over the locking range. The limit of the U-shape on the left side of the graph is a direct result of the effect of  $\alpha_\phi$  (the MTR is "U"-shaped when  $\alpha_\phi=0$ ). The non-zero value of  $\alpha_\phi$  also causes the detuning at which the minimum of the U-shape occurs to become non-zero. Additionally, it should be noted that when this "U" shape was plotted at various modulation frequencies (below 10MHz), all of the curves were found to be graphically indistinguishable from each other. This indicates that, as was predicted by (4.25), the MTR of the slave laser is weakly dependant of the modulation frequency.

Figure 4.02 depicts this ratio for various injected intensities. As can be seen from this figure, although the minimum of the “U” shape is less than one (indicating a suppression of the modulation of the injected signal) it does not go to zero. Instead, this minimum value is approximately proportional to the intensity of the injected master signal (at low modulation frequencies and low injected noise levels). Thus for the case of a multi-mode slave laser, other than some differences between the overall “U”-shape (due to the effect of  $\alpha_\phi$ ), there is no appreciable difference between the behavior as the injected power is varied.

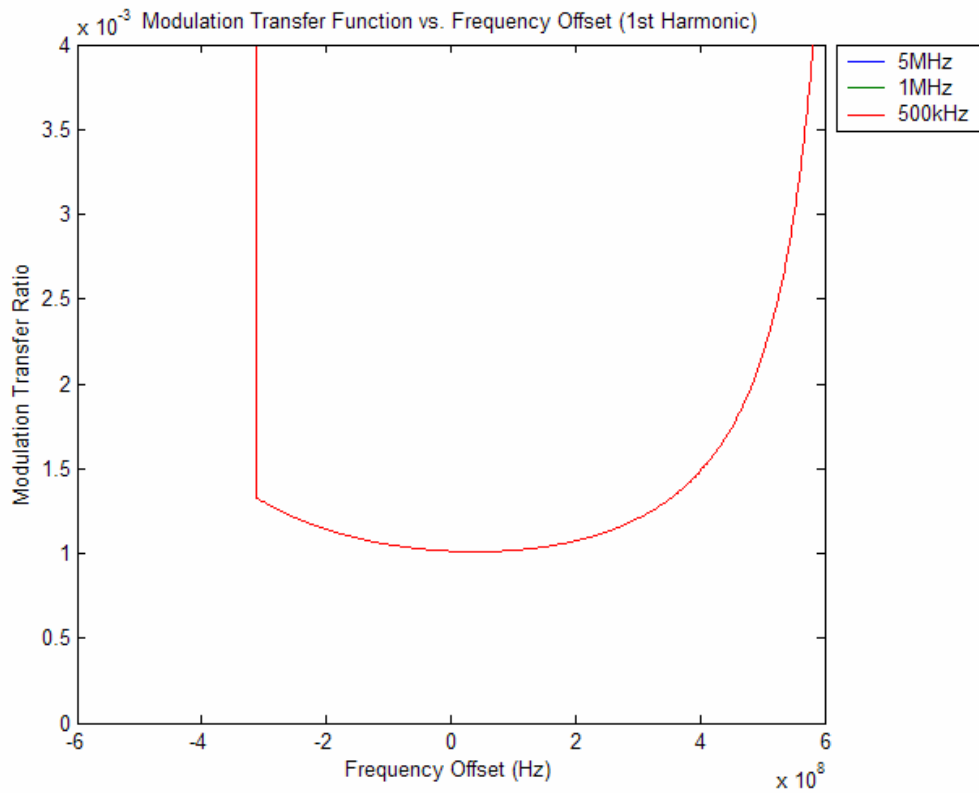


Figure 4.01 – 1<sup>st</sup> Order Modulation Transfer Ratio vs. Frequency Offset (At Various Modulation Frequencies)

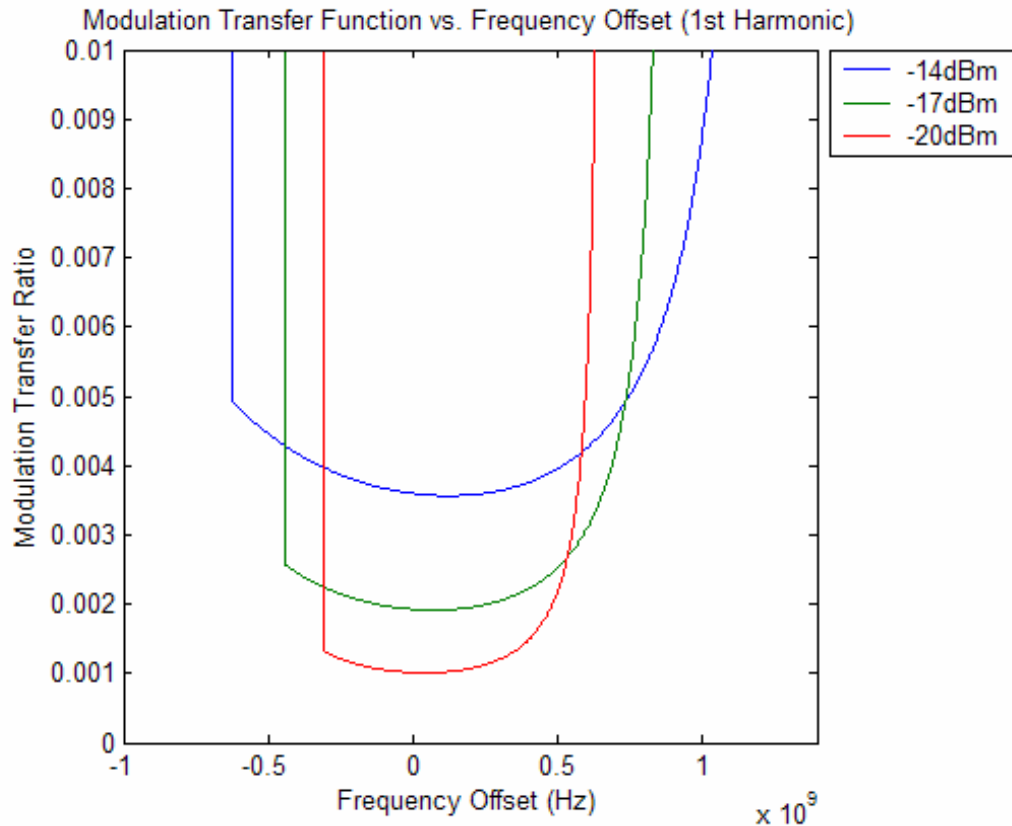


Figure 4.02 – 1<sup>st</sup> Order Modulation Transfer Ratio vs. Frequency Offset (At Various Injected Powers)

#### 4.3.1.5 Experimentally Verifying the Injection Locking Theory

To confirm these theoretical results, the setup depicted in Figure 4.03 was assembled. Similar to the setup depicted in Figure 3.05, a CW with a 10MHz modulation applied to it (with ~10% modulation depth) is diverted by Circulator #1 into the slave laser, which also diverts the output of the slave laser to Circulator #2. Circulator #2 directs the output from the slave laser into a Bragg grating, whose center frequency is the same as the frequency of the master laser. The output from the Bragg grating is then

directed to an optical detector. Additionally, the signal reflected by the Bragg grating is re-directed by Circulator #2 to another detector.

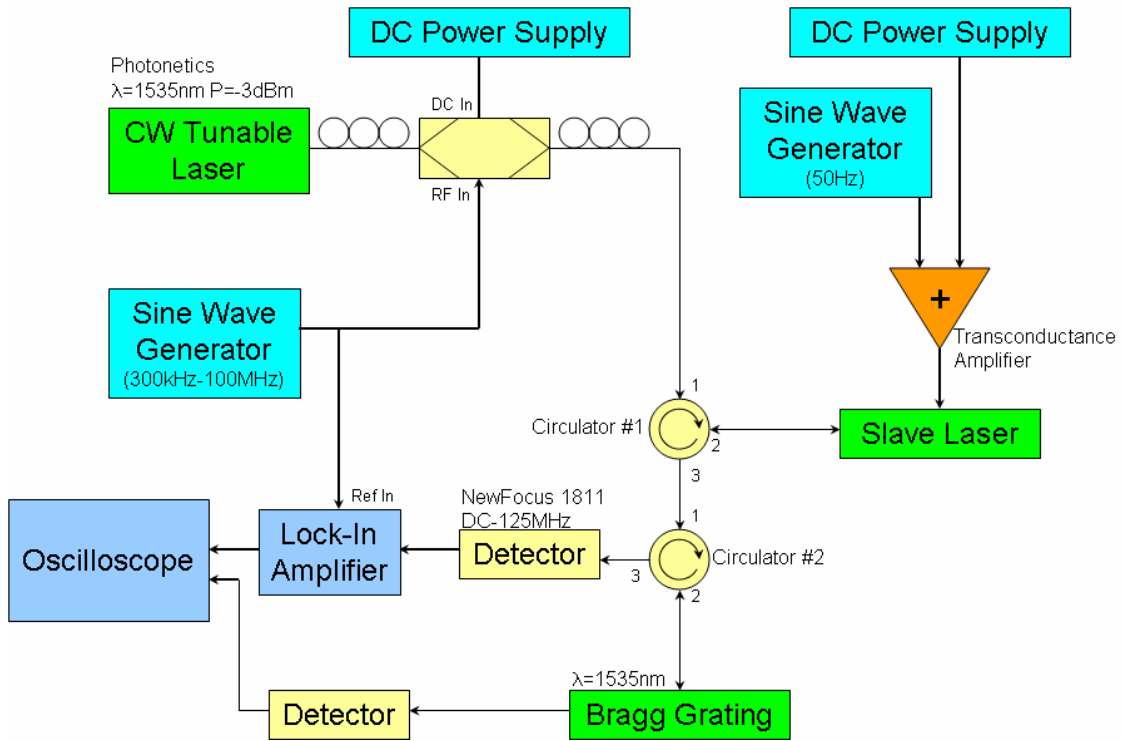


Figure 4.03 – Layout of Injection Locking Experiment

The output from the detector that monitors the signal transmitted through the Bragg grating is proportional to the intensity of the unwanted modes, while the output from the detector that monitors the signal reflected by the Bragg grating (port 3 of Circulator #2) is proportional to the intensity of the main mode. The purpose of monitoring the unwanted modes is simply for the purposes of comparison with monitoring the MTR of the main mode, and is presented in Section 4.3.4.

The output of the detector that monitors the main mode is directed to a lock-in amplifier whose reference signal is the same as the modulation frequency that was applied to the master laser signal (10MHz). For this, the lock-in amplifier is at a

sensitivity of 30mV[rms], with its filter disabled. Thus, the real-component ( $[X^2+Y^2]^{1/2}$ ) output of the lock-in amplifier is proportional to the magnitude of the modulation at the 10MHz modulation frequency that is on the portion of the output of the slave laser that is at the optical frequency of the master laser.

In order to detect the change in both the magnitude of the modulated signal and the power level of the unwanted modes across the entire locking range, the free-running frequency of the slave laser is slowly swept across a 3GHz range, by adding a 50Hz sinusoidal modulation to the current source of the slave laser. This setup allows for both the modulation transfer ratio and the power level of the unwanted modes to be measured before the laser has a chance to drift.

#### 4.3.2 Varying the Free-Running Frequency of the Slave Laser

Before the MTR's dependence on detuning can be utilized by a feedback loop, a method for adjusting the free-running frequency of the slave laser is required. As was the case with the single-mode slave laser, the frequency of the multi-mode slave laser is tuned by changing the control current. However, the Fabry-Perot slave laser that was used in this experiment requires 10 times the current required by the DFB laser. Also, a different laser controller was desired in order to allow us to more easily add modulation to the drive current. Thus, a current source needed to be designed and assembled for this purpose.

The circuit for generating the driving current for the Fabry-Perot slave laser is depicted in Figure 4.04. In this circuit, the current provided by the 5V source is used to control the Fabry-Perot laser. The magnitude of this current is equal to the current

entering the collector of the transistor, which in turn is determined by the current leaving the emitter of the transistor. The emitter current is controlled by the output voltage of the top-right op-amp, and by the value of the resistors that separate the emitter from ground. The output of this op-amp is proportional to the sum of the 50Hz dither signal, the output from the lock-in amplifier, and a bias voltage. The “optional additional modulation” is for testing purposes, and will be explained later. The values of the resistors can be changed via a jumper select. This way, the maximum current that can be provided by the circuit can be switched between 40mA and 400mA. Also, the +5V, +15V, and -15V sources are connected to ground via a 0.1uF capacitor and a polarized 4.7uF capacitor in parallel. This filters the ripple from the power supplies, which in turn reduces the number of glitches in the circuit.

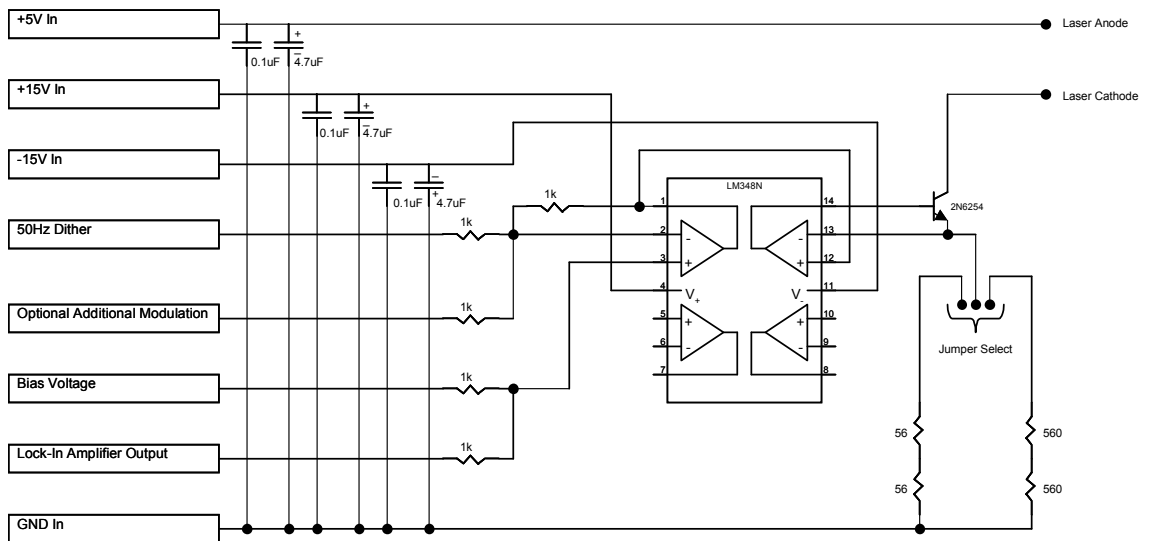


Figure 4.04 – Fabry-Perot Laser Controller

### 4.3.3 Modeling the Modulation Transfer Ratio of the Slave Laser

Figures 4.05 and 4.06 depict the modulation transfer ratio of the slave laser over the full locking range, as seen on the oscilloscope following the lock-in amplifier. Similar to what is predicted in the theory, the minimum value of this limited “U”-shape is approximately proportional to the intensity of the injected master signal (at low modulation frequencies). Also, it should be noted that the curvature of the MTR remains fairly constant for modulation frequencies below 5MHz. The small variation in these limited “U”-shapes at the different frequencies is due to noise in the control circuit of the slave laser.

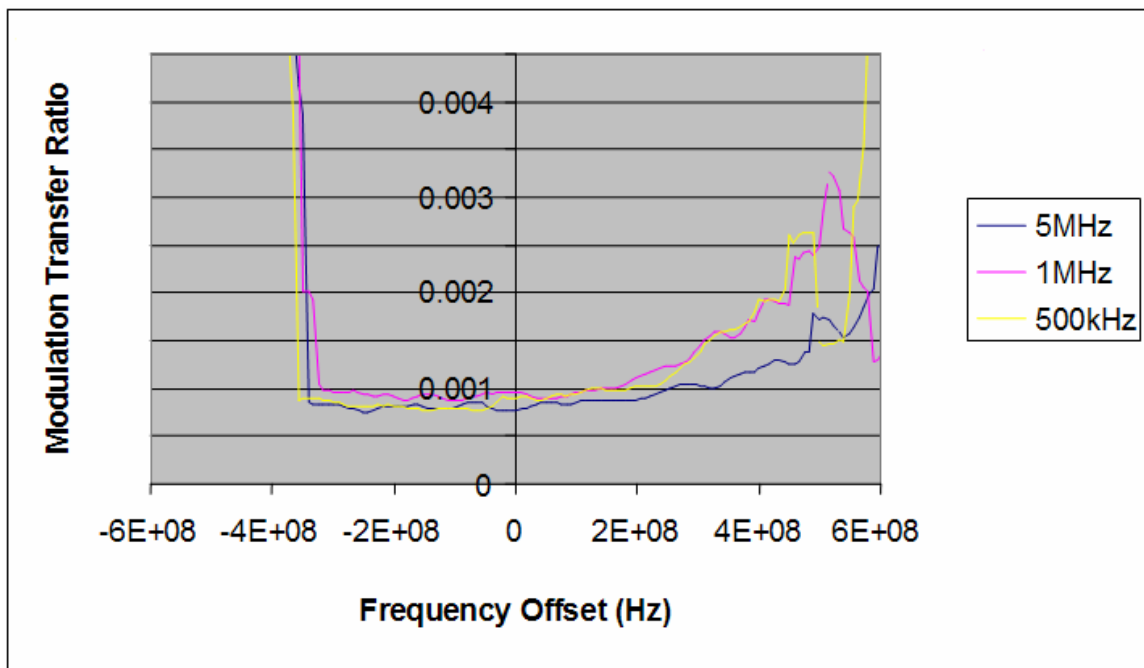


Figure 4.05 – 1<sup>st</sup> Order Modulation Transfer Ratio vs. Frequency Offset (At Various Frequencies)

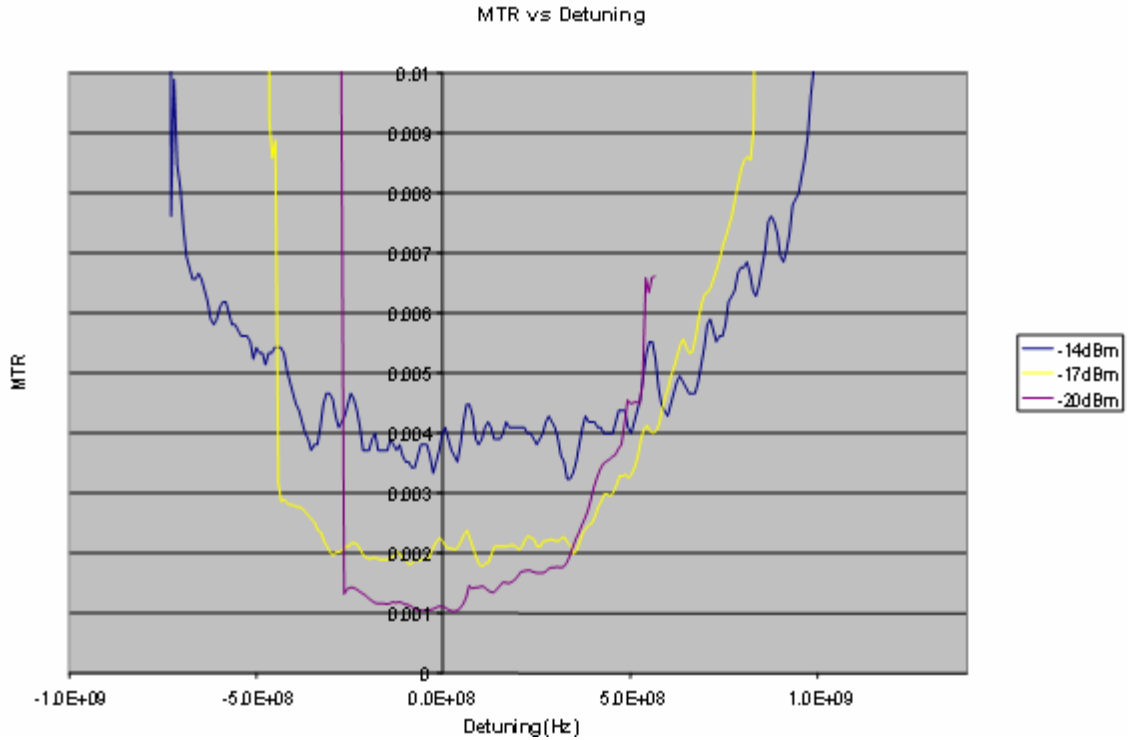


Figure 4.06 – 1<sup>st</sup> Order Modulation Transfer Ratio vs. Frequency Offset (At Various Injected Powers)

#### 4.3.4 Suppressing the Unwanted Modes in the Slave Laser

Several oscillatory modes may be present in a free-running Fabry Perot Laser. Injection locking the Fabry-Perot laser will help to suppress these unwanted oscillatory modes, as is seen in Figure 4.07.

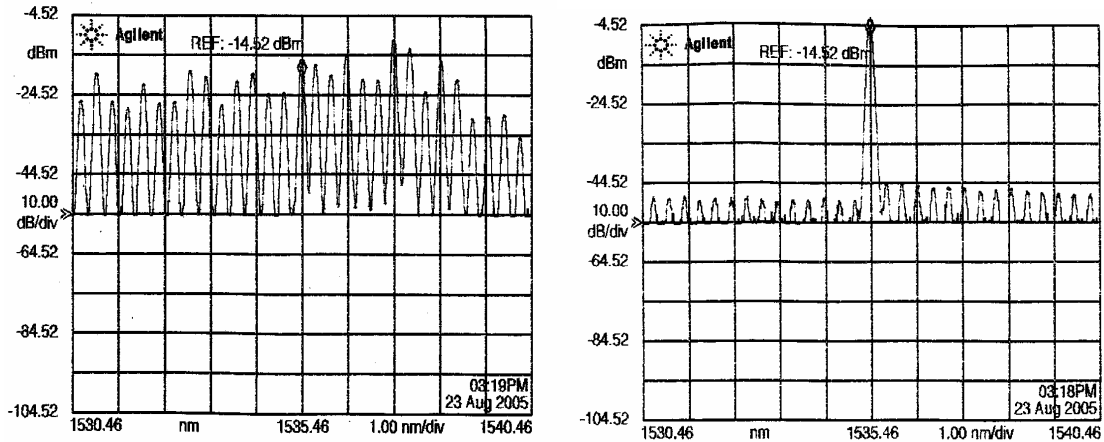


Figure 4.07 - Frequency Spectrum of Unlocked (left) and Locked (right) Fabry-Perot Laser

Figure 4.08 shows both the modulation transfer ratio and the intensity of the unwanted modes across the locking range (normalized to each other). As can be seen from this graph, the intensity of the unwanted modes remains at nearly a minimum while inside the locking range. Additionally, it exhibits a threshold-like transition at the edge of the locking range. Since there is not necessarily a gradual change in the intensity of the unwanted modes with detuning, this intensity can be used as a binary indicator to see whether or not the slave laser is locked, but not as an alternative to the modulation transfer function as a feedback signal.

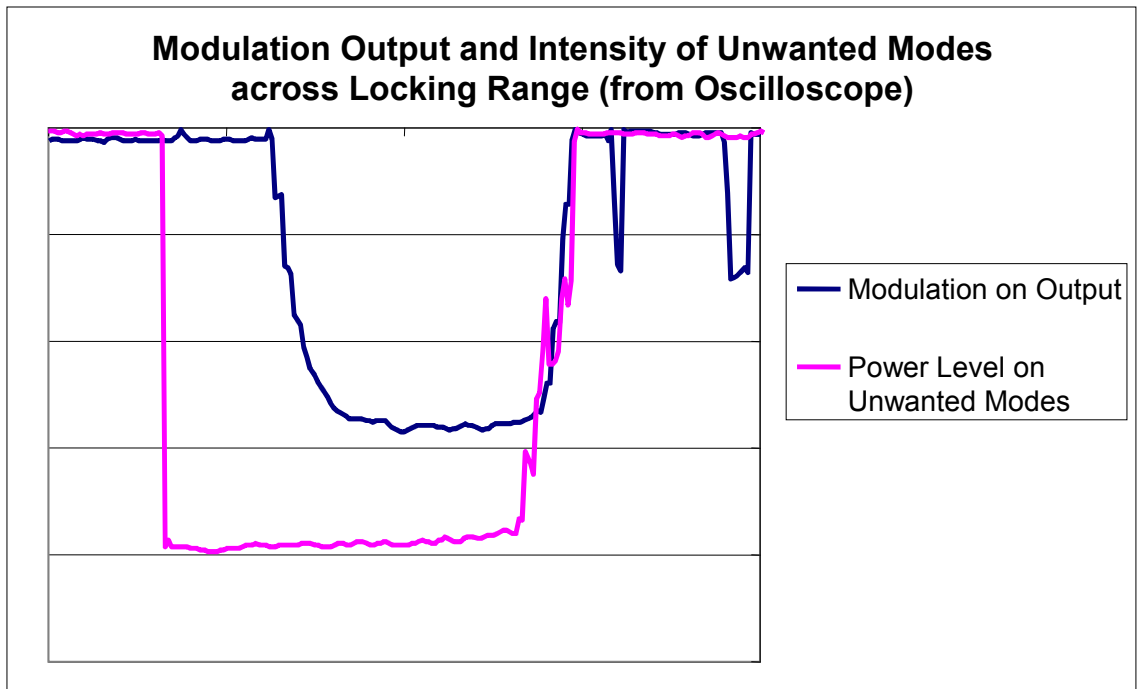


Figure 4.08 - Modulation Transfer Ratio and Intensity of Unwanted Modes Across Locking Range

#### 4.3.5 Creating the Feedback System for the Injection Lock

Similar to what was seen in the case of a DFB slave laser, the modulation transfer ratio of a laser that is locked to a modulated optical signal is essentially “U” shaped. If the free-running frequency of the slave laser is then dithered by modulating its drive current, then the amplitude of the modulation on the output from the slave laser at the dither frequency will be proportional to the derivative of the “U” shape. Also, as was the case with the DFB laser, this derivative will be used as an input threshold for a digital feedback loop.

Figure 4.09 depicts the setup of the digital feedback loop. This setup is very similar to the one used to stabilize the DFB slave laser (Figure 3.09). In this, a modulated optical signal (approximately a 10% modulation depth at a frequency of 1MHz) is

amplified by an EDFA before being directed into the slave laser via a circulator. The EDFA is required, since a higher injected signal is required to effectively suppress the unwanted modes of the Fabry-Perot slave laser. A 50Hz sinusoid is applied to the bias port of the slave laser controller that effectively tunes the free-running frequency of the slave laser over ~10% of the locking range.

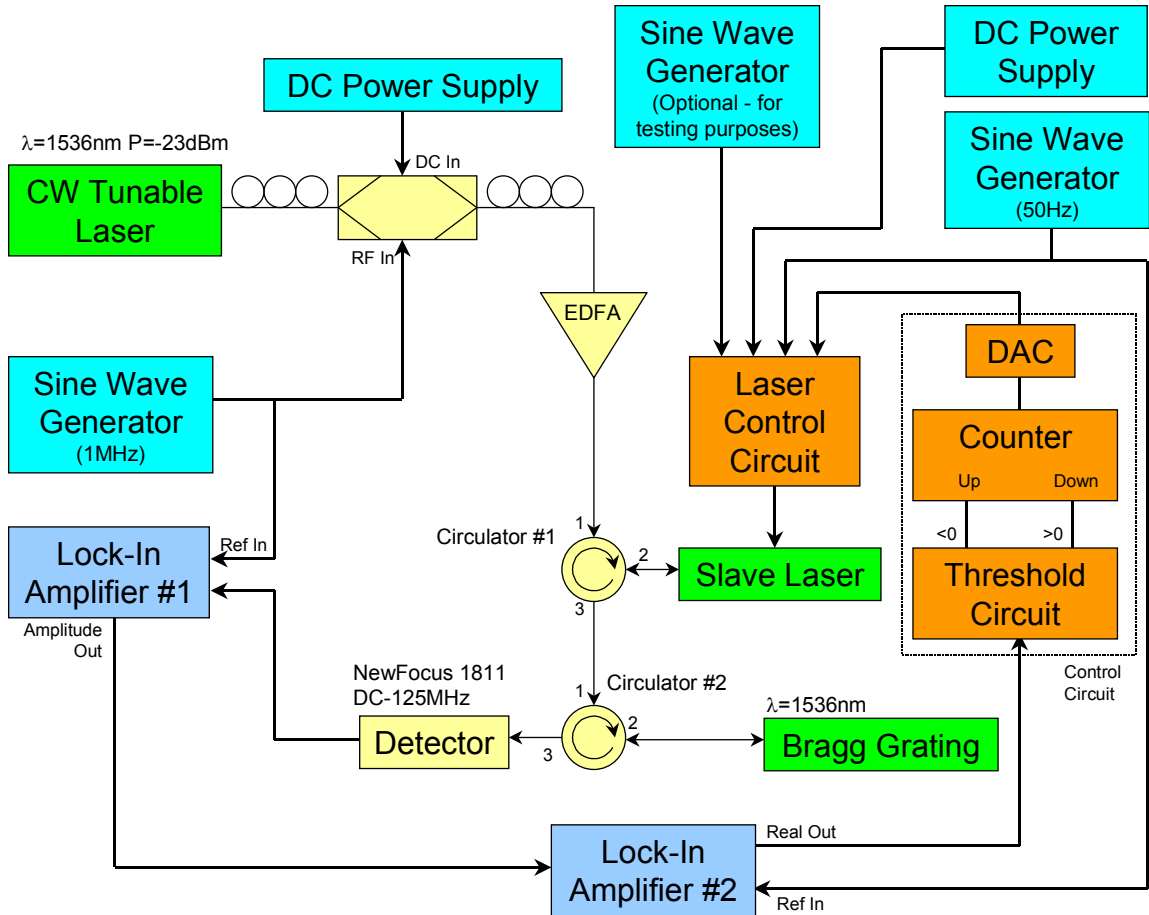


Figure 4.09 –Layout of Automated Injection Lock

Circulator #1 redirects the signal emitted from the slave laser to Circulator #2, which directs the signal into a Bragg Grating (as was done in the setup depicted in Figure 4.04). In this case, the purpose of the Bragg grating is to filter off the background ASE emitted by the EDFA (a Fabry-Perot filter could also have been used for this purpose).

Also, although not shown in the figure, the signal that is transmitted through the Bragg grating may be used to monitor the effectiveness of the feedback control loop.

Circulator #2 redirects the signal reflected by the Bragg grating to an optical detector, whose output is directed to the input of a lock-in amplifier whose reference signal is the signal that is driving the amplitude modulator this lock-in. The output of the amplitude port of the lock-in amplifier is directed to a second lock-in amplifier, whose reference signal is the same 50Hz sinusoid that was used to modulate the free-running frequency of the slave laser (the setting for both lock-in amplifiers are summarized in Table 2). This second lock-in amplifier is set to maximum sensitivity so that it saturates. Thus, the in-phase output of this lock-in amplifier will be a large, positive (negative) voltage when the difference between the free-running frequency of the slave laser and the frequency of the master laser is positive (negative).

	<b>Lock-In Amplifier #1</b>	<b>Lock-In Amplifier #2</b>
<b>Filter Type</b>	24dB/oct Low Pass	6dB/oct Bandpass
<b>Integration Time</b>	300us	300ms
<b>Sensitivity</b>	Variable	300nV <sub>rms</sub>

Table 2 – Lock-In Amplifier Settings for Fabry-Perot Feedback

This signal is then directed to the control circuit, the layout of which is depicted in Figure 4.10. The output voltage of this control circuit will step up (down) if the input from the 2<sup>nd</sup> lock-in amplifier is greater (less) than zero voltage. The control circuit output is then added to the bias port of the slave laser controller.

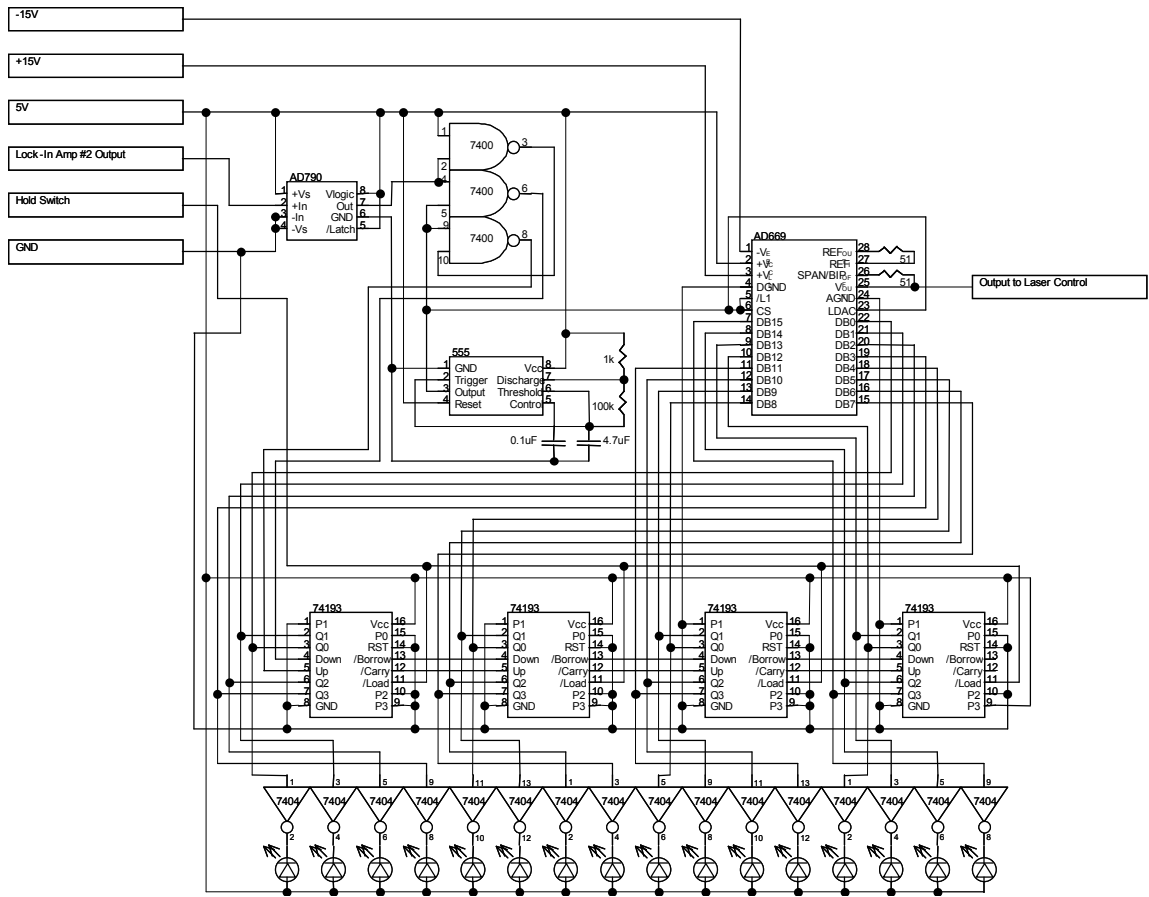


Figure 4.10 – Control Circuit for Fabry-Perot Laser

In order to test the effectiveness of the feedback loop, the intensity of the unwanted modes was monitored over a period of 50 seconds. As discussed in Section 4.3.4, the intensity of the unwanted modes can be used to indicate if the slave is locked to the injected signal. Thus, this intensity is a good indicator of the effectiveness of the feedback loop.

Unlike the DFB laser, the free-running frequency of the Fabry-Perot laser used in this experiment is stable over long periods of time. Thus, in order to test the loop locking stability and recovery response, an additional modulation was added to the laser control

circuit (Figure 4.05). The additional modulation periodically forces the slave laser to leave the locking range. Thus, the intensity of the unwanted modes over the course of 50 seconds will look like what is depicted in Figure 4.11. Figure 4.12 shows this same intensity with the feedback loop activated. From this, it can be seen that the feedback loop successfully adjusts the free-running frequency of the slave laser so that it is consistently within the locking range.

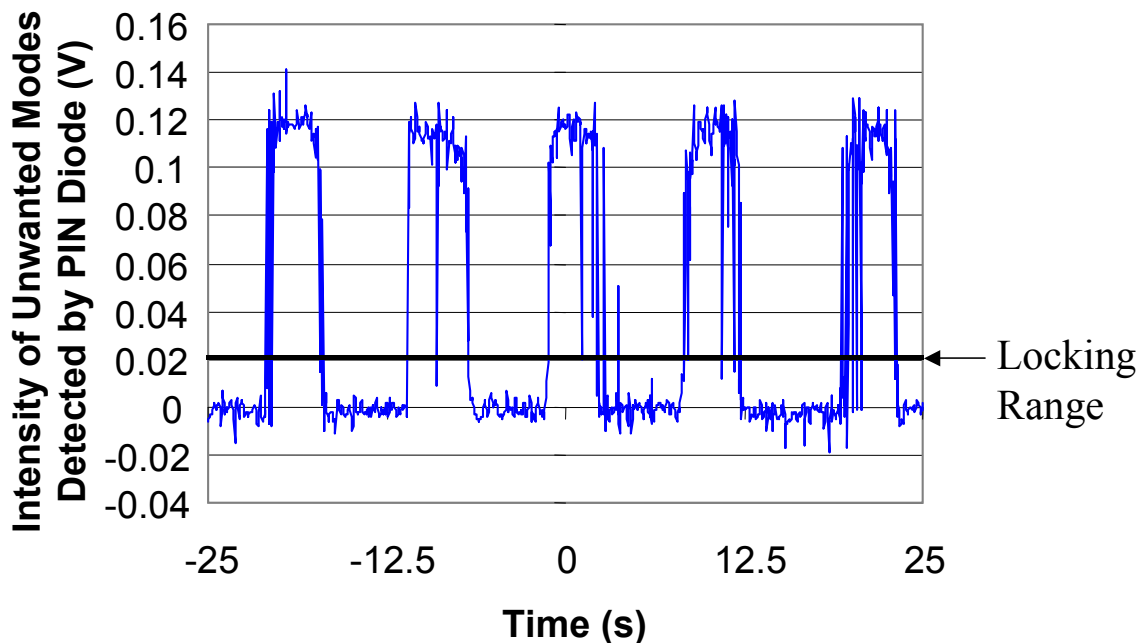


Figure 4.11 – Output of Lock-In Amplifier #1 Without Feedback

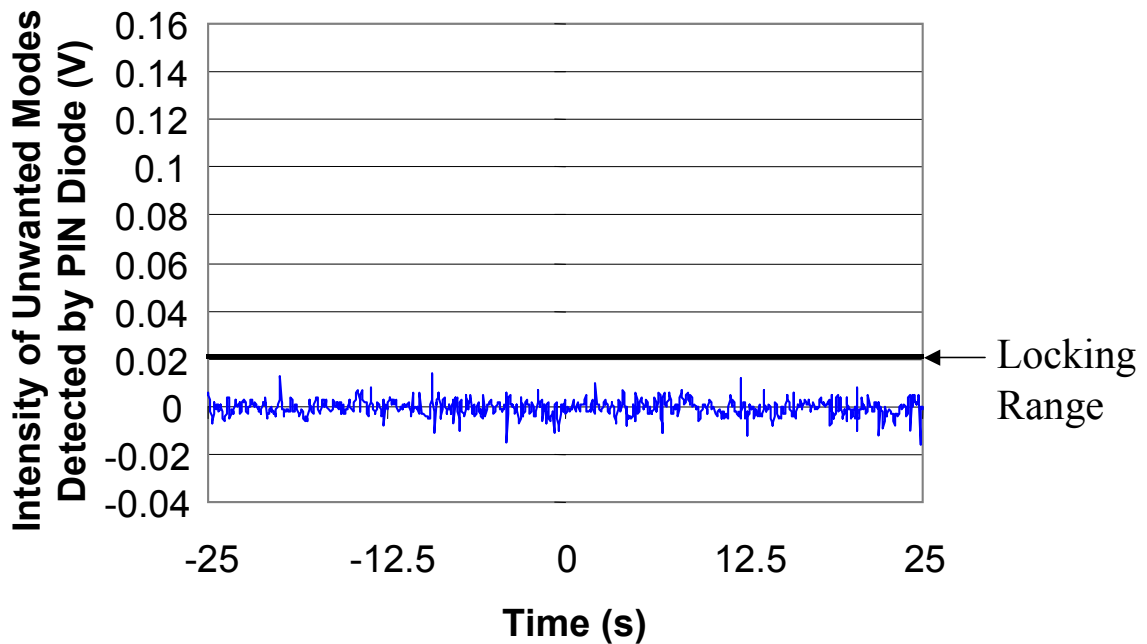


Figure 4.12 – Output of Lock-In Amplifier #1 With Feedback

From this it was found that, for a -24dBm injected signal with a modulation frequency of 1MHz, the difference between the free-running frequency of the slave laser and the frequency of the master laser was maintained within ~60% of the full locking range. As a result, the phase difference between the injected signal and the output of the slave laser was approximately  $\pm 37^\circ$  (calculated by monitoring the output voltage from the first lock-in amplifier and assuming a one-sided locking range of  $90^\circ$ ).

## V. CHAPTER 5 – Characterizing the Local Oscillator Signal

### 5.1 Characteristics of the Fabry-Perot Filter

In order to determine the quality of the local oscillator signal, we first focus on the filter's ability to suppress the modulation of the incident optical signal. Figure 5.01 depicts the spectrum from an OC48 SONET transmission of random data. In order to determine how well the Fabry-Perot filter is expected to suppress this modulation, the setup depicted in Figure 5.02 was assembled. A CW optical signal is modulated with OC48 SONET data using a Mach-Zehnder interferometer. This signal is then applied to the Fabry-Perot optical filter, whose output is monitored by both an optical power meter and a detector and RF spectrum analyzer combination.

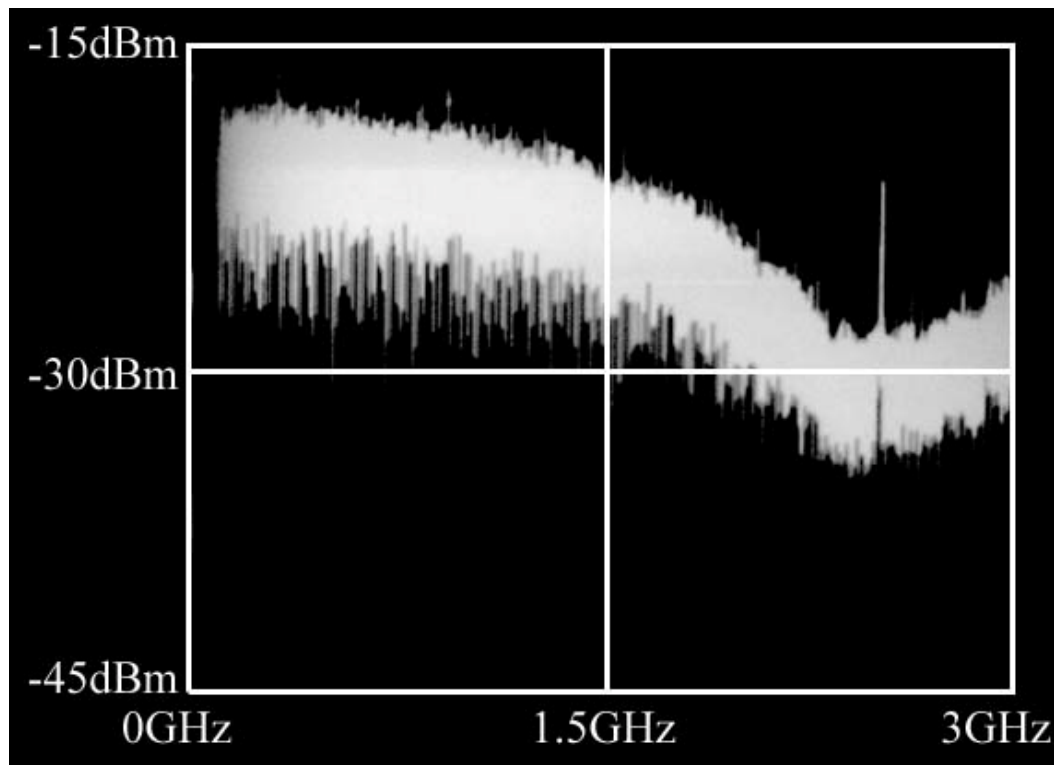


Figure 5.01 – Spectrum from an OC48 SONET Transmission (Random Data)

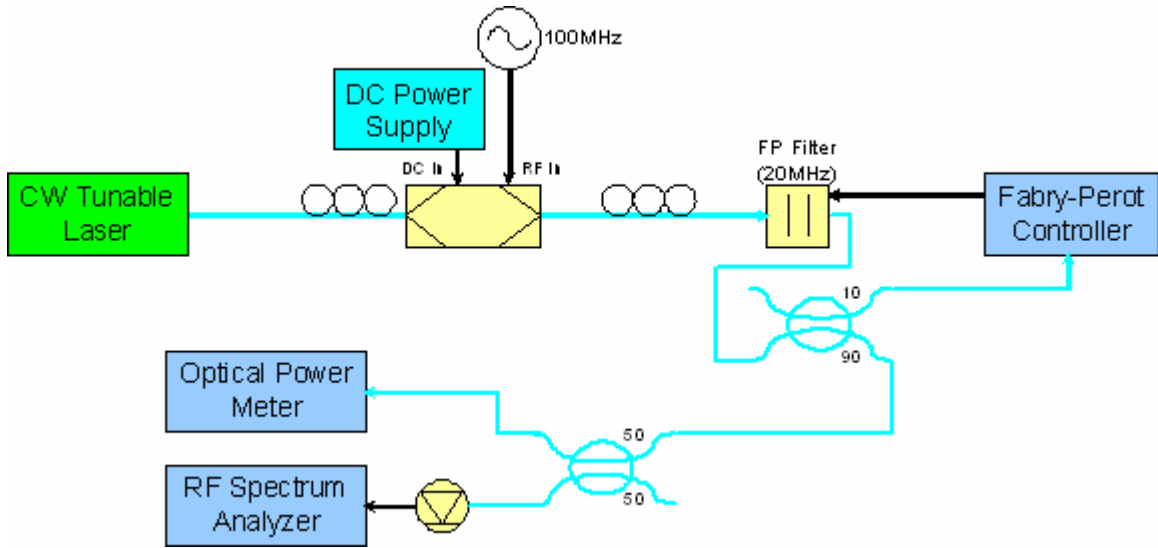


Figure 5.02 – Layout for Testing Modulation Transfer Ratio of Fabry-Perot Filter

With this setup, the bandpass of the Fabry-Perot filter can be recorded for modulation frequencies ranging from 3-200MHz, as is depicted in Figure 5.03. From this it can be seen that, for modulation frequencies less than 20MHz, attenuation provided by the Fabry-Perot filter is approximately 0dB. As the modulation frequency is tuned to frequencies that are greater than 20MHz, this attenuation rapidly increases as the modulation frequency increases.

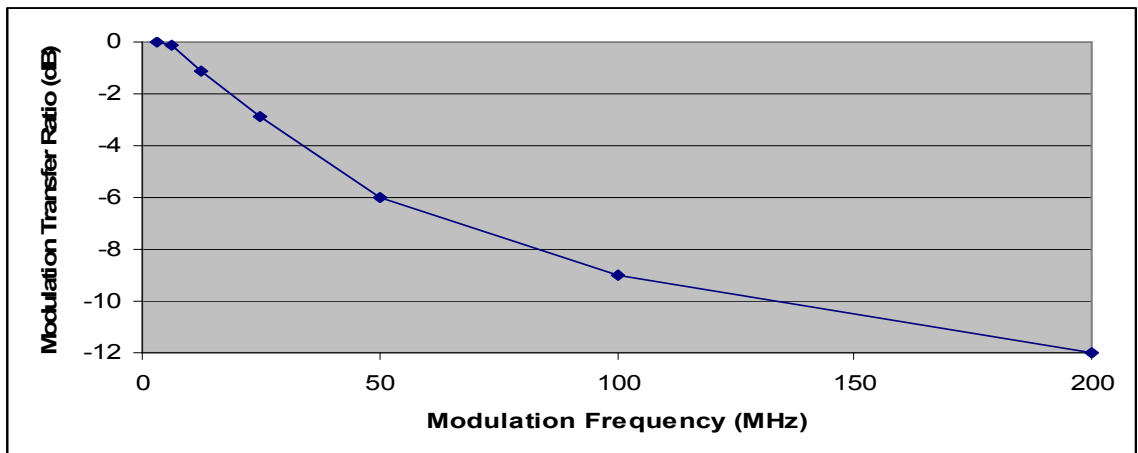


Figure 5.03 – MTR of Fabry-Perot Filter for Various Modulation Frequencies

Figure 5.04 depicts the RF spectrum of the OC48 SONET transmission of random data, after the Fabry-Perot filter. As was predicted by the bandpass function of the filter, the incident modulation is strongly suppressed at higher frequencies.

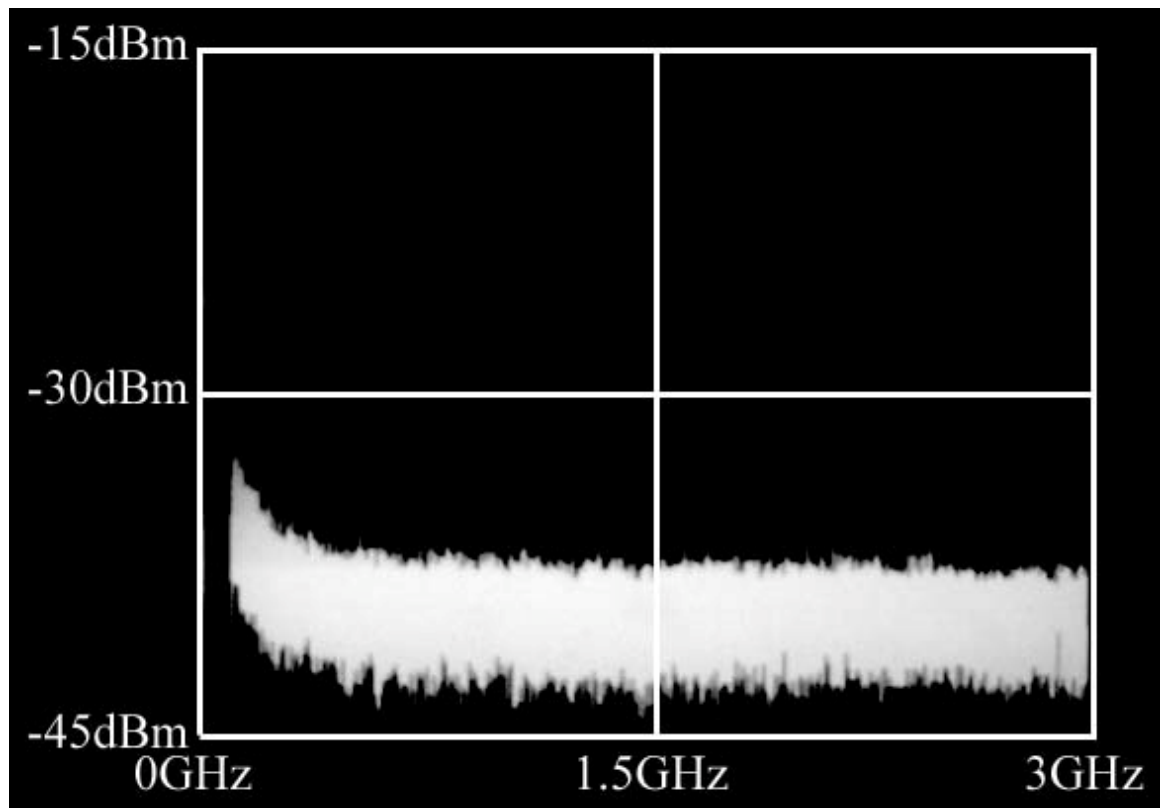


Figure 5.04 – Spectrum from an Optically Filtered OC48 SONET Transmission (Random Data)

If we assume that the OC48 SONET transmission is NRZ, the data on the received signal is essentially the square of a 2.5GHz sinc function in frequency space. In addition, the modulation transfer function of the Fabry-Perot filter is a Lorentzian lineshape with a 20MHz bandwidth. As such, it can be assumed that the modulation on the received signal over the bandwidth of the Fabry-Perot filter is constant. Given this, the fraction of

the residual modulation that is present on the filtered signal is equal to the ratio between the integral of the normalized Lorentzian lineshape to the integral of the normalized sinc function. From this, it is found that the residual modulation on the filtered signal is 2.5% of the initial modulation.

## 5.2 Quality of the Injection Locked Fabry-Perot Laser

Now we investigate the quality of the signal generated by the injection-locked Fabry-Perot laser. One of the main incentives for using a Fabry-Perot laser, as opposed to a DFB laser, is its high degree of wavelength acceptability. A Fabry-Perot laser can be injection locked as long as one of its modes can be tuned to the frequency of the received optical signal. Since the bandgap of the semiconductor material that comprises the Fabry-Perot laser can be altered by changing the temperature of the material, the gain region of the Fabry-Perot laser can be shifted. Experimentally, it was found that the center of the gain region of the Fabry-Perot laser could be tuned over a range of 30nm, as can be seen in Figures 5.05a and 5.05b. As a direct result of this, it is possible to injection lock this laser using a wide range of received optical wavelengths, as is shown in Figures 5.06a and 5.06b. From these figures, it can be seen that the Fabry-Perot laser can be effectively injected by signals whose wavelengths range from 1520nm to 1560nm. The difference in both the peak output power and the power of the unwanted modes vary in each case, due to differences in the particular region of the gain region of the Fabry-Perot laser that we are injecting into.

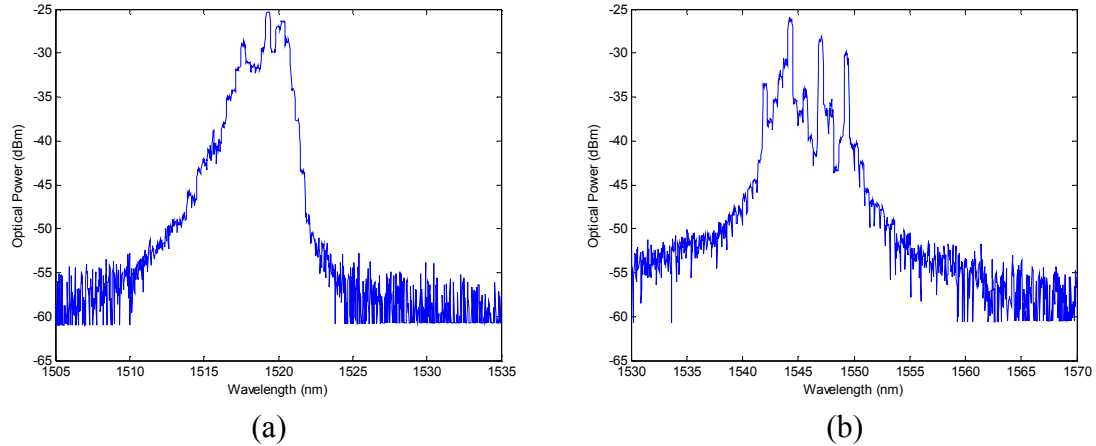


Figure 5.05 – Gain Curve for F-P Laser Temperature Tuned to 1520nm and 1545nm

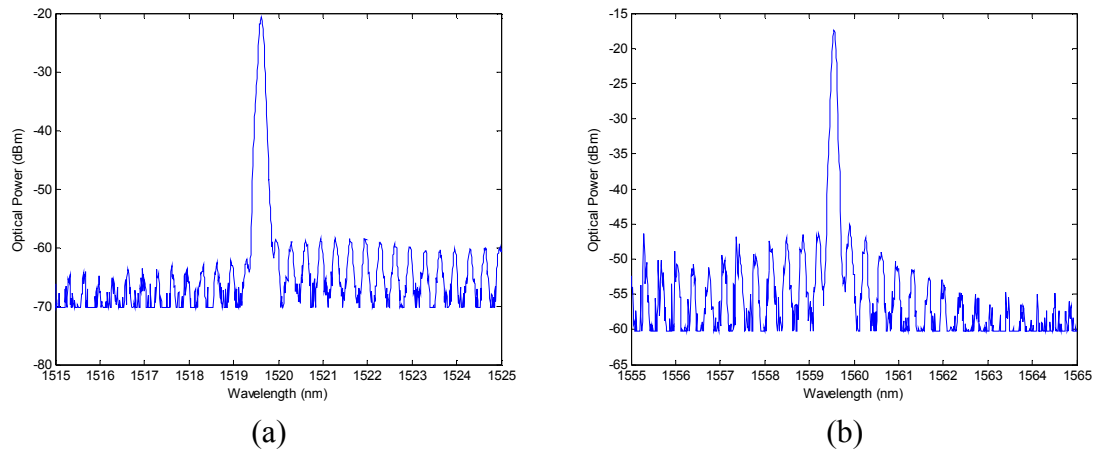


Figure 5.06 – Output of Injection Locked Fabry-Perot Laser Given a Received Optical Wavelength of 1520nm and 1560nm

### 5.2.1 Noise on the Output of the Fabry-Perot Laser

As discussed in Section 4.3.1.4, the Fabry-Perot laser will suppress noise on the injected signal. However, the Fabry-Perot laser will also add its own noise to the local oscillator signal. Experimentally, it was found that the majority of this noise is intensity noise at the relaxation oscillation frequency.

When a laser is disturbed during operation, its output power does not immediately return to its steady state, but rather exhibits so-called relaxation oscillations. The

frequency at which these damped oscillations occur is known as the relaxation oscillation frequency. Experimentally it was shown that, when free-running, the relative intensity noise (RIN) on the output of the Fabry-Perot laser peaks at approximately 2.5 GHz.

Coherent injection induced stimulated emission dominates spontaneous (random) emission. When the slave laser is injected, the relaxation oscillations are more strongly damped, and forced to a higher frequency. Furthermore, the relaxation oscillation frequency will shift towards a higher frequency as the intensity of the injected signal is increased [29]. This shift can be predicted by the laser rate equations (similar to those in Section 3.1), provided that we no longer ignore non-radiative excitation. For this, we would take into account the current pumping term for the slave laser, which can be represented by Langevin noise forces [30].

In order to test this phenomenon, the Fabry-Perot laser, whose threshold driving current is  $\sim 30\text{mA}$ , was driven with a current of  $100\text{mA}$ . Also, the gain curve of the Fabry-Perot laser was tuned so that its peak coincided with the wavelength of the injected signal (Figure 5.07). Figures 5.08 and 5.09 show the RF spectrum of the output of the slave laser given injected intensities of  $-6\text{dBm}$  and  $-12\text{dBm}$ . These figures demonstrate the frequency shift of the RIN as the intensity in the locking signal is varied.

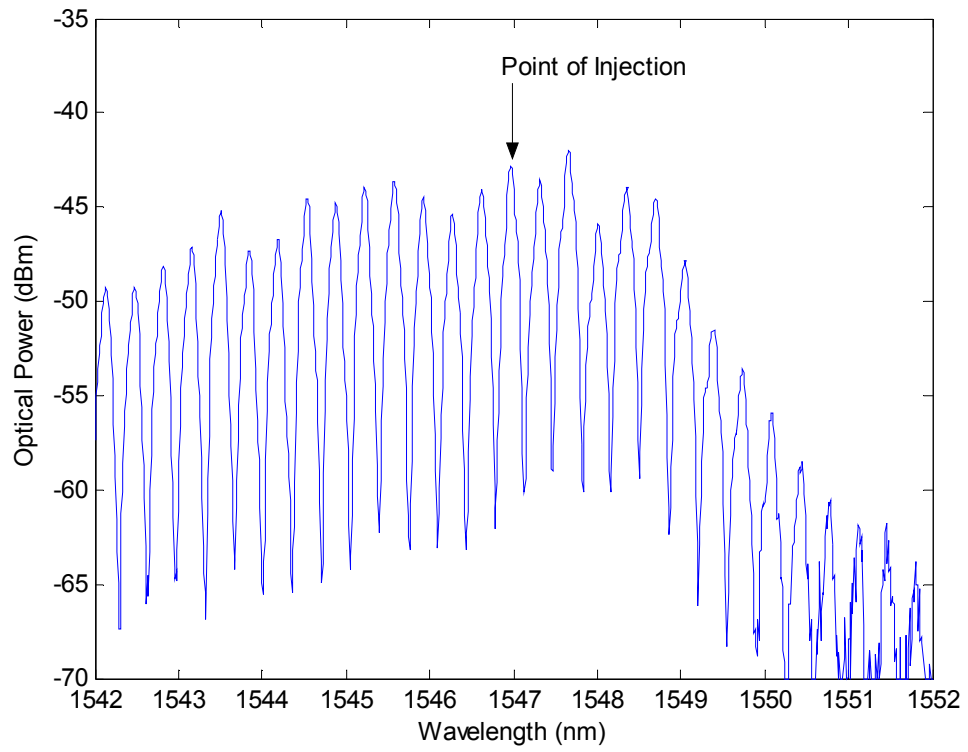


Figure 5.07 – Point of Injection for Received Optical Signal

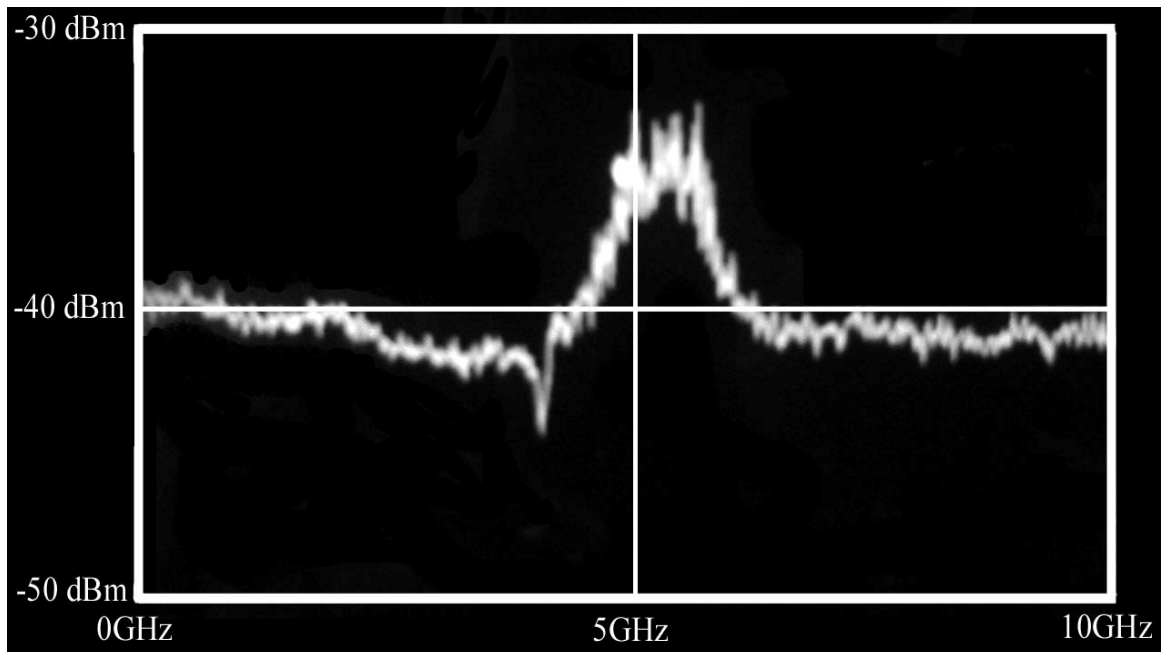


Figure 5.08 - RF spectrum on Output of Slave Laser (Injected Intensities = -6dBm)

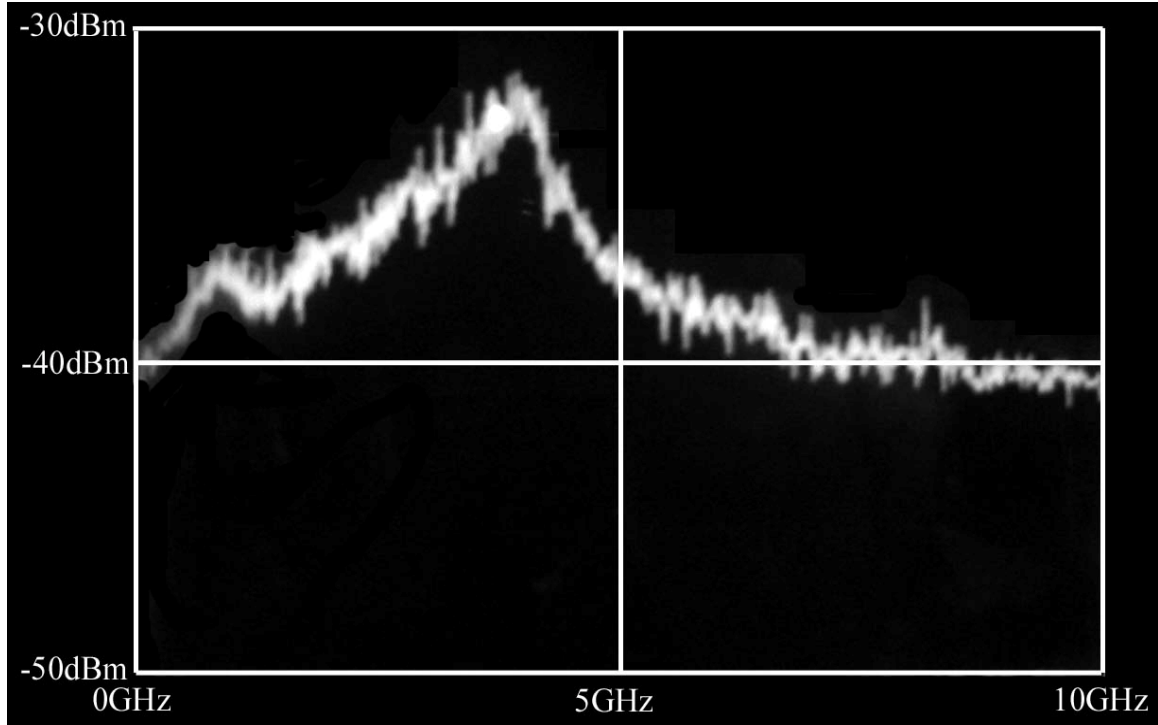


Figure 5.09 - RF spectrum on Output of Slave Laser (Injected Intensities = -12dBm)

Thus, in order to minimize the noise on the detected signal, the RIN on the local oscillator must be shifted to a frequency that is higher than the data rate of the received optical signal. The RIN must be shifted to a frequency that is greater than 2 times the data-rate in order to avoid in-band signal-RIN beat noise. Sufficiently shifted, the RIN can then be filtered off of the detected signal with the use of a low-pass filter.

To demonstrate RIN shift, we record the center of the RIN peak for various injected intensities, and compare this to the S/N ratio (ratio of power to variance), as recorded by a detector with a 1GHz bandwidth. This detector effectively ignores all noise at frequencies greater than 1GHz. Figures 5.10 and 5.11 show the results of this.

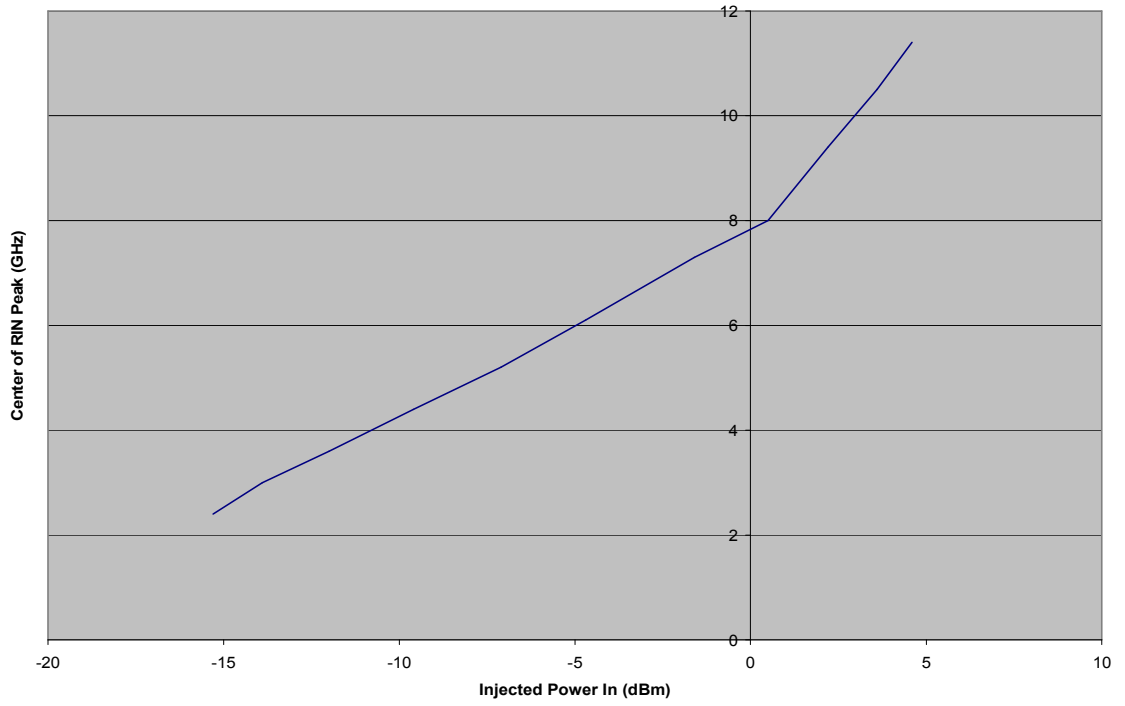


Figure 5.10 - Center of the RIN Peak for Various Injected Intensities

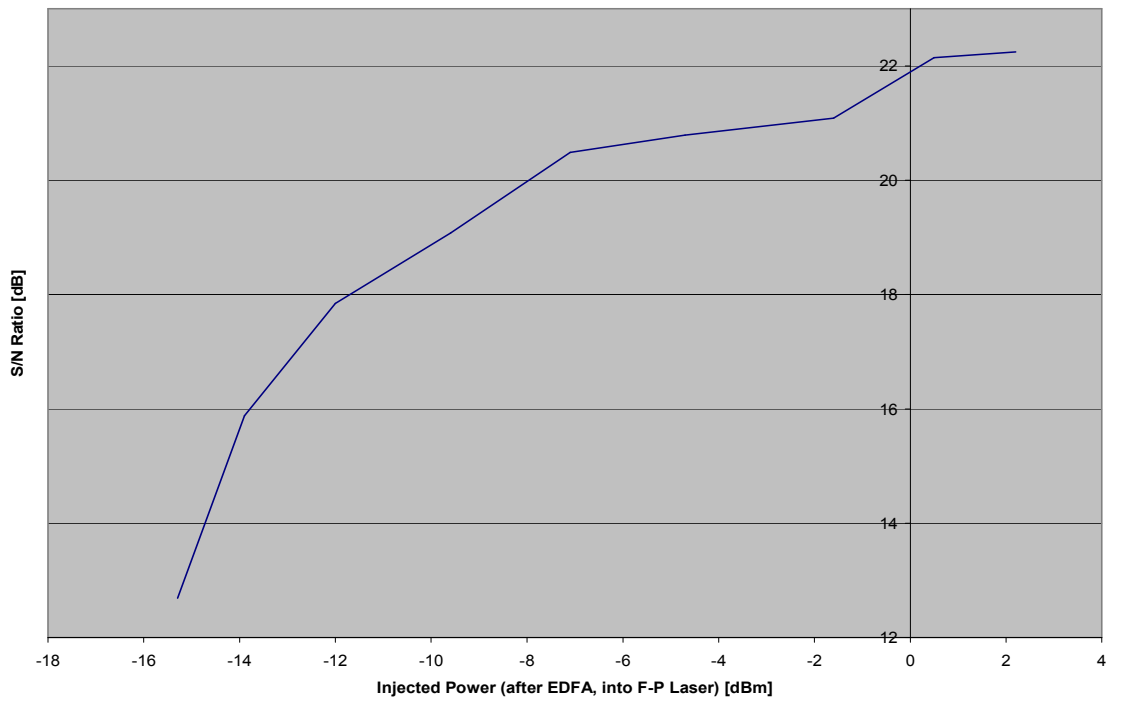


Figure 5.11 – S/N Ratio for Various Injected Intensities (As Seen on 1GHz Receiver)

As can be seen from these figures, a  $-8\text{dBm}$  injected signal will ensure a S/N ratio of more than 20dB (the desired S/N for our experimental system). This corresponds to a RIN peak of  $\sim 5\text{GHz}$ . The 5GHz RIN peak effectively generates 1GHz noise, due to the width of the RIN peak, as seen in Figure 5.09.

### 5.2.2 Modulation Transfer Ratio of the Fabry-Perot Laser

As was discussed in Section 4.3.1.4, the Fabry-Perot slave laser is capable of further suppressing amplitude modulation on the incident optical signal. The effectiveness of this suppression is dependant on the intensity of the injected signal. Figure 5.12 shows the modulation transfer function of the slave laser for various injected powers. For this case, the modulation frequency used is 128MHz, and the current used to pump the slave laser is approximately 100mA. From this, it can be seen that the intensity of the modulation on the output of the slave laser decreases as the injected intensity decreases. This indicates, just as the theory described in Section 4.3.1.4 predicted (depicted in Figure 4.02), that the Fabry-Perot slave laser is more effective at suppressing the incident modulation as the intensity of that incident modulation is decreased. However, as the injected intensity is decreased, the overall noise on the output of the slave laser, as well as the difficulty in maintaining the injection lock, is increased.

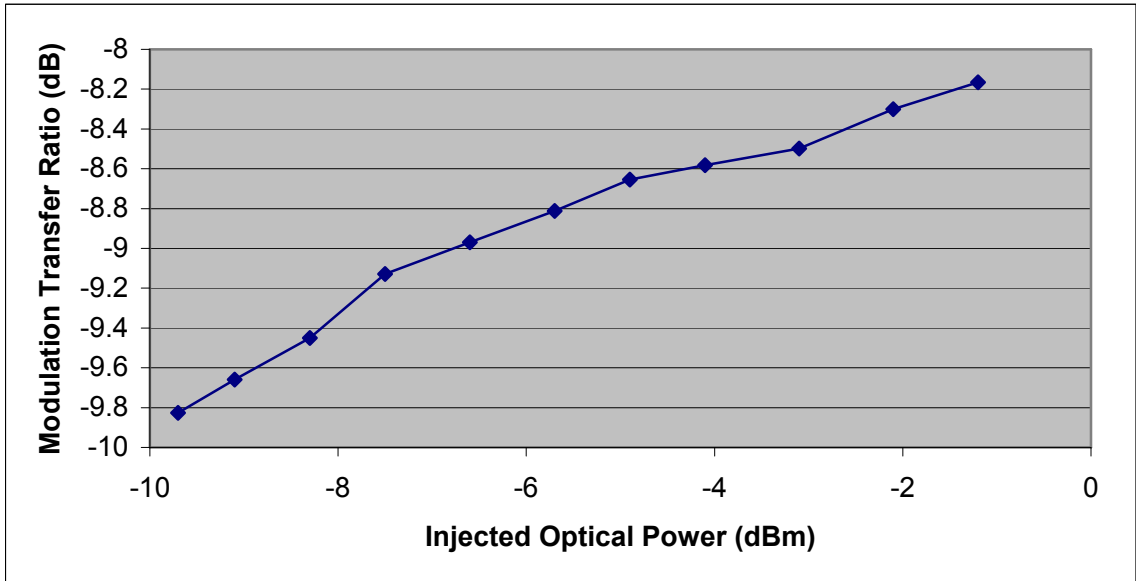


Figure 5.12 - MTR of Fabry-Perot Laser for Various Injected Powers (at 128MHz)

### 5.2.3 Linewidth of Fabry-Perot Laser

Before analyzing the output of the injection locked Fabry-Perot laser in further detail, it is useful to determine its linewidth. Since the linewidth of the laser is due to the phase variation on the output of the laser, the linewidth can serve as an indicator of how well the phase of the injected signal compares to the phase of the local oscillator signal. Ideally, the phase variation, and thus the linewidth, of the injected signal will be the same as the phase variation of the local oscillator signal. This implies that the phase of the output of the Fabry-Perot laser follows that of the injected signal.

The method of delayed-self heterodyne is used to measure linewidth, the setup for which depicted in Figure 5.13. The Fabry-Perot is first injected with a CW signal in order to force the slave laser into a single mode. The single-mode output of the slave laser is directed into the input of an Acousto-Optic (AO) modulator. The AO modulator has two outputs, the 0<sup>th</sup> order output and the 1<sup>st</sup> order output. The 0<sup>th</sup> order output is at

the same frequency as the input, while the 1<sup>st</sup> order output is shifted by the acoustic frequency, which in this case is 400MHz. The first order output is then transmitted through a 100km delay line, after which it is beat with the 0<sup>th</sup> order output from the AO modulator at a detector. The output from the detector is monitored on a RF spectrum analyzer.

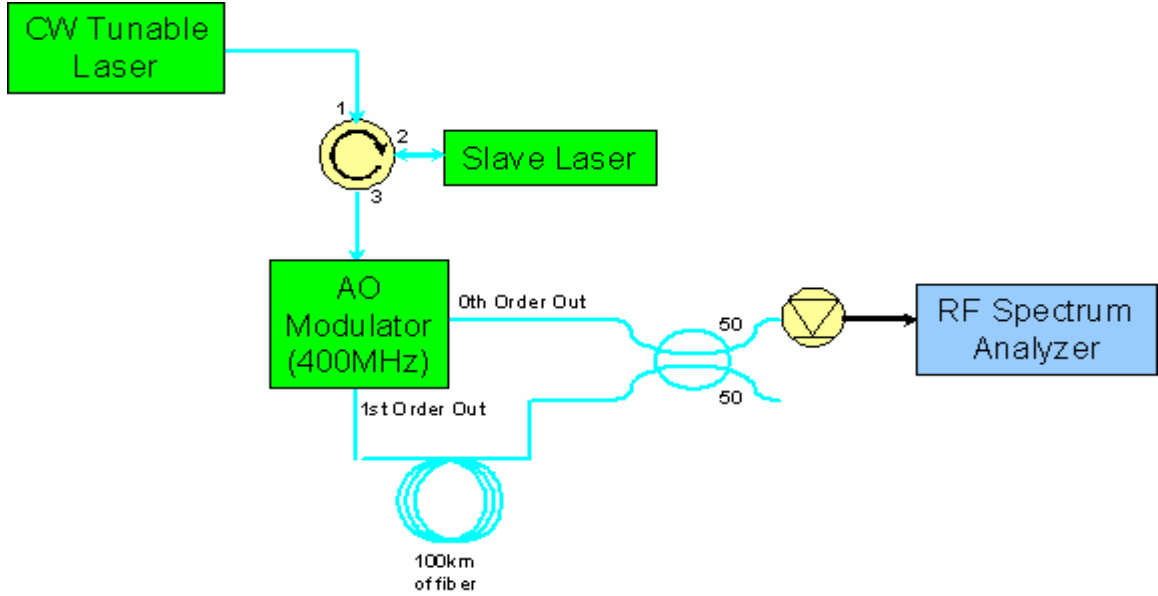


Figure 5.13 – Layout for Testing Linewidth of Fabry-Perot Laser

If it is assumed that the lineshape of the output of the Fabry-Perot laser can be approximated as a Lorentzian lineshape, then the power spectral density of the output of the detector can be expressed as [28]:

$$S = \frac{\frac{1}{2} P_0^2 t_c^2}{1 + (\omega \pm \Omega)^2 t_c^2} \left\{ 1 - e^{-|t|/t_c} \cdot \left[ \cos(\omega \pm \Omega)|t| + \frac{\sin(\omega \pm \Omega)|t|}{(\omega \pm \Omega)t_c} \right] \right\} + \frac{1}{2} P_0^2 \pi e^{-|t|/t_c} \delta(\omega \pm \Omega) \quad (5.01)$$

where  $P_0$  is the signal power,  $t_c$  is the coherence length of the receiver signal,  $\Omega$  is the offset frequency (400MHz in this case), and  $t$  is the delay time due to the added length of fiber (100km in this case). Since the coherence length of the Fabry-Perot laser is much less than 100km, it can be assumed that the two mixed signals are mutually incoherent. In other words, by adding the 100km delay line we ensure that  $t \gg t_c$ . From this (and by noting that  $\omega > 0$ ), we can reduce (5.01) to:

$$S = \frac{\frac{1}{2} P_0^2 t_c^2}{1 + (\omega - \Omega)^2 t_c^2} \quad (5.02)$$

This power spectrum is a Lorentzian function whose FWHM is  $2/t_c$ . From this it can be seen that, given sufficient delay, the RF spectrum analyzer of the mixed signal is a Lorentzian function whose linewidth is double that of the linewidth of the laser itself [27, 28].

Figure 5.14 shows a total of three RF spectrums from the detector. The red curve is the spectrum of the signal that is injected into the Fabry-Perot laser. The blue and yellow curves are both spectrums of the output of the injection-locked Fabry-Perot laser, where the free-running frequency of the slave laser is either near the center of the locking range (yellow) or approximately mid-way between the center and edge of the locking range (blue). The optical spectrums for the yellow and blue RF curves are depicted in Figures 5.15a and 5.15b respectively, in which the intensity of the unwanted modes serve as an estimate of the difference between the free-running frequency of the slave laser and the frequency of the injected signal (as was discussed in Chapter 4). Additionally, Figure 5.16 depicts the RF spectrum of the unlocked Fabry-Perot laser.

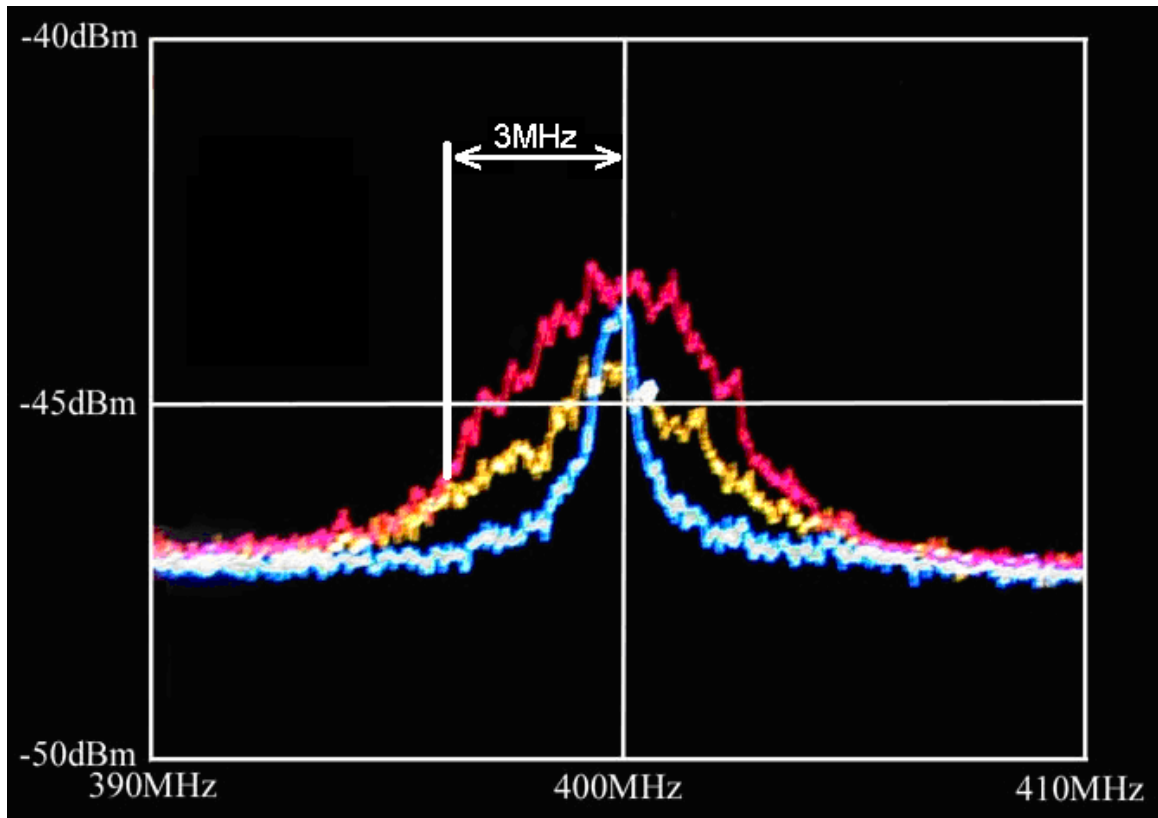


Figure 5.14 – RF Spectra of Heterodyne Mixing. Red = Injected Signal, Yellow = Strongly Locked FP Laser, Blue = Weakly Locked FP Laser

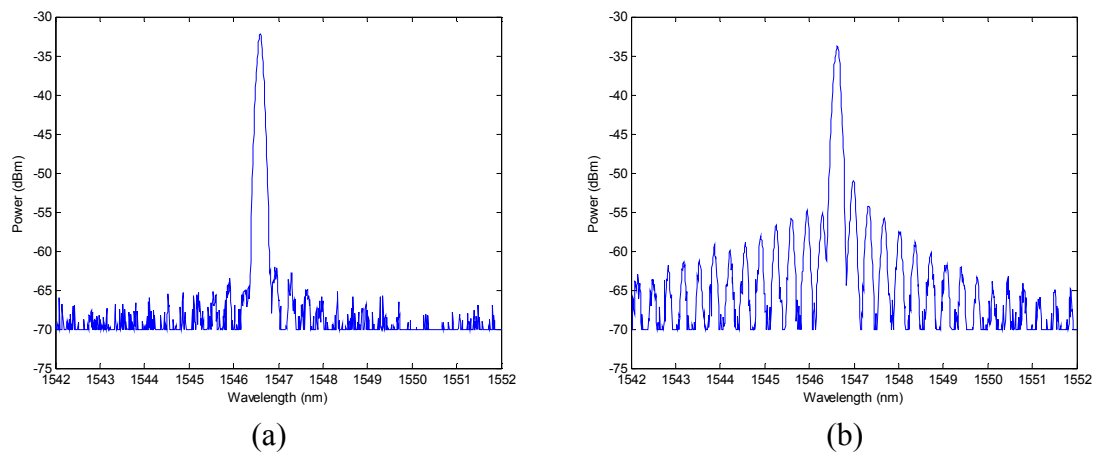


Figure 5.15 – Optical Spectrums for Strongly (a) and Weakly (b) Locked FP Laser

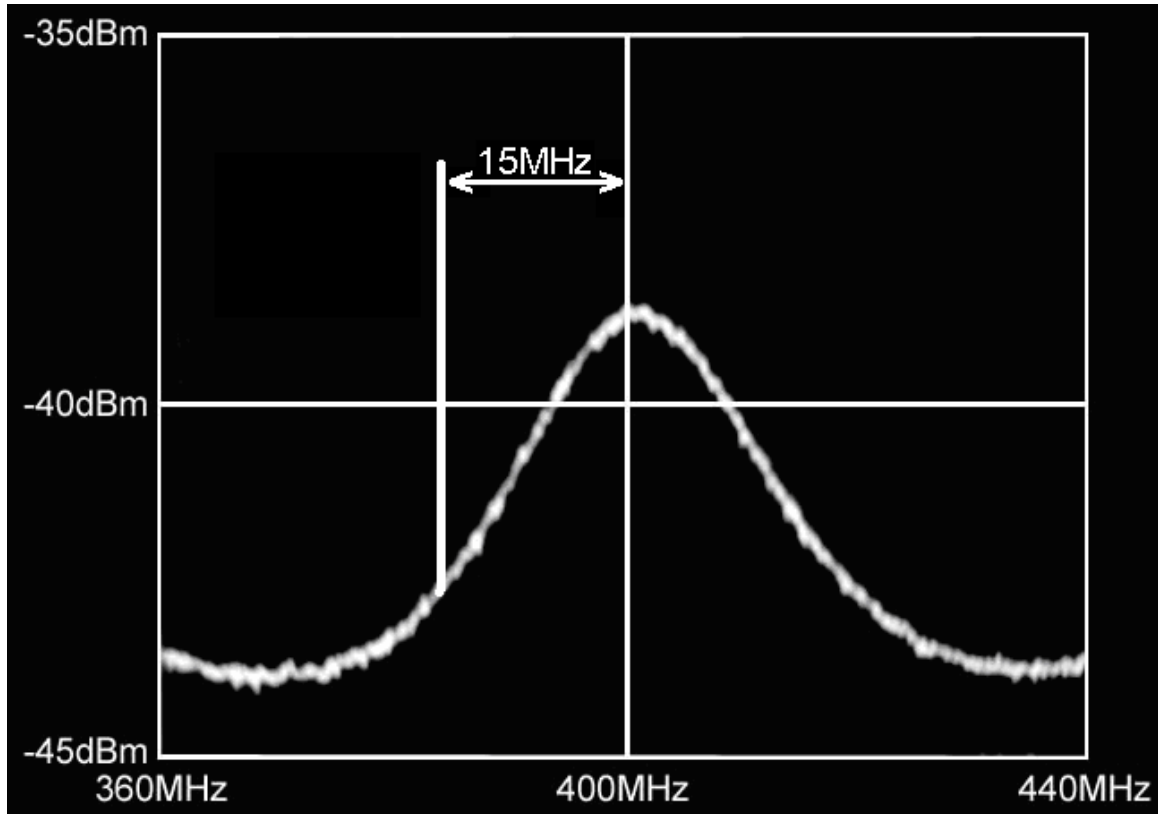


Figure 5.16 – RF Spectrum of Heterodyne Mixing of Unlocked Fabry-Perot Laser

As can be seen from Figures 5.14 and 5.16, as the free-running frequency of the slave laser approaches the center of the locking range, the output of the slave laser effectively tracks the phase of the injected signal, independent of its free-running linewidth. However, the linewidth of the output of the slave laser decreases as it is detuned, indicating a reduction in the level of the phase noise. This is detrimental to the generation of a suitable local oscillator, since it indicates that the generated signal is no longer phase coherent with the injected signal.

The small signal approximations of the laser rate equations predict that the phase noise on the output of the slave laser should always equal the phase noise on the injected signal. This discrepancy indicates that these equations are insufficient in predicting this

phase reduction effect, and a more detailed model will need to be implemented in the future.

#### 5.2.4 Phase Noise Generated by Amplitude Noise

As was done in Chapter 3 and 4, if we assume that  $r$  (the unsaturated gain to loss ratio) is a complex value

$$r = r_1 + ir_2 \quad (5.03)$$

and single-mode operation, then the laser rate equations, as in Chapter 3, can be written as:

$$\frac{d\phi}{dt} - \frac{r_2}{2\tau_c} + (\omega_1 - \omega_0) = -\frac{\gamma_e E_1}{E} \sin \phi \quad (5.04)$$

$$\frac{dE}{dt} + \frac{r_1 - 1}{2\tau_c} E = (\gamma_c - \gamma_m) E_1 \cos \phi = \gamma_e E_1 \cos \phi \quad (5.05)$$

$$\frac{dr_1}{dt} = P - r_1 \frac{1}{T_1} \left( 1 + \frac{I}{I_{sat}} \right) = P - r_1 \frac{1}{T_1} \left( 1 + \frac{E^2}{I_{sat}} \right) \quad (5.06)$$

Following the method used in Section 3.2.1.1, small perturbations are applied to  $E_1$ ,  $E$ ,  $r_1$ ,  $r_2$ , and  $\phi$

$$E_1 = E_{10} + \Delta E_1 \quad (5.07)$$

$$E = E_0 + \Delta E \quad (5.08)$$

$$r_1 = r_{10} + \Delta r_1 \quad (5.09)$$

$$r_2 = r_{20} + \Delta r_2 \quad (5.10)$$

$$\phi = \phi_0 + \Delta \phi \quad (5.11)$$

Once again, the phase factor is defined as

$$\alpha_\phi = \frac{\Delta r_2}{\Delta r_1} \quad (5.12)$$

Thus, the equations for  $d\Delta E/dt$ ,  $d\Delta r_1/dt$ , and  $d\Delta\phi/dt$  can be written to the 1<sup>st</sup> order as:

$$\frac{d\Delta E}{dt} + \frac{\Delta r_1}{2\tau_c} E_0 + \frac{r_{10} + \Delta r_1 - 1}{2\tau_c} \Delta E = \gamma_e (\Delta E_1 \cos \phi_0 - E_{10} \Delta\phi \sin \phi_0) \quad (5.13)$$

$$\frac{d\Delta r_1}{dt} = -\frac{1}{T_1} \left( \Delta r_1 + \frac{2E_0 \Delta E r_{10} + E_0^2 \Delta r_1}{I_{sat}} \right) \quad (5.14)$$

$$\frac{d\Delta\phi}{dt} - \frac{\alpha_\phi \Delta r_1}{2\tau_c} = -\frac{\gamma_e}{E_0} \left[ \Delta E_1 \sin(\phi_0) + E_{10} \Delta\phi \cos(\phi_0) - \frac{E_{10} \Delta E}{E_0} \sin(\phi_0) \right] \quad (5.15)$$

From Sections 3.2.1.1.3 and 4.3.1.4, we know that if the perturbations on  $E$ ,  $E_I$ ,  $\phi$ , and  $r_I$  are assumed to be harmonic, then the resulting modulation transfer function is only weakly dependant on the modulation frequency for low frequencies. Thus, we can assume that in the limit  $\Omega \rightarrow 0$ , the perturbations on  $E$ ,  $E_I$ ,  $\phi$ , and  $r_I$  can be modeled as a constant deviation that can be expressed as:

$$\Delta E_1 = A \quad (5.16)$$

$$\Delta E = B \quad (5.17)$$

$$\Delta\phi = C \quad (5.18)$$

$$\Delta r_1 = D \quad (5.19)$$

Substituting the results from (5.16-5.19) into (5.13-5.15) results in the following three equations:

$$0 = -\frac{1}{T_1} \left( D + \frac{2E_0 B r_{10} + E_0^2 D}{I_{sat}} \right) \quad (5.20)$$

$$0 = \frac{\alpha_\phi B \left( \frac{DE_0}{B} \right)}{2\tau_c E_0} - \frac{\gamma_e}{E_0} \left[ CE_{10} \cos \phi_0 + A \sin \phi_0 - B \frac{E_{10}}{E_0} \sin \phi_0 \right] \quad (5.21)$$

$$B \frac{\frac{DE_0}{B} + r_{10} - 1}{2\tau_c} = \gamma_e (-CE_{10} \sin \phi_0 + A \cos \phi_0) \quad (5.22)$$

If we then solve (5.22) for  $D$ , we get:

$$D = -\frac{2E_0 B r_0}{I_{sat} + E_0^2} \quad (5.23)$$

This equation can then be written as:

$$\frac{D}{B} = -\frac{2r_{10}E_0}{I_{sat} + E_0^2} \quad (5.24)$$

In addition, if we combine (5.21) and (5.22) for  $B$ , we get:

$$\frac{\gamma_e CE_{10} \cos \phi_0 + \gamma_e A \sin \phi_0}{\alpha_\phi \left( \frac{DE_0}{B} \right) + \frac{\gamma_e E_{10}}{E_0} \sin \phi_0} = \frac{-C\gamma_e E_{10} \sin \phi_0 + A\gamma_e \cos \phi_0}{\left( \frac{DE_0}{B} \right) + r_{10} - 1} \quad (5.25)$$

Eliminating  $D/B$  with (5.24) yields:

$$\frac{\gamma_e CE_{10} \cos \phi_0 + \gamma_e A \sin \phi_0}{-\frac{r_{10}E_0^2 \alpha_\phi}{I_{sat} + E_0^2} + \frac{\tau_c \gamma_e E_{10}}{E_0} \sin \phi_0} = \frac{-C\gamma_e E_{10} \sin \phi_0 + A\gamma_e \cos \phi_0}{-\frac{r_{10}E_0^2}{I_{sat} + E_0^2} + \frac{r_{10}}{2} - \frac{1}{2}} \quad (5.26)$$

from which:

$$C = \frac{\left( \frac{\cos \phi_0}{\frac{r_{10} - 1}{2} - \frac{r_{10} E_0^2}{I_{sat} + E_0^2}} - \frac{\sin \phi_0}{\frac{\tau_c \gamma_e E_{10}}{E_0} \sin \phi_0 - \frac{r_{10} E_0^2 \alpha_\phi}{I_{sat} + E_0^2}} \right)}{\left( \frac{E_{10} \sin \phi_0}{\frac{r_{10} - 1}{2} - \frac{r_{10} E_0^2}{I_{sat} + E_0^2}} + \frac{E_{10} \cos \phi_0}{\frac{\tau_c \gamma_e E_{10}}{E_0} \sin \phi_0 - \frac{r_{10} E_0^2 \alpha_\phi}{I_{sat} + E_0^2}} \right)} A \quad (5.27)$$

Given this and using (3.51), the magnitude of the phase modulation  $|C|$  can be plotted. Figure 5.17 depicts the magnitude of the phase modulation for various saturation intensities, while Figure 5.18 depicts this magnitude for various Henry-Alpha factor values. For these plots, the effective saturation intensity of the slave laser is assumed to be -10dBm, the perturbation on the injected electric field is assumed to be 5% (effectively a 10% perturbation on the intensity of the injected signal), the unsaturated cavity gain to loss ratio ( $r$  when  $E=0$ ) is assumed to be 2, the cavity lifetime ( $\tau_c$ ) is assumed to be  $5 \cdot 10^{-10}$  s, the carrier lifetime ( $T_I$ ) is assumed to be  $5 \cdot 10^{-10}$  s. The code for generating these plots is located in Appendix C.

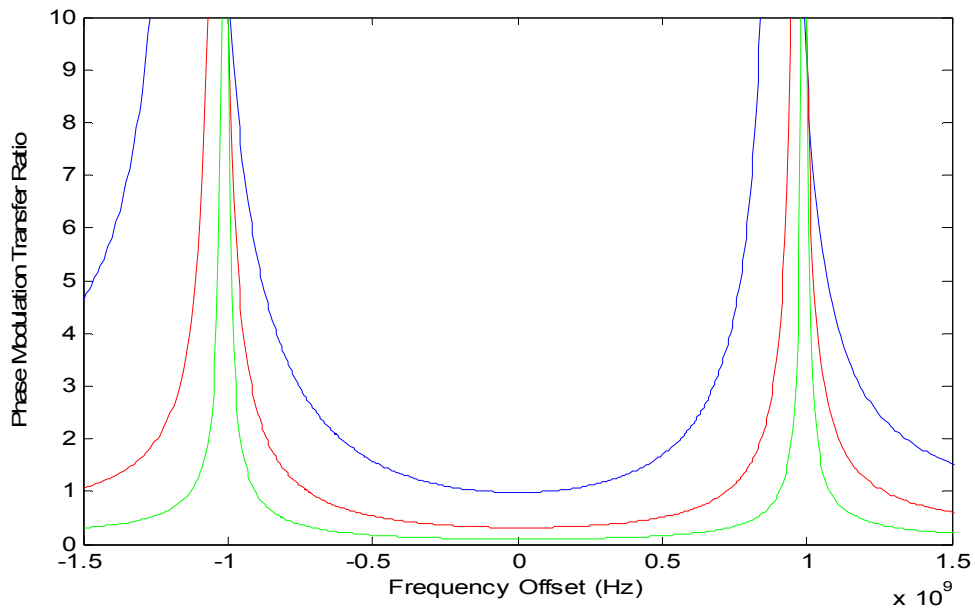


Figure 5.17 – Magnitude of Phase Noise over Locking Range [ $\alpha_H = 10$ ] for Saturation Intensities of -10dBm (blue), -15dBm (red), and -20dBm (green)

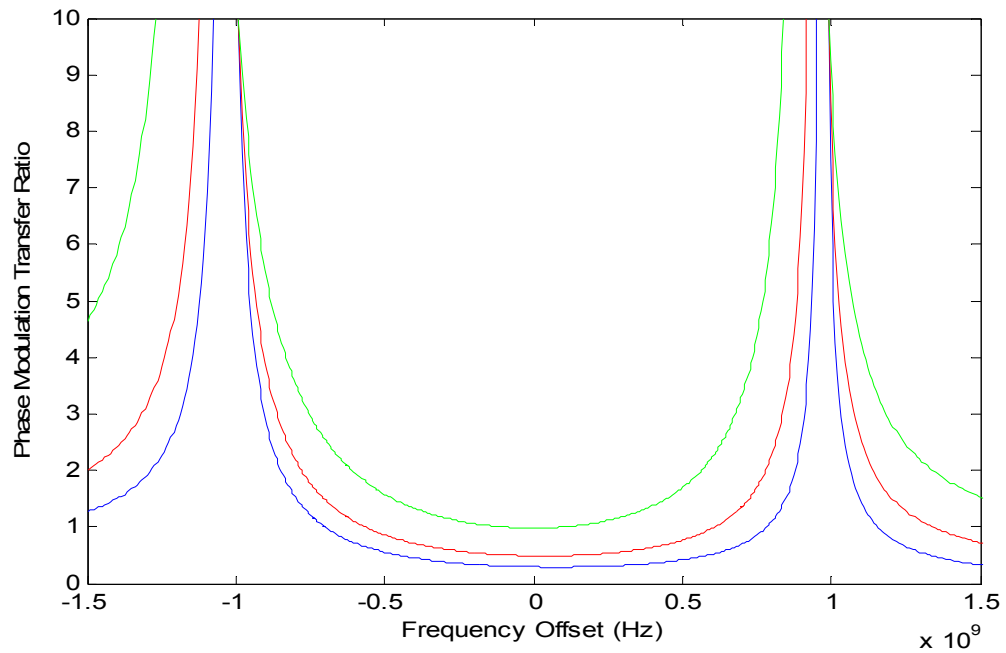


Figure 5.18 – Magnitude of Phase Noise over Locking Range [ $I_s = -10\text{dBm}$ ] for Henry-Alpha Factors of 3 (blue), 5 (red), and 10 (green)

From this, it can be seen that the phase transfer will be minimal at the center of the locking range. Additionally, the amount of phase noise that is generated by amplitude noise can be reduced by selecting a laser with either a low phase factor and/or with a low saturation intensity.

In order to measure the severity of the phase modulation on the output of the local oscillator signal due to suppressed amplitude modulation, we employ the configuration depicted in Figure 5.19. This setup is the same as the one depicted in Figure 5.13, except that now a 10%, 25MHz modulated signal is injected into the Fabry-Perot slave laser.

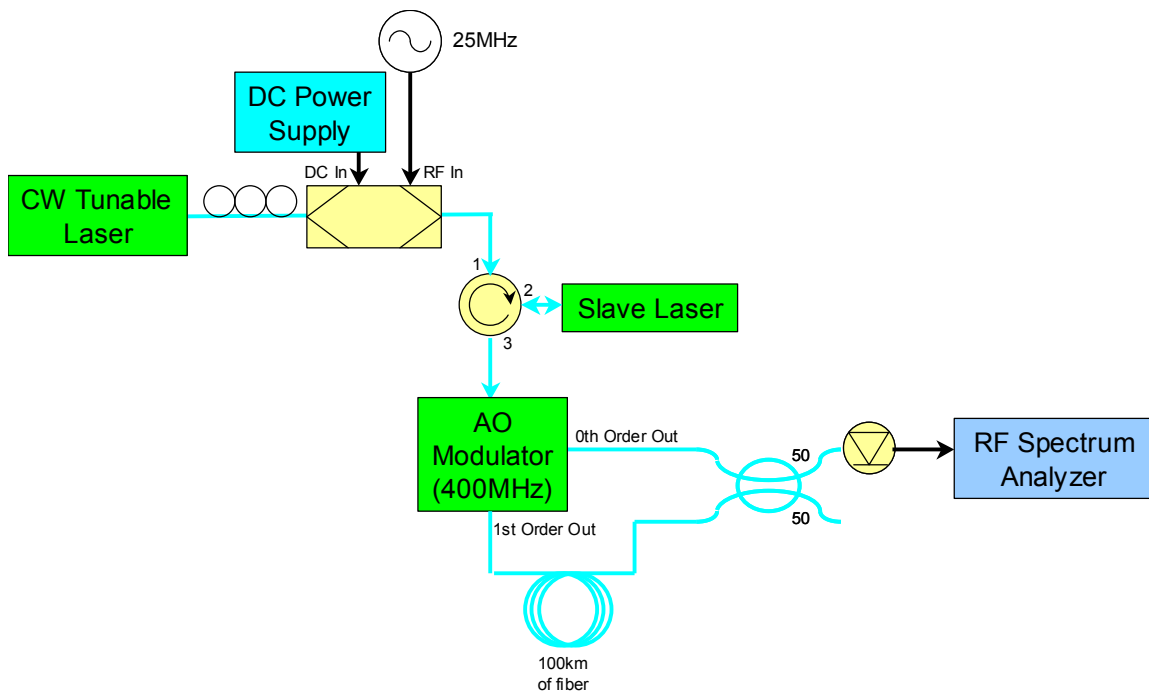


Figure 5.19 – Layout for Monitoring Total Modulation on Output of Fabry-Perot Laser

The resulting spectrum is depicted in Figure 5.20. In this, the yellow line represents the spectrum of the injected signal, while the blue line represents the spectrum of the output of the injection locked slave laser (near the center of the locking range).

The ratio between the power of the center peak to the power of the sidebands indicates the total amplitude and phase modulation on the signal. In the case of the injected signal, all of this modulation is in the form of amplitude modulation. For the output of the injection locked Fabry-Perot laser, the total modulation on the signal is comparable to the total modulation on the injected signal. However, as was discussed in Section 5.2.2.2, the amplitude modulation is reduced by approximately 10dB by the injection locking process. This indicates that the phase noise added by the present process is comparable in magnitude to the amplitude modulation that was suppressed. In addition, we observed that the amount of phase noise on the output of the slave laser increases with detuning.

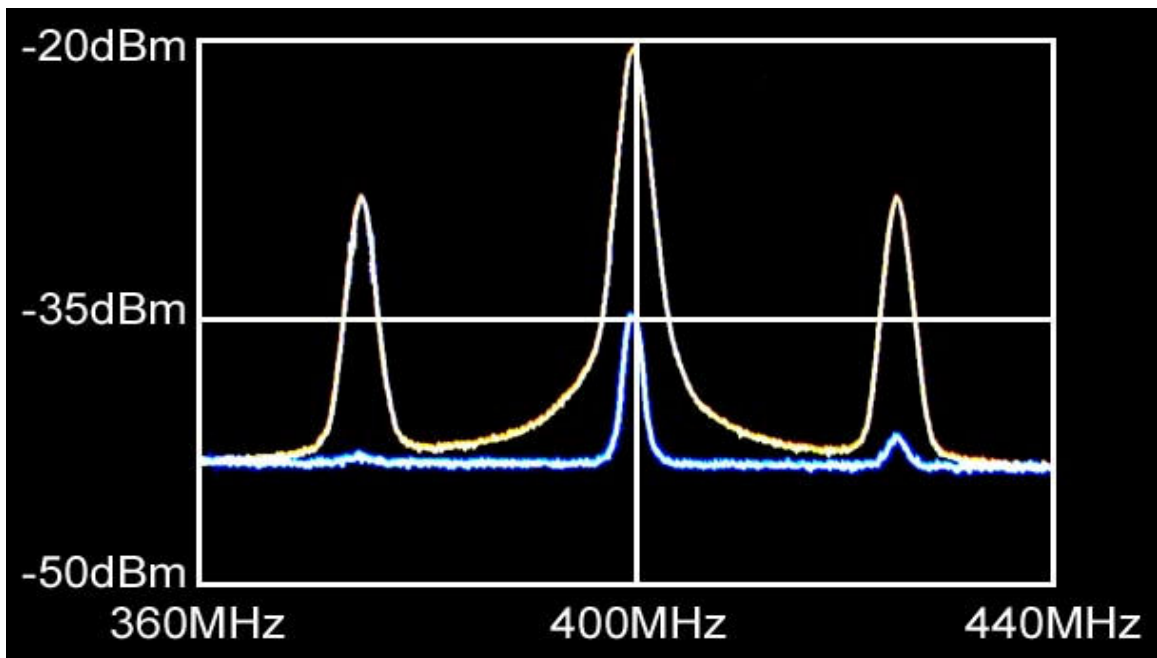


Figure 5.20 – RF Spectrums of Heterodyne Mixing. Yellow = Injected Signal, Blue = Strongly Locked FP Laser

The injection-locking process converts much of the incident amplitude noise to phase noise. However, a homodyne receiver is much less sensitive to this type of noise.

We can see this by first considering the signal from a homodyne receiver:

$$P = \sqrt{P_s P_{lo}} \cos(\phi_s - \phi_{lo}) \quad (5.28)$$

If it is assumed that the phase differences are small, then this can be re-written as:

$$P = \sqrt{P_s (P_{lo} + \Delta P_{lo})} \cos(\Delta \phi_{lo}) \quad (5.29)$$

where  $\Delta P_{lo}$  and  $\Delta \phi_{lo}$  is the amplitude and phase noise on the local oscillator signal, respectively. If it is assumed that assumed that the noise is small, then (5.29) can be re-written as:

$$P = \sqrt{P_s P_{lo}} \left( 1 + \frac{\Delta P_{lo}}{2 P_{lo}} \right) \left( 1 - \Delta \phi_{lo}^2 \right) \quad (5.30)$$

Eliminating the 3<sup>rd</sup> order term yields:

$$P = \sqrt{P_s P_{lo}} \left( 1 + \frac{1}{2} \frac{\Delta P_{lo}}{P_{lo}} - \Delta \phi_{lo}^2 \right) \quad (5.31)$$

Since the phase noise only affects the detected power in the second order, it can be neglected (assuming small modulation).

### 5.2.5 Phase Coherence Between Injected Signal and Fabry-Perot Laser Output

One of the requirements of a local oscillator signal is for it to be phase coherent with the received signal. To demonstrate this, an equi-path heterodyne interferometer, as depicted in Figure 5.21, was employed. In this, half of the received optical signal is injected into the Fabry-Perot laser. The output of the Fabry-Perot laser is then shifted by 400MHz and beat with the remaining portion of the received signal at a detector. The RF

spectrum of the output of the detector is then analyzed. The 50m delay line is added in order to compensate for the added fiber length that was required to generate the local oscillator signal.

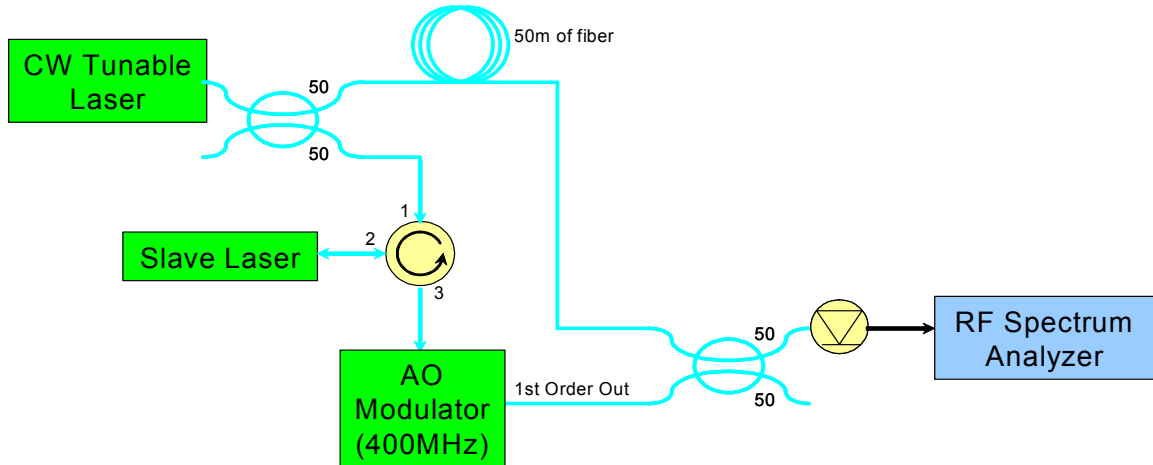


Figure 5.21 – Layout for Determining Phase Coherence Between Injected Signal and Fabry-Perot Laser Output

The linewidth of the resulting RF spectrum indicates the fluctuations between the phases of these two signals. Figure 5.22 shows three of these RF spectrums, given injected powers of -16dBm (yellow plot), -44dBm (blue plot), and -62dBm (red plot). From the previous section we know that, if the phases of the two signals are incoherent with each other, the observed RF linewidth will be approximately 4MHz wide, as was the red plot in Figure 5.14. Instead, the yellow plot of Figure 5.22 shows a linewidth that is less than 300Hz. This indicates that the received and local oscillator signals are strongly phase coherent. The residual phase variation (the phase noise within the 300Hz bandwidth) is either due to thermal or acoustic fluctuations in the optical fiber, and can be compensated for by implementing a phase tracking feedback loop, by isolating the system from thermal and/or acoustic sources, or by reducing the lengths of fiber used in

the system. If a phase tracking system is used, the yellow plot in Figure 5.22 indicates that this feedback system will need to track the phase difference between the two signals as speeds greater than 3.3ms.

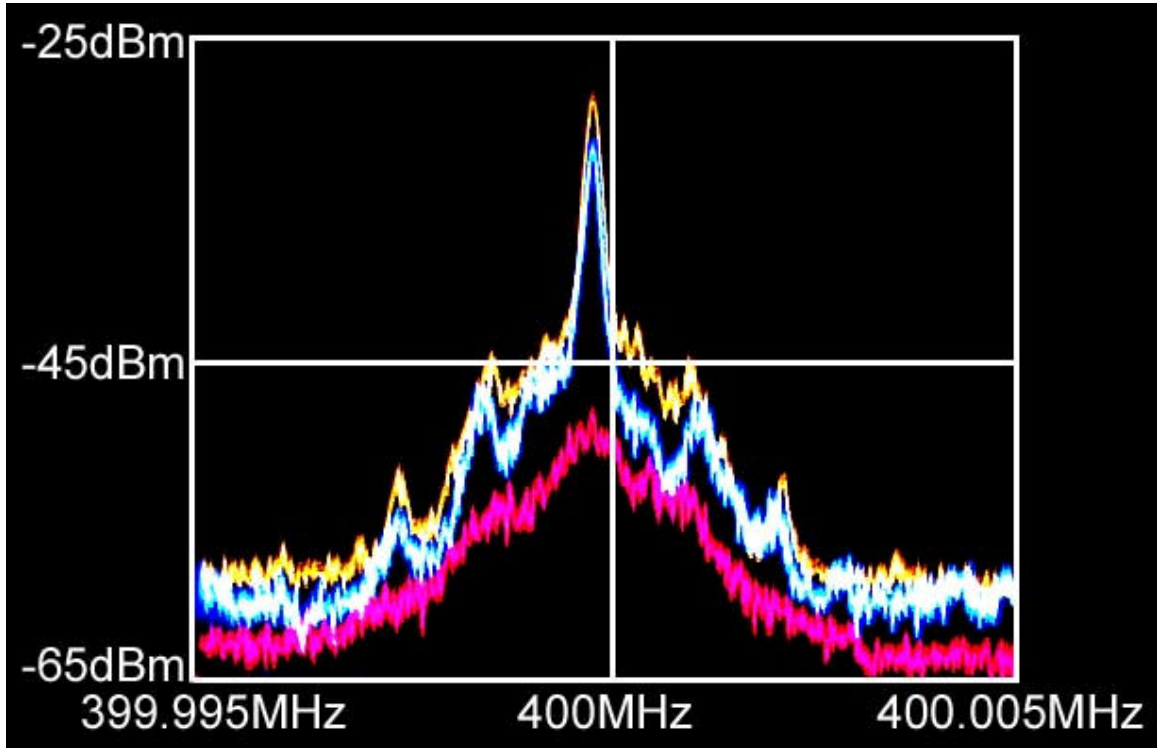


Figure 5.22 – RF Spectrum of Heterodyne Mixing for Various Injected Powers

By varying the injected power, we are able to determine the minimum input power that is required to maintain coherence with the received optical signal. Figure 5.23 depicts the peak of the RF linewidth for various injected powers. From both Figures 5.22 and 5.23, we can see that, given injected powers of more than approximately -35dBm (yellow plot in Figure 5.22), the received and local oscillator signals are coherent with each other. At an injected power of approximately -40dBm (blue plot in Figure 5.22), the slave laser begins to lose coherence with the received optical signal. At injected powers

of less than -50dBm (red plot in Figure 5.22), the local oscillator signal is no longer coherent with the received signal.

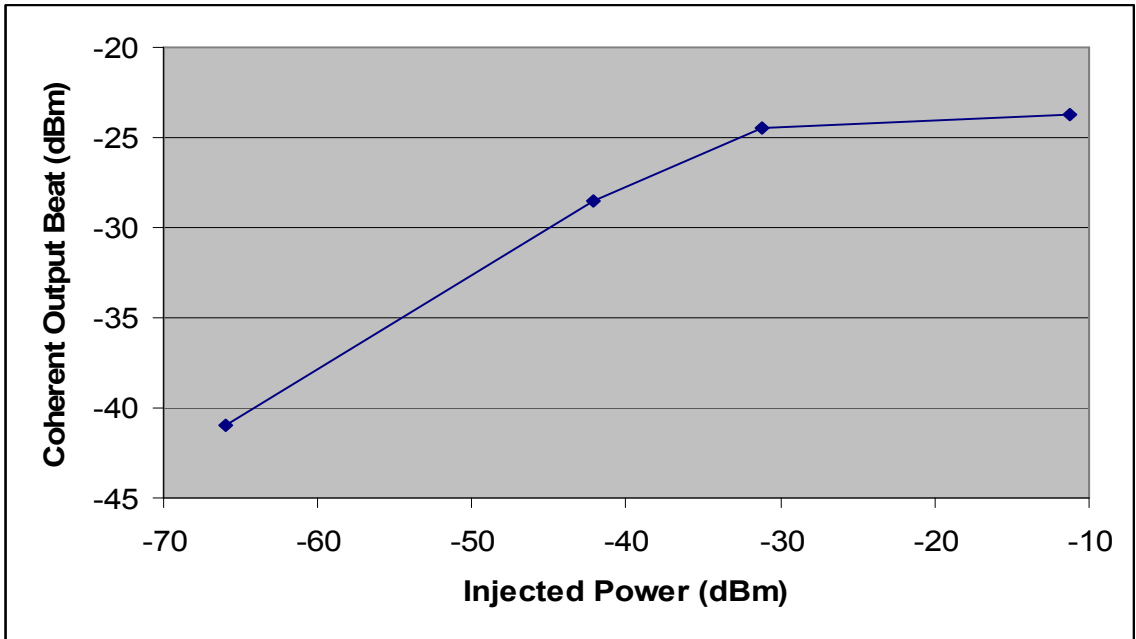


Figure 5.23 – Peak of RF Spectrum of Heterodyne Mixing for Various Injected Powers

### 5.2.6 Gain of the Fabry-Perot Laser

Since we are effectively using the Fabry-Perot laser as a regenerative optical amplifier, it is important to know its effective coherent gain. Assuming that the free-running frequency of the slave laser is centered in the locking range, it is expected that the gain of the Fabry-Perot laser will be strongly dependent on the intensity of the injected signal. Specifically, it is expected for the gain to increase as the injected power decreases.

In order to determine the gain of the Fabry-Perot laser, the layout depicted in Figure 5.21 (from the previous section) was used to monitor the output power of the coherent signal. Figure 5.24 shows this gain for varying injected powers. In this case,

the current used to pump the slave laser is approximately 120mA. From this it can be seen that the gain of the Fabry-Perot slave laser increases as the injected intensity decreases. However, just as in the case of the modulation transfer ratio of the slave laser, both the overall noise on the output of the slave laser and the difficulty in maintaining the injection lock increases as the injected intensity is decreased.

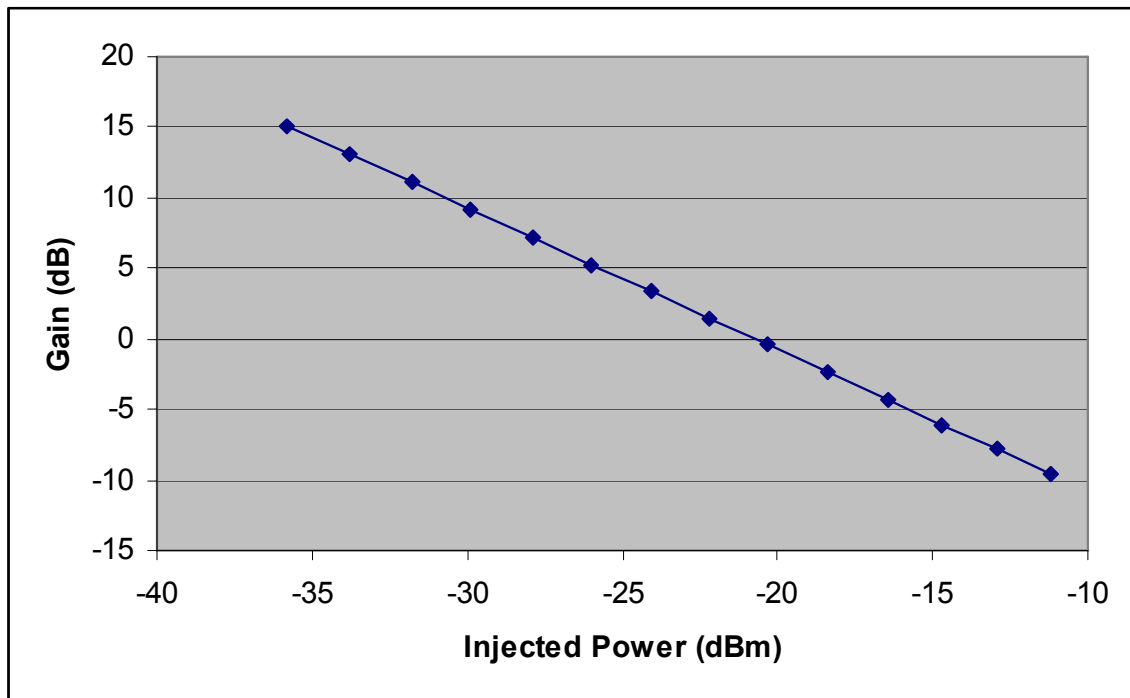


Figure 5.24 - MTR of Fabry-Perot Laser for Various Injected Powers (at 128MHz)

### 5.2.7 Parasitic Oscillations

In order to effectively injection lock the Fabry-Perot laser, the laser must be manufactured without internal isolators. One common problem that can occur as a result of this is parasitic oscillations. Specifically, if a small amount of backscatter is present

after the output of the laser, it is capable of creating additional oscillating modes. This effect is illustrated in Figure 5.25.

In order to detect the noise due to parasitic oscillations, we introduce a small point of reflection between the slave laser and port #2 of the circulator. This will create an oscillator between this point and the slave laser, which will generate a series of modes spaced approximately 70 MHz apart in frequency space.

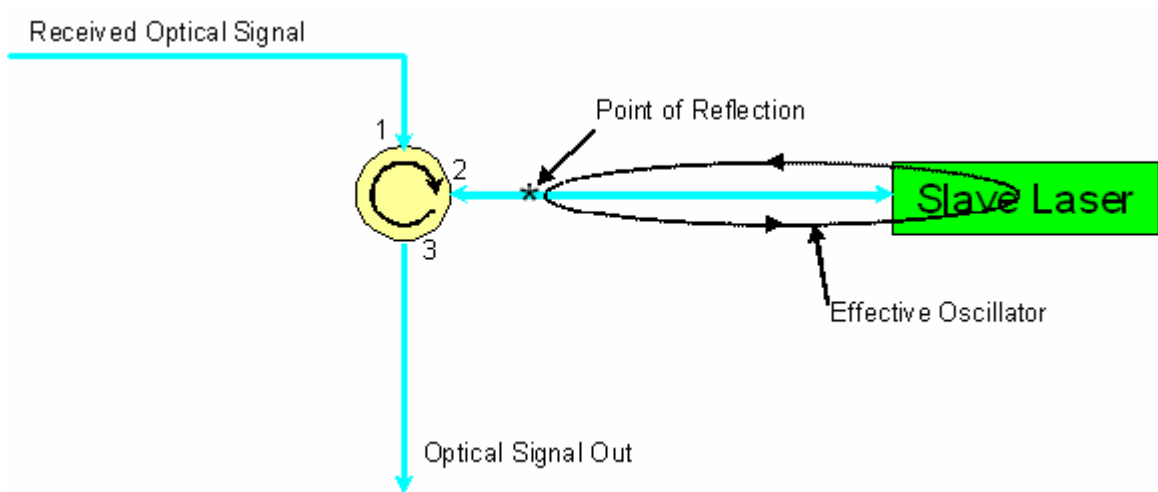


Figure 5.25 – Source of Additional Oscillatory Modes

Figures 5.26-5.28 show the optical and RF spectrums from the injection locked slave laser, at injected intensities of -20dBm (Figure 5.26), -30dBm (Figure 5.27), and -40dBm (Figure 5.28). For this the Fabry-Perot laser, whose threshold driving current is ~30mA, was driven with a current of 200mA. Also, the gain curve of the Fabry-Perot laser was tuned so that its peak coincided with the wavelength of the injected signal (Figure 5.07). As can be seen from these figures, the intensity of the unwanted modes varies inversely with the intensity of the received optical signal. Also, the 70MHz peaks vary by approximately the same amount as the unwanted modes. Thus, similar to the

case of RIN, the effect of this noise on the local oscillator signal can be minimized by using a sufficiently strong received optical signal. In this case, the amplified received optical signal power must be greater than -30dBm. However, this power depends on the amount of backscatter present, as well as the magnitude of the electrical current used to pump the slave laser.

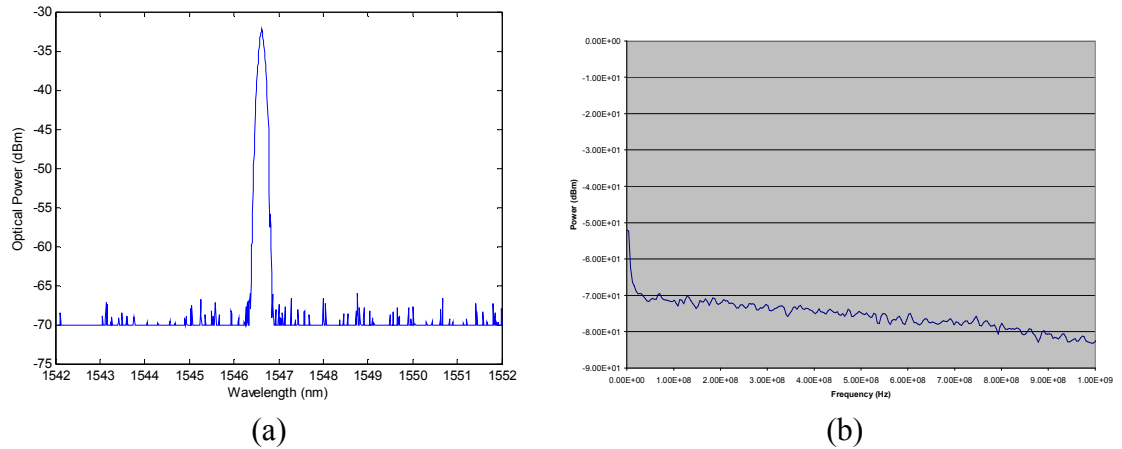


Figure 5.26 – Optical (a) and RF (b) Spectrum from Fabry-Perot laser (pumped at 200mA – Injected near peak of gain curve) with an injected power of -20dBm

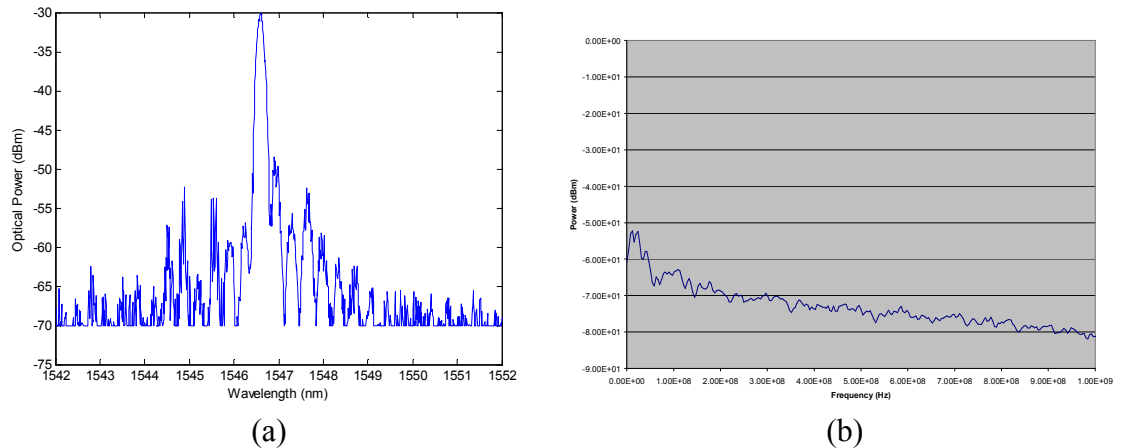


Figure 5.27 – Optical (a) and RF (b) Spectrum from Fabry-Perot laser (pumped at 200mA – Injected near peak of gain curve) with an injected power of -30dBm

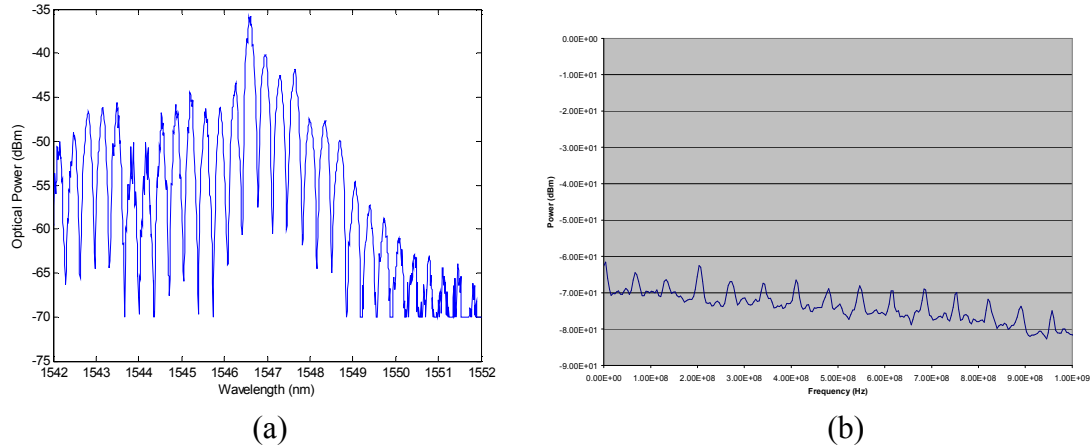


Figure 5.28 – Optical (a) and RF (b) Spectrum from Fabry-Perot laser (pumped at 200mA – Injected near peak of gain curve) with an injected power of -40dBm

### 5.3 Modulation Suppression as a Function of Modulation Frequency

As was discussed in Section 4.4, injection locking theory predicts that the modulation transfer ratio of the Fabry-Perot laser is weakly dependent on the modulation frequency. In order to confirm this, the modulation transfer ratio of the Fabry-Perot laser was recorded at frequencies ranging from 1MHz to 200MHz. Figure 5.29 shows the results of this, given an injected power of -1dBm. Additionally, Figure 5.30 shows the results of this, given an injected power of -10dBm. From these two graphs, it can be seen that, unlike what is predicted by the theory, the modulation transfer ratio of the Fabry-Perot laser increases at a modulation frequency of approximately 50MHz.

The cause of this breakdown in the theory of the modulation transfer ratio is most likely due to the influence of thermal vibrations within the laser cavity. Previous studies have shown that thermal effects will have an effect on frequencies that are below a specific threshold, typically between 1MHz and 100MHz [31]. These thermal effects most likely aid in the suppression of the incident modulation at lower modulation frequencies. As a result, in order to effectively use the Fabry-Perot laser as an ultra low-

bandwidth filter, it may be necessary to combine it with a 50MHz Fabry-Perot filter. This would be used to uniformly suppress the incident modulation at all modulation frequencies.

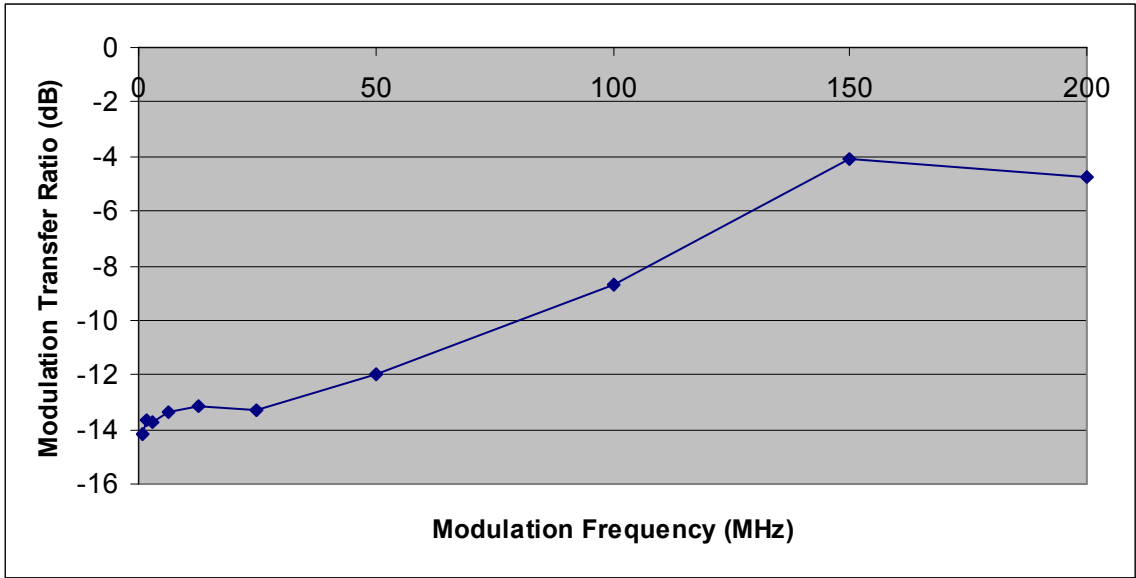


Figure 5.29 – MTR vs. Modulation Frequency (Injected Power = -1dBm)

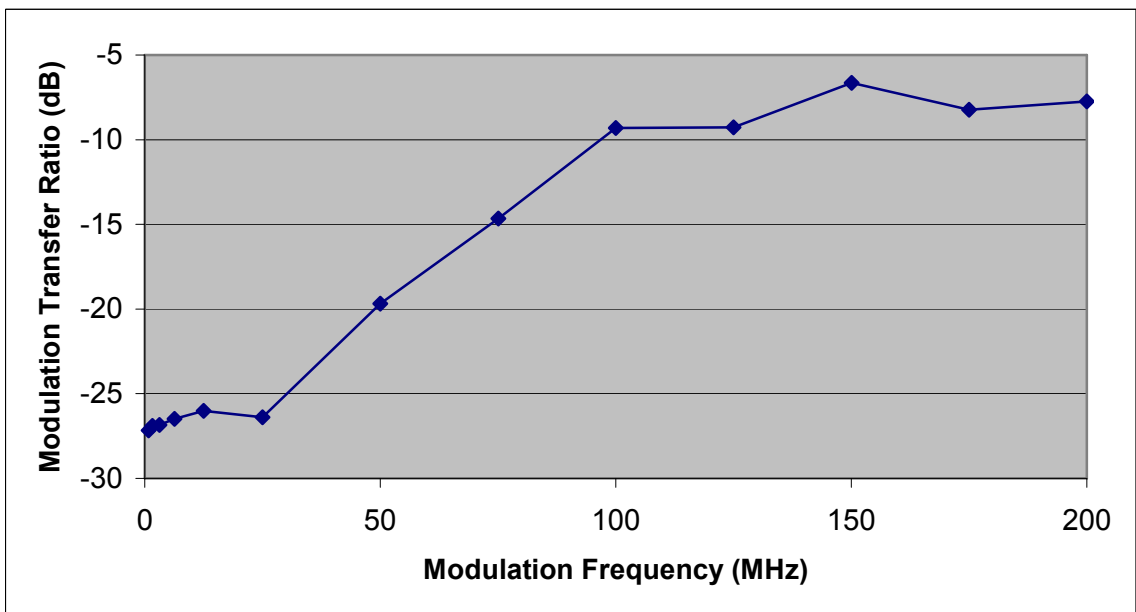


Figure 5.30 – MTR vs. Modulation Frequency (Injected Power = -10dBm)

## 5.4 Generating a Local Oscillator Signal

Now that the quality of the local oscillator signal has been established, we can generate a local oscillator signal. The layout for the local oscillator generator is depicted in Figure 5.31. In this, 10% of the received optical signal is diverted into an EDFA, which is followed by a 20MHz Fabry-Perot optical filter. In order to lock the center frequency of the filter to the received signal, the feedback loop previously described in Chapter 2 (Section 2.2) is implemented. After the filter, the signal is re-amplified via a second EDFA, and diverted into an optical modulator. The purpose of this modulator is to apply the 100kHz modulation that will be used to implement the feedback control loop for the injection lock, as was discussed in Chapter 3 (Section 3.2.3) and Chapter 4 (Section 4.3.5). From the modulator, the signal is directed into the Fabry-Perot slave laser via a circulator. The output of the slave laser can then be used as the local oscillator signal.

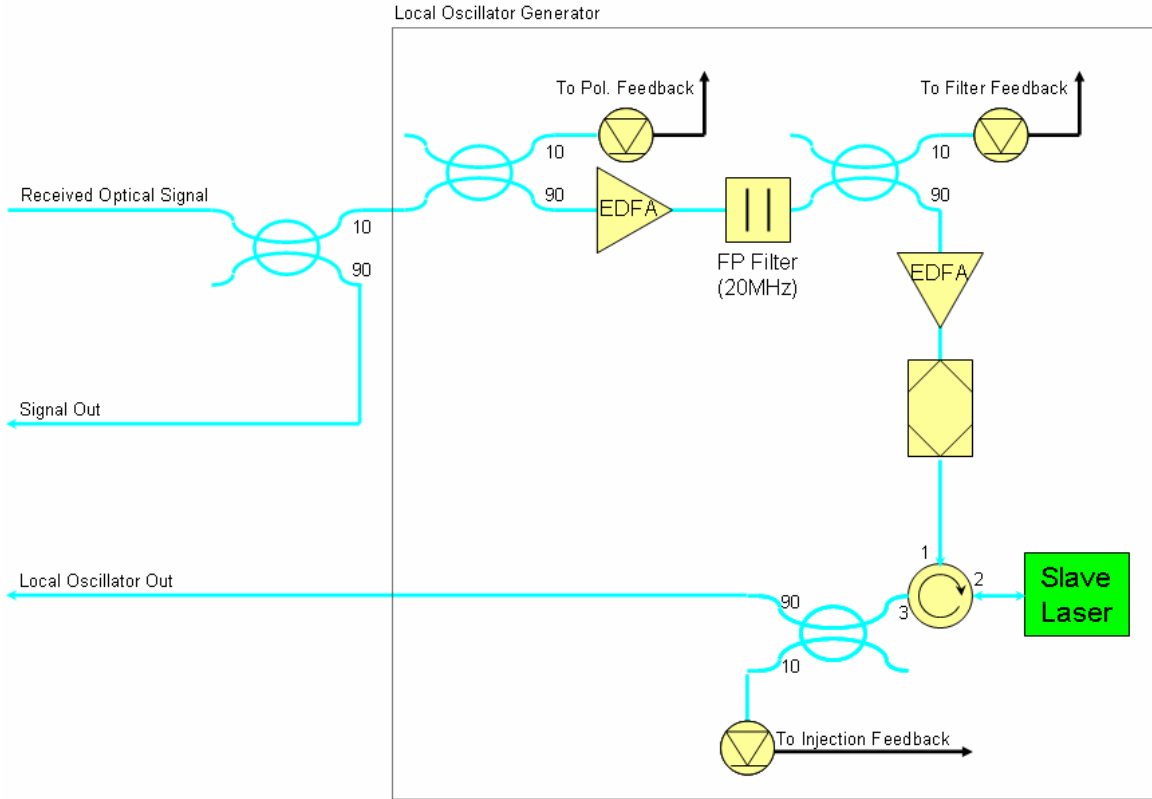


Figure 5.31 – Layout of Local Oscillator Generator (Feedback Loops Omitted)

## VI. CHAPTER 6 – Design of Homodyne Receiver

The primary goal for this project is the creation of a practical homodyne receiver for use with high-speed optical transmissions. Specifically, we are creating a stand-alone, rack-mountable, receiver. In order to do this, the feedback loops for both the filter and the injection lock must be implemented without the use of rack-mountable lock-in amplifiers and laser controllers. Also, a phase lock should be implemented, so that the receiver can be used in an environment that is not as precisely temperature controlled as the one in the experiment. Finally, for a practical homodyne receiver, the receiver itself must be capable of initiating itself, automatically obtaining the filter and injection locks.

### 6.1 Phase Locking

The phase of the received and local oscillator signals must be aligned for the homodyne receiver to achieve maximum sensitivity. In order to accomplish this, a feedback system will be required to align the phases of these two signals together.

#### 6.1.1 Background

As discussed in Chapter 1, the magnitude of the resulting signal from this detector is dependant on the phase difference between the two signals. Specifically, the signal from the overall receiver can be described as:

$$P = \sqrt{P_s P_{lo}} \cos(\phi_s - \phi_{lo}) \quad (6.01)$$

In this,  $P_s$  and  $P_{lo}$  are the powers of the signal and local oscillator, respectively, and  $\phi_s$  and  $\phi_{lo}$  are the phases of the signal and local oscillator, respectively.

In order to create the phase locked loop, the setup depicted in Figure 6.01 can be created. In this, a phase shifter is added to one of the arms of the interferometer. A 10kHz modulation can then be added to the phase shifter, along with the output of a lock-in amplifier. A portion of the received signal from the detector is then input to this lock-in amplifier whose reference signal is the 10kHz modulation. The lock-in amplifier will effectively filter off the high-frequency data from the received signal, and its in-phase output (X) will be the derivative of the sinusoidal signal of (6.01).

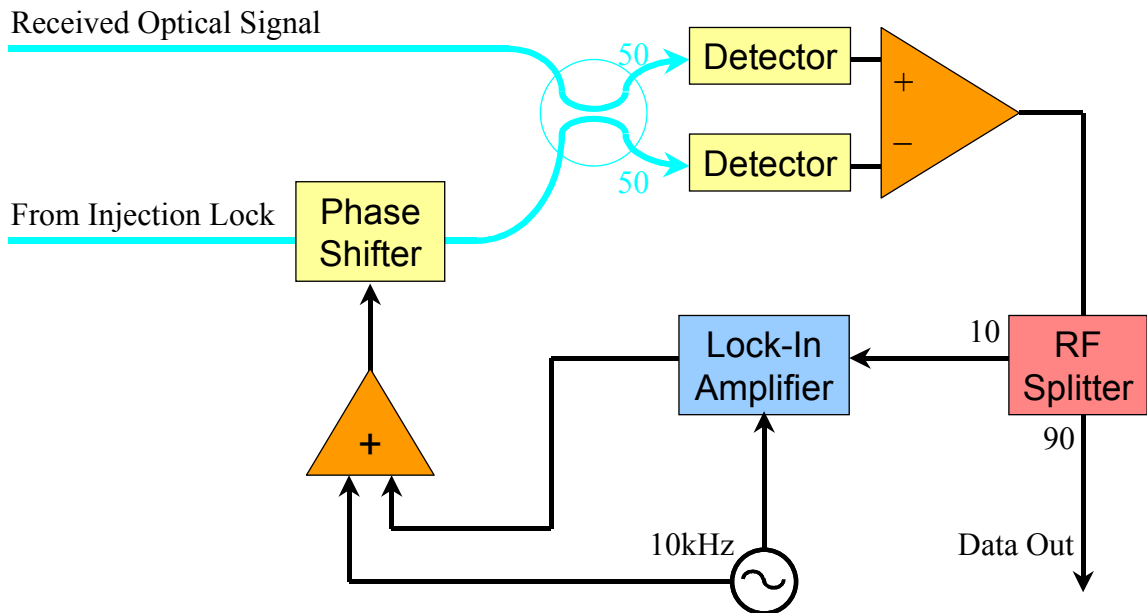


Figure 6.01 – Layout of Phase-Locked Loop

## 6.2 Practical Feedback Systems

More practical versions of the filter, and injection, and phase lock feedback loops are depicted in Figures 6.02-6.04. These layouts differ from the ones depicted in Figures 2.02, 4.12, and 6.01 in that a microcontroller has now been added to the systems. The purpose of the microcontroller is to automate the initial lock. After the microcontroller

has found the correct bias to apply to the filter, it will hold that position, and allow the lock-in amplifier to maintain the filter lock.

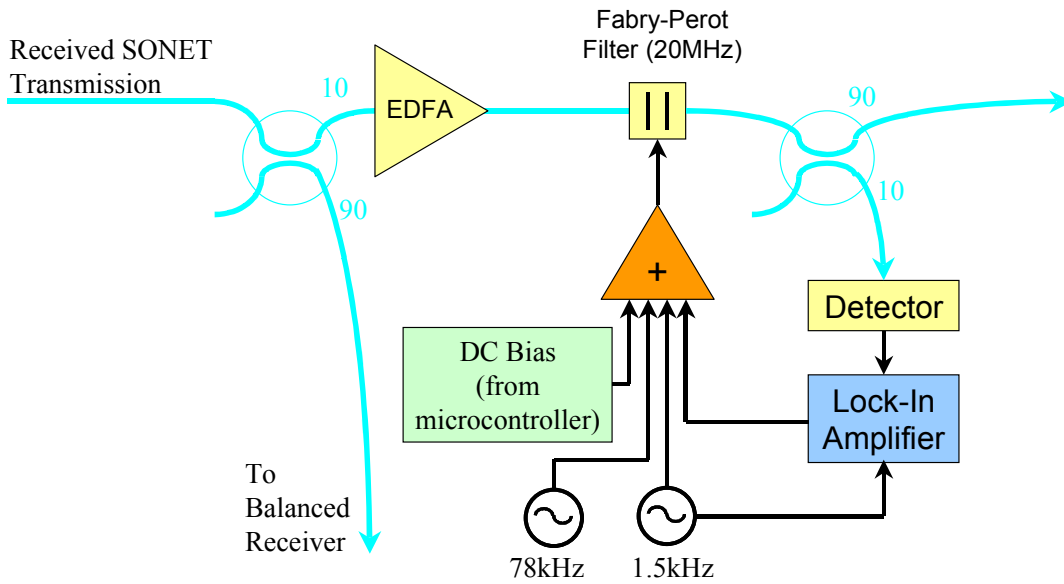


Figure 6.02 – Practical Filter Feedback Loop

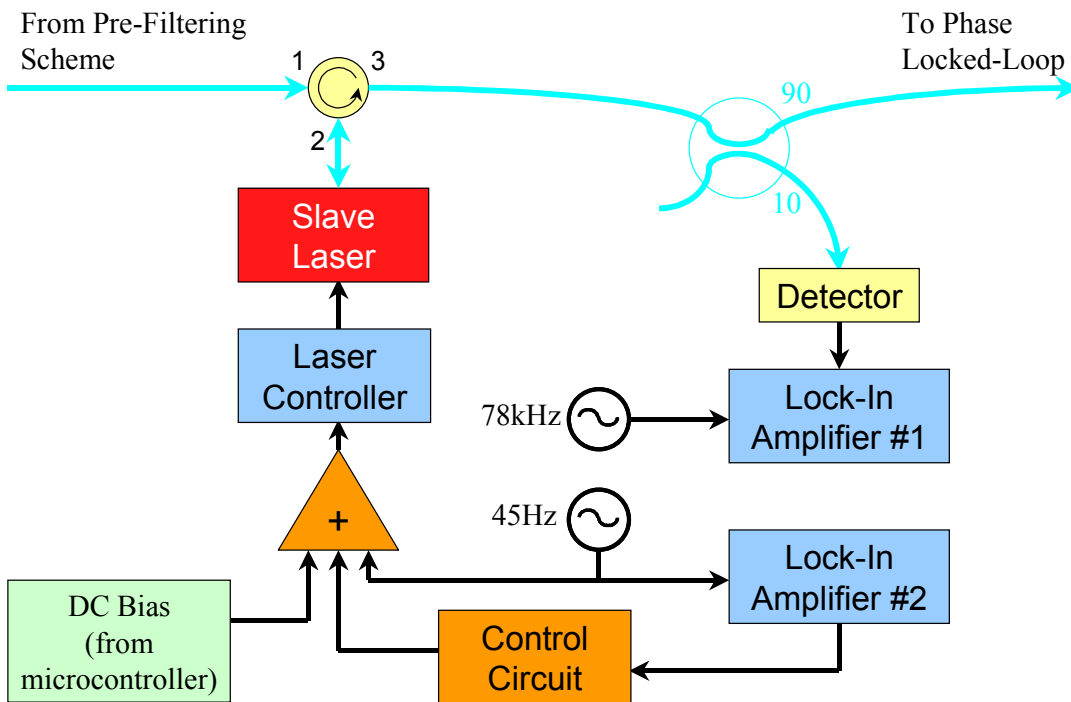


Figure 6.03 – Practical Injection Lock Feedback Loop

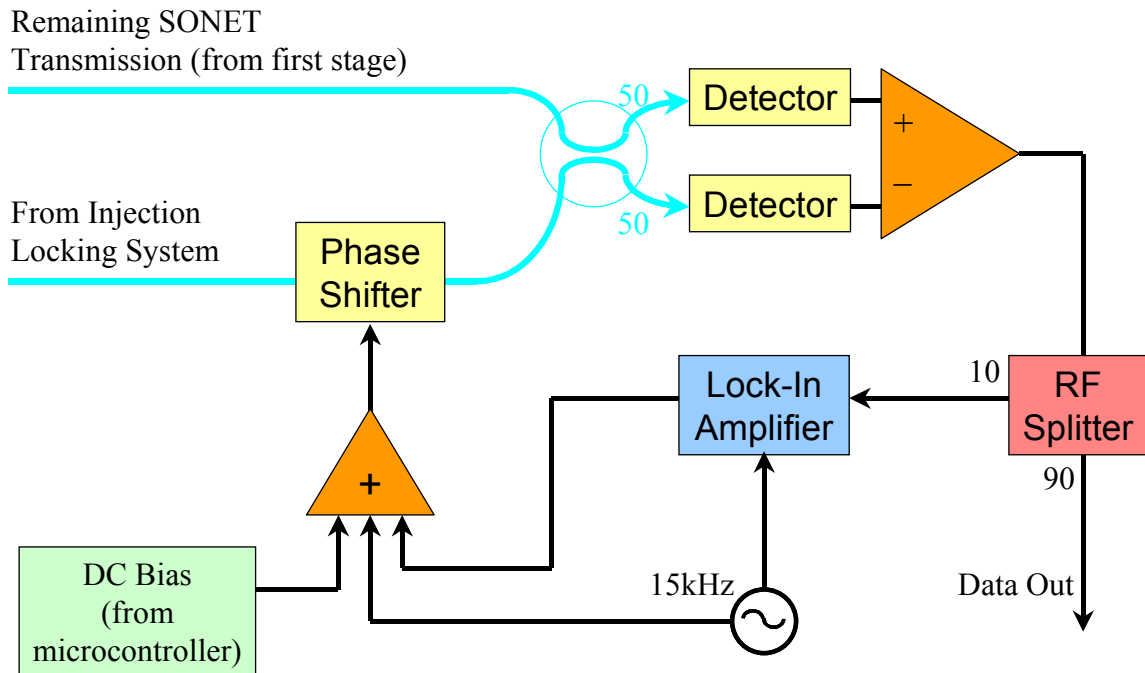


Figure 6.04 – Practical Phase-Locked Loop

In addition, the 78kHz modulation used to control the injection lock feedback loop is now applied to the Fabry-Perot filter. This allows modulation of the received optical signal without incurring the additional 6dB loss from an additional optical modulator.

Figures 6.05-6.07 depict the layouts of the circuits that have been designed to control the receiver. Additionally, Figures 6.08-6.10 are photographs of the actual circuit boards that have been created. Board 0 (depicted in Figures 6.05 and 6.08) is responsible for adding the electronic signals together, which is controlled by the four LM348N chips and their corresponding resistors. The relay switches in the upper-left of Figure 6.05 are used to enable the analog feedback for the optical filter and phase shifter (controlled by the lock-in amplifier) once the appropriate bias point has been set. The feedback control



is greater than zero (ground) and one corresponding to a signal that is less than zero.

These two clock signals each control either the up or down pin of the Counter, comprised of the four 74193 chips. The digital output of this counter is then converted by the DAC (AC669) to an analog output. In addition, the four LM348N chips to the right of Figure 6.06 are used to generate the sinusoidal signals that are used in the feedback control loops.

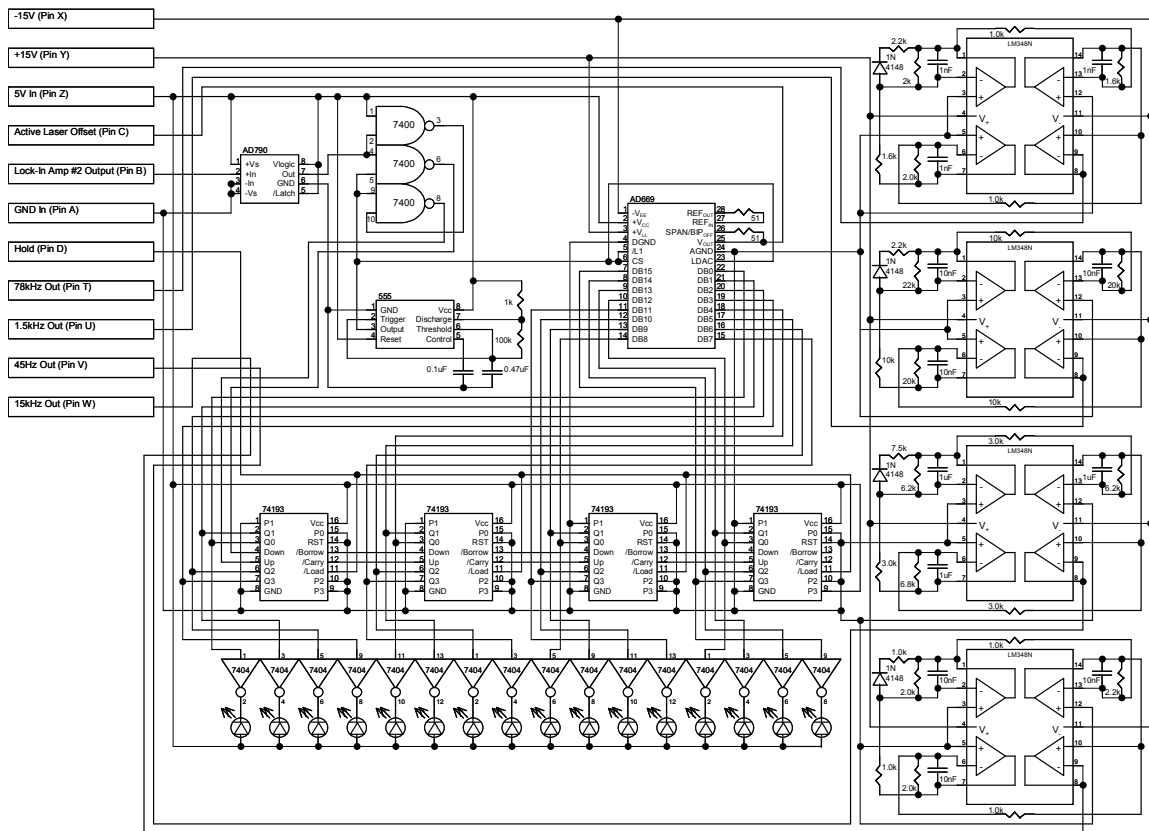


Figure 6.06 – Board #1 (Slave Laser Control and Oscillators)

Board 2 (plugs into Board 0), depicted in Figures 6.07 and 6.10, contains the microcontroller and corresponding logic used to set the initial bias for the controllers. In this, the three DACs (ADS7812) convert the signals from the detectors that monitor the

output of the filter, slave laser, and final signal to a digital value. The microcontroller is programmed to select a particular data source (either the filter, slave laser or final output monitor) via a three-pin output and the logic gates, and use the information from this data source to choose an appropriate bias (the code for this is in Appendix D). This bias is then converted to an analog signal via the three ADCs (DAC7611) and sent to Board 0. In addition, the three-pin data source selector is also used to control the two relay switches on Board 0, as well as the hold pin of the up/down counter on Board 1. This allows the microcontroller to enable the analog feedback loops once it has successfully set the bias points.

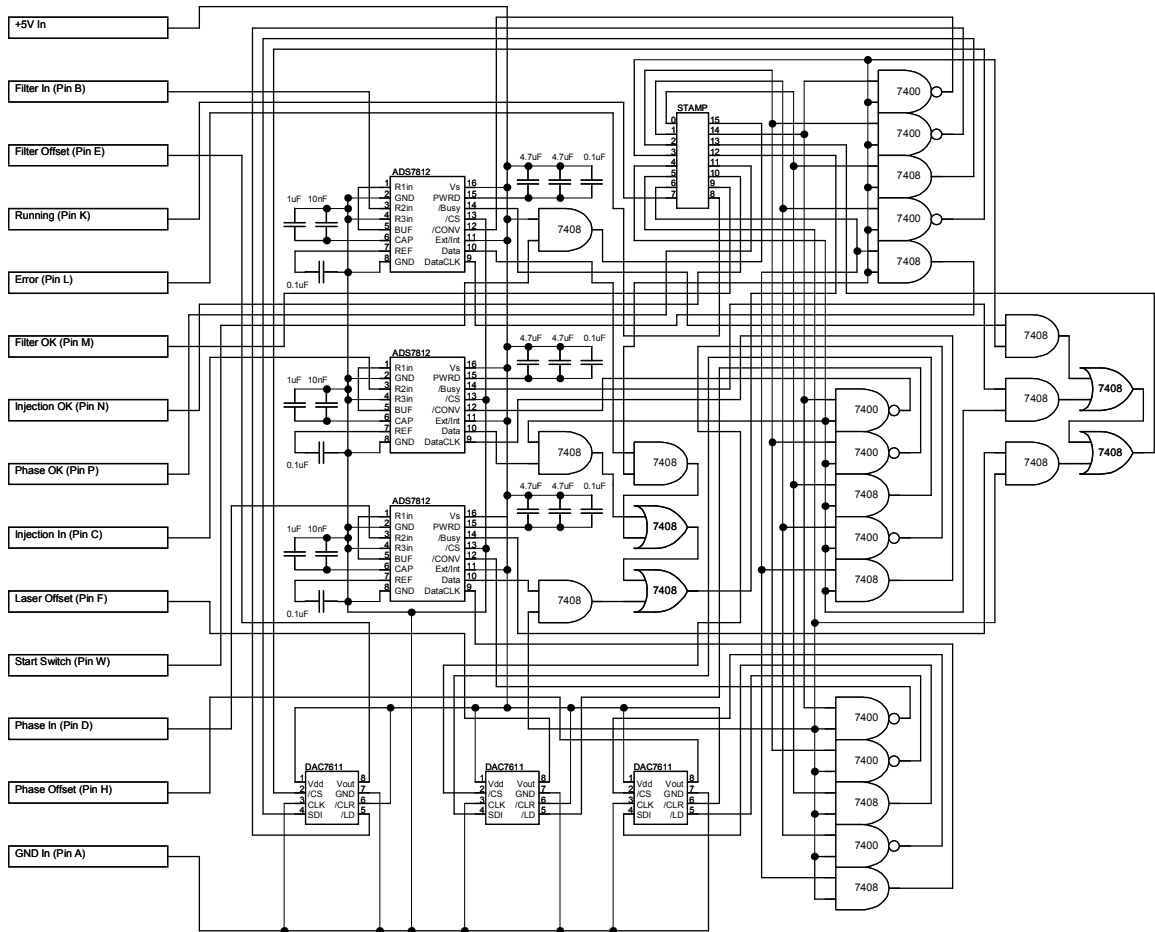


Figure 6.07 – Board #2 (Microcontroller Logic)

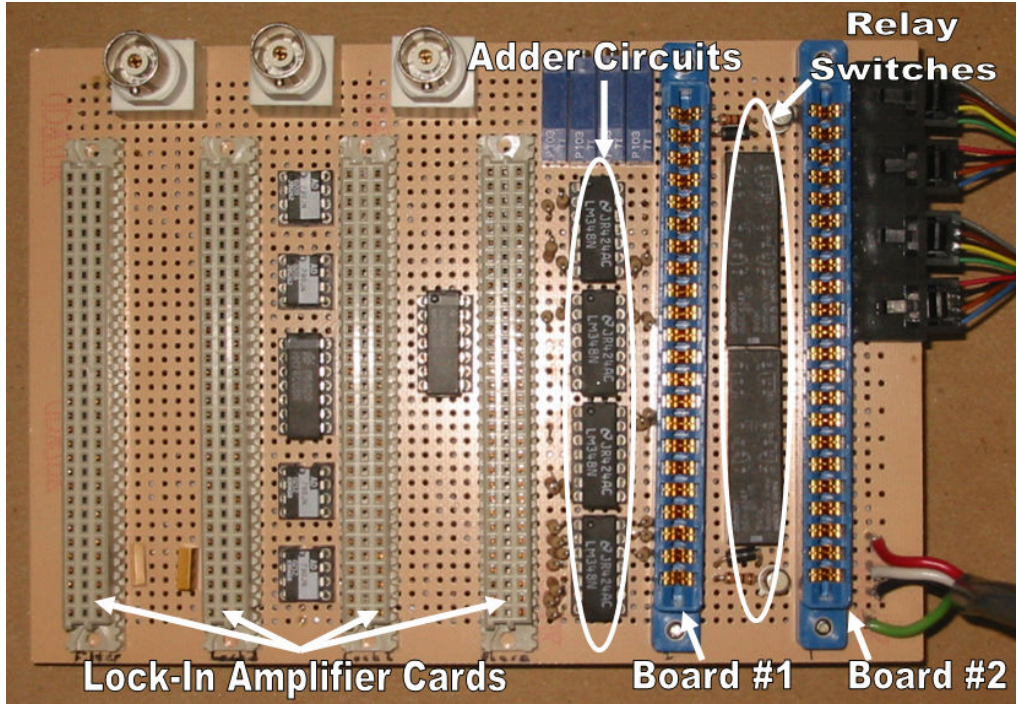


Figure 6.08 – Photograph of Board #0 (Front Board)

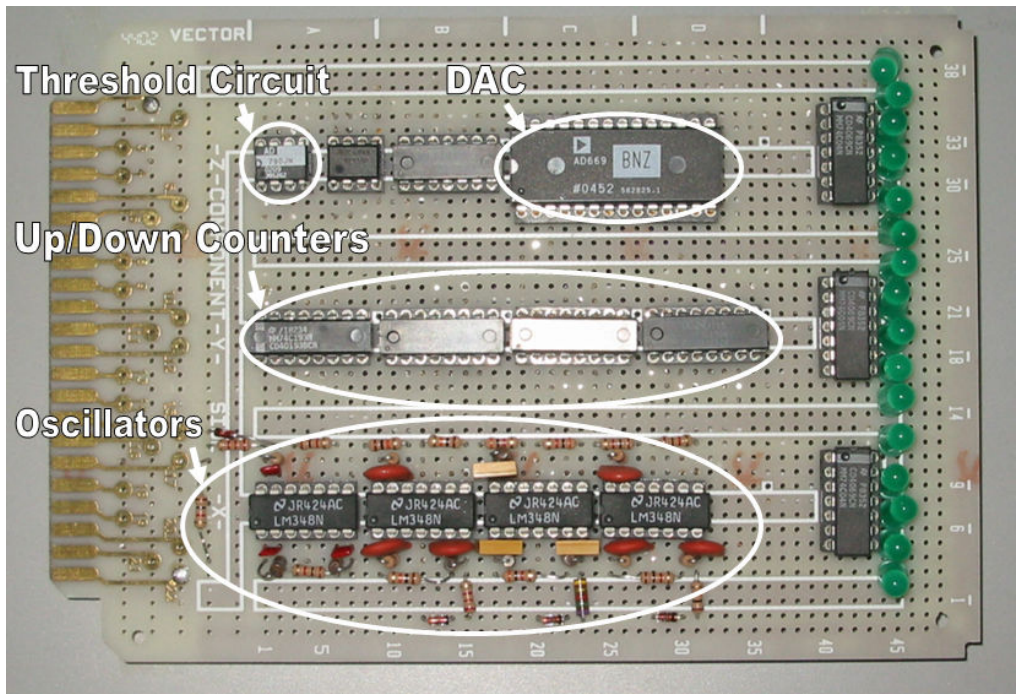


Figure 6.09 – Photograph of Board #1 (Slave Laser Control and Oscillators)

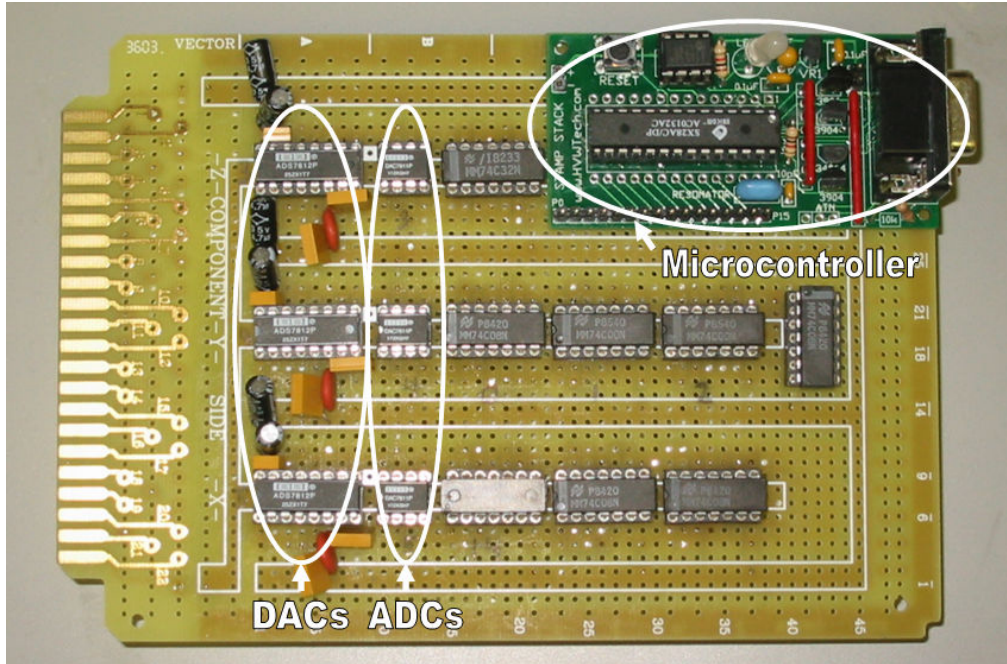


Figure 6.10 – Photograph of Board #2 (Microcontroller Logic)

After the button on the front panel is pressed (denoted by the switch in Figure 6.05), a signal is sent to the microcontroller on Board #2 to begin its routine. First, the microcontroller determines the proper bias for the filter, given the output from the detector in Figure 6.02. After this, the microcontroller sends a signal to a relay switch to activate the signal from the lock-in amplifier card, thus maintaining the filter lock.

Once the proper bias point for the filter is determined, the microcontroller biases the slave laser, given the output of the detector in Figure 6.03. After the proper bias for the slave laser is found, the microcontroller sends a signal to the hold pin of the up/down counter. This allows for the counter to properly track the difference between the free-running frequency of the slave laser and the received optical signal, as in explained in Chapters 3 and 4.

At this point, the microcontroller biases the phase shifter by maximizing the average power of the signal from the balanced receiver (Figure 6.04). Similar to the feedback circuit for the filter lock, once the proper bias for the phase shifter is found, the microcontroller will activate a relay switch that allows for the lock-in amplifier card to maintain the phase lock.

## 6.3 Future Work

### 6.3.1 Polarization Control

Up to this point, the topic of polarization control has not been mentioned. Since several of the electro-optic devices in this setup are polarization sensitive, as well as the final mixing of the received and local oscillator signals, it becomes necessary to ensure that the polarization of the received signal is known. This can be accomplished in one of two ways, polarization feedback or polarization diversity.

In the case of polarization diversity, the received optical signal would need to be split via a polarizing beam cube into two known polarization states. The main problem with this method is that it effectively doubles the complexity of the system, since we now require two local oscillator generators. Also, the decrease in the effective magnitude of the received optical signal may require additional optical amplifiers, which would add noise to the local oscillator signal.

Thus, a polarization feedback loop would be the more practical solution. Such a system is depicted in Figure 6.11. In this, the received optical signal is incident on a polarization controller, followed by a polarizer, before a portion of the signal is split off for local oscillator signal generation. After this portion is split off, a portion of that signal

is diverted to a detector. This detected signal is directed to a lock-in amplifier, whose output (along with a sinusoidal dither) controls the polarization controller. It should be noted that, since a polarization controller usually has at least 3 inputs, it would either be necessary to have separate feedback loops for each control, or have a microcontroller switch between the input ports in order to maintain the proper polarization.

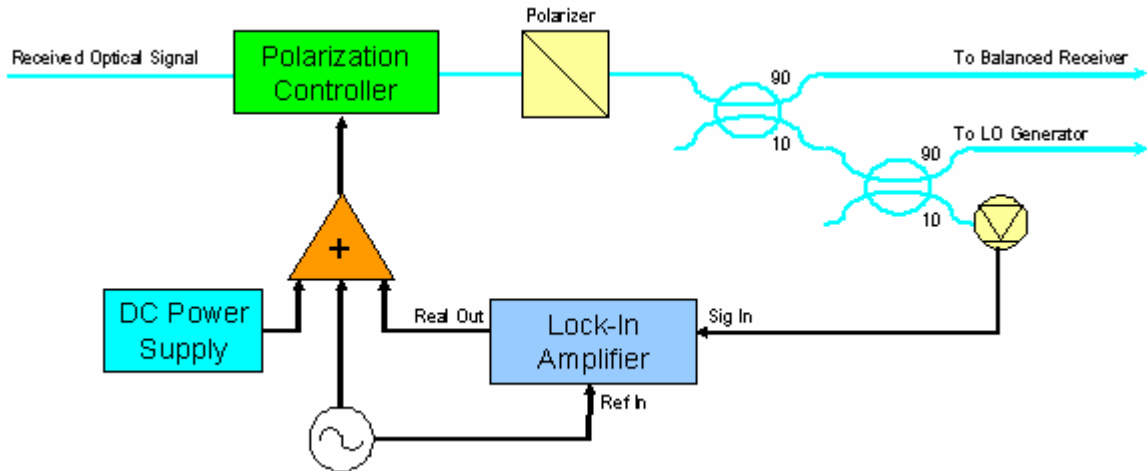


Figure 6.11 – Layout of Polarization Feedback Control Loop

### 6.3.2 Final Receiver Layout

The overall expected design for the receiver is depicted in Figure 6.12 (the feedback loops are not shown in order to simplify the diagram). In this, 10% of the received optical signal is diverted from the received optical signal. After this, 10% of the diverted signal is used for the polarization feedback loop (explained in section 6.2.2).

The remaining portion of the diverted signal is directed into an EDFA. From the EDFA, the signal goes through the filtering, injection locking, and phase locking stages (discussed in section 6.2.1). After this, a balanced receiver detects the signal. The purpose of the balanced receiver is to reduce the effect of any common-mode noise that is present on the local oscillator [32].

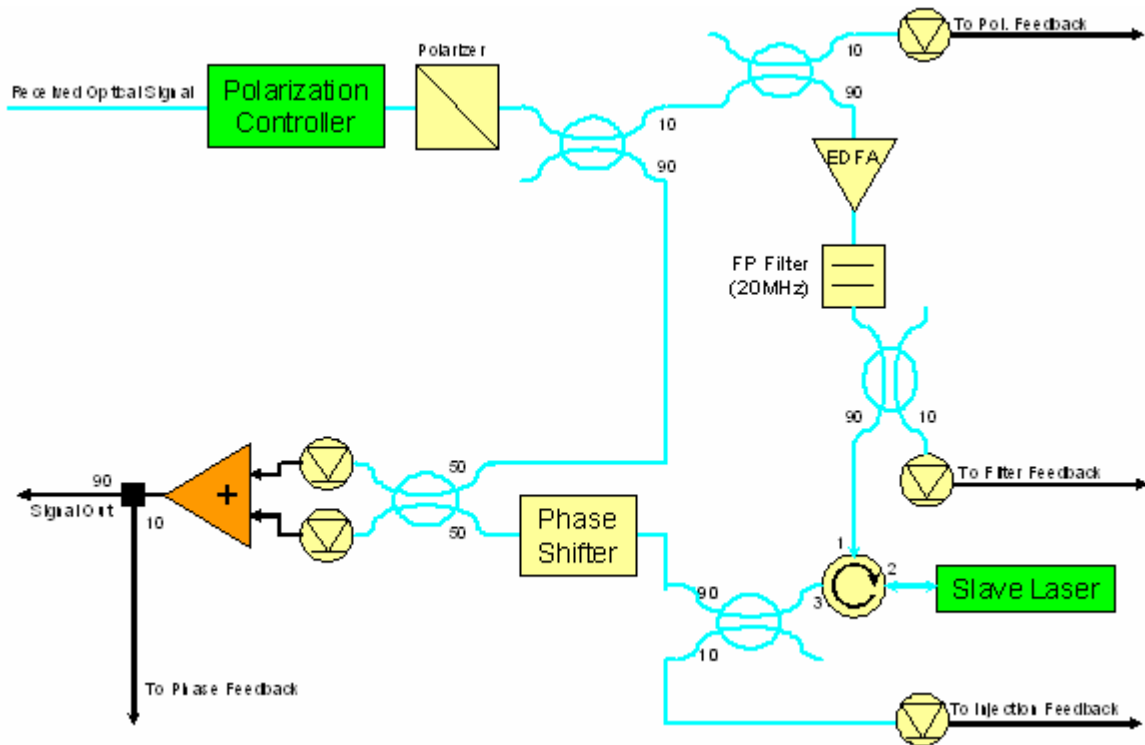


Figure 6.12 – Layout of Homodyne Receiver (Feedback Loops Omitted)

Once assembled, this homodyne receiver should be capable of receiving SONET transmissions at data rates up to 10GHz (limited by the bandwidth of the detectors used in the balanced receiver). In addition, this receiver should be capable of effectively detecting transmissions whose optical power is less than -30dBm.

### 6.3.3. Support for PSK transmissions

The system described above can be used for homodyne detection or as a pump for parametric amplification. In addition, our previous work has shown that our OIL system can be used to generate an acceptable LO signal from a NRZ OC192 SONET transmission, provided that the signal is first pre-filtered via a Fabry-Perot optical filter (Micron Optics, 20MHz bandwidth) [47].

It is also desirable to use this LO generator with more complex phase modulation schemes, such as PSK [49]. However, because these transmissions do not have a carrier to recover, they are not compatible with OIL without additional pre-processing. As such, a method must be developed to generate a Fourier component of the carrier before the OIL LO generator can be utilized.

One possible method to generate a carrier for the PSK signal is depicted in Figure 6.13. A two-armed interferometer with a digitally-variable phase shift is used to generate the carrier. The phase shifter is controlled by the output of the interferometer, which is proportional to an optical mixing of the received signal and the output of the slave laser. The phase shifter will shift the phase of the incident signal by either 0 or  $\pi$ , depending on if the input signal is greater or less than a pre-defined threshold value. Note that an optical delay has also been added before the phase shifter to ensure that the bit input into the phase shifter is the same as the bit that is mixed with the local oscillator signal used to bias the phase shifter at that instance.

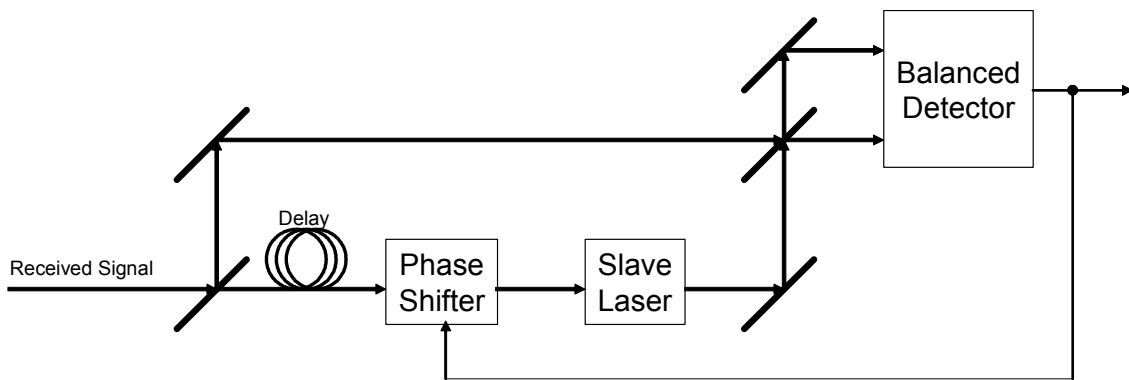


Figure 6.13 - Possible layout for retrieving the carrier of the received optical signal

We assume that the bits that comprise the received signal can be represented as a series of values equaling either 1 or -1 (depending on the phase). If we assume that the

round trip time of the slave laser is on the order of the bit period, the output of the phase shifter can be modeled as:

$$B_{out} = B_{in} \cdot (2 \cdot U(|B_{lo} + B_{in}| - 1) - 1) \quad (6.02)$$

such that  $B_{in}$  is the bit value of the phase shifter (1 or -1),  $B_{lo}$  is the normalized output of the slave laser, and  $U(x)$  is a step function that returns 0 if  $x \leq 0$  and 1 if  $x > 0$ . Note that if that the intensity of the injected signal is much less than the free-running intensity of the slave laser,  $B_{lo}$  will be approximately equal to the running average  $B_{out}$ .

Given this, we can simulate the signal generated by this system, given an input of random data. The result of this is depicted in Figure 6.14. Note that for this figure, the spacing between points is equal to a bit period (which we also set equal to the round-trip time of the laser cavity). In this case, given random data, the output of the phase shifter eventually settles on a value of 1 (either 1 or -1 are possible results) for a random input, forcing the coherent portion of the LO signal to approach a steady value. Our future work will focus on developing a more robust theory to describe the operation of the PSK LO generator, and will experimentally verify the process.

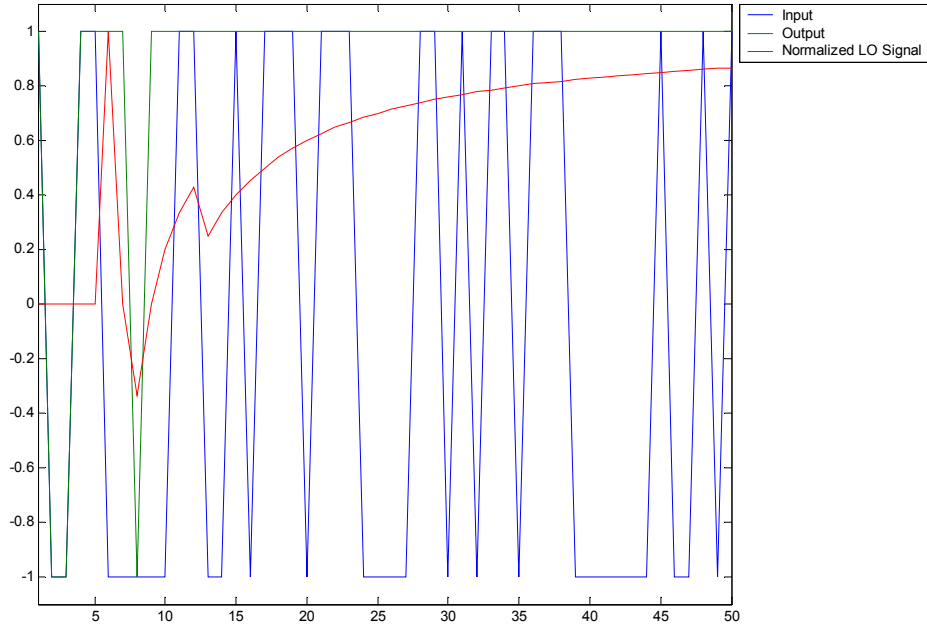


Fig. 6.14 - Theoretical LO signal produced from LO generator that utilizes the proposed carrier retrieval method (blue: input to carrier retrieval module, green: output of carrier retrieval module, red: LO output).

## VII. CHAPTER 7 – Conclusions

It has been shown that a suitable local oscillator for a homodyne receiver can be generated from a slave laser that is injected with a filtered portion of the received optical signal. For this, the slave laser can either be a Fabry-Perot laser, or a Distributed Feedback laser. The advantage of using a Fabry-Perot laser is its lower cost and higher degree of wavelength acceptability, while the Distributed Feedback laser allows for a simpler receiver design. However, either laser will effectively reduce the amplitude modulation on the incident signal, while providing a signal whose intensity is that of the free-running slave laser.

Additionally, it has been shown that the injection locking process can be stabilized by monitoring the modulation transfer ratio of the slave laser. The modulation transfer function of an injected laser is at a minimum at the center of the locking range, and increases with detuning. This behavior can be utilized by a feedback loop to keep the modulation transfer ratio of the slave laser to a minimum. Furthermore, it has been shown that this trend holds true for both Fabry-Perot lasers and Distributed Feedback lasers. Finally, it has been demonstrated that this effect is sufficiently well understood, and that it can be modeled with simple laser rate equations.

## Appendix A – Matlab Code for Plotting Results for DFB Injection Locking

```

%MatLab Code for Ploting Magnitude and Phase of 1st Harmonic
%for various modulation frequencies
clear
fudge=400;
op=linspace(-pi/2,pi/2,100);
e1=sqrt(10^-3.0/1000)/sqrt(fudge);
isat=10^-2.08/1000*fudge;
runsat=2;
tc=4e-12;
T1=.5e-9;
gammae=-1./(tc);
P=runsat./T1;
A=e1*sqrt(.1);
U=isat.*T1;
%wp=[1e5,2.5e5,5e5,7.5e5,1e6,2.5e6,5e6,7.5e6,1e7,2.5e7,5e7,7.5e7,1e8,2.
5e8,5e8,7.5e8,1e9,2.5e9,5e9];
%wp=logspace(5,10,15);
wp=[5e5,1e6,2e6];
for loop=1:1:length(wp)
    w=wp(loop);
    strings(loop,:)=sprintf('Modulation Frequency=%0.2e',w);
    loop2=0;
    for o=op
        loop2=loop2+1;
        e0(loop,loop2)=solve_e0(isat,tc,gammae,e1,o,P,T1);
        etemp(loop,loop2)=e1./e0(loop,loop2);
        r=(P.*T1)./(1+e0.^2./isat);
        f(loop,loop2)=-gammae.*(e1./e0(loop,loop2)).*sin(o);
        D=-
        (e0(loop,loop2).^2.*r(loop,loop2))./(i.*w.*T1.*isat+isat+e0(loop,loop2)
        .^2);
        k=1./(i.*w+(D+r(loop,loop2)-1)./(2.*tc));
        B(loop,loop2)=(gammae.*e1+i.*w.*e0(loop,loop2).*cos(o))...
        ./((e1.^2./e0(loop,loop2)).*gammae.*sin(o).^2+(i.*w.*e0(loop,loop2))./(
        gammae.*k)+(e1.*cos(o))./k)).*A;
        C(loop,loop2)=(k.*gammae.^2.*e1.*sin(o).*cos(o)-
        gammae.*e1.*sin(o))...
        ./(gammae.*e0(loop,loop2).*e1.*cos(o)+i.*w.*e0(loop,loop2).^2+k.*gammae
        .^2.*e1.^2.*sin(o).^2)).*A;
        B2(loop,loop2)=((-
        C(loop,loop2).^2.*e1.*sin(o))./2+A.*C(loop,loop2).*cos(o)...
        -
        (B(loop,loop2).*C(loop,loop2).*e1.*cos(o))./e0(loop,loop2)-
        (A.*B(loop,loop2).*sin(o))./e0(loop,loop2)...
        +(B(loop,loop2).^2.*e1.*sin(o))./e0(loop,loop2).^2.0...
        +(2.*i.*w.*e0(loop,loop2))./gammae+e1.*cos(o)).*(-
        C(loop,loop2).^2./(2.*tan(o))-A.*C(loop,loop2))./e1...
        -(-
        (isat.*e0(loop,loop2).*B(loop,loop2).^2.*r(loop,loop2).*(i.*w.*T1+1))./
        (i.*w.*T1.*isat+isat+e0(loop,loop2).^2).^2.0...

```

```

+ (e0(loop,loop2).*B(loop,loop2).^2.*r(loop,loop2))./(i.*w.*T1.*isat+isat+e0(loop,loop2).^2))./(2.*tc.*gammae.*e1.*sin(o)))./...

((e1.*sin(o))./e0(loop,loop2)+((2.*i.*w.*e0(loop,loop2))./gammae+e1.*cos(o)).*...
    ((4.*i.*w.*tc-
(e0(loop,loop2).^2.*r(loop,loop2))./(i.*w.*T1.*isat+isat+e0(loop,loop2).^2)+r(loop,loop2)-1)...
    ./ (2.*tc.*gammae.*e1.*sin(o))));
    end
end

figure(1)
plot(f', (sqrt(B'.*conj(B'))).*(etemp')./A).^2.*fudge)
axis([-4e8,4e8,0,1.6e-2])
title('Modulation Transfer Function vs. Frequency Offset (1st Harmonic)')
xlabel('Frequency Offset (Hz)')
ylabel('Modulation Transfer Ratio')
legend(strings,-1);
figure(2)
plot(f', (sqrt(B2'.*conj(B2'))).*(etemp')./A).^2.*fudge)
axis([-4e8,4e8,0,5e-8])
title('Modulation Transfer Function vs. Frequency Offset (2nd Harmonic)')
xlabel('Frequency Offset (Hz)')
ylabel('Modulation Transfer Ratio')
legend(strings,-1);

```

```

%MatLab Code for Ploting Magnitude and Phase of 1st Harmonic
%for various injected powers

clear
fudge=400;
op=linspace(-pi/2,pi/2,100);
e1=sqrt(10^-3.0/1000)/sqrt(fudge);
isat=10^-2.08/1000*fudge;
runsat=2;
tc=4e-12;
T1=.5e-9;
gammae=-1./(tc);
P=runsat./T1;
U=isat.*T1;
w=1e6;
elp=[sqrt(10^-2.6/1000)/sqrt(fudge),sqrt(10^-
2.8/1000)/sqrt(fudge),sqrt(10^-3.0/1000)/sqrt(fudge)];
%A=1e-5;
Ap=elp./sqrt(10);
for loop=1:1:length(elp)
    e1=elp(loop);
    A=Ap(loop);
    strings(loop,:)=sprintf('Incident Power =
%2.0fdBm',30+10*log10(fudge*e1^2));
    loop2=0;
    for o=op
        loop2=loop2+1;
        e0(loop,loop2)=solve_e0(isat,tc,gammae,e1,o,P,T1);
        etemp(loop,loop2)=e1./e0(loop,loop2);
        r=(P.*T1)./(1+e0.^2./isat);
        f(loop,loop2)=-gammae.*(e1./e0(loop,loop2)).*sin(o);
        D=-
(e0(loop,loop2).^2.*r(loop,loop2))./(i.*w.*T1.*isat+isat+e0(loop,loop2)
.^2);
        k=1./(i.*w+(D+r(loop,loop2)-1)./(2.*tc));
        B(loop,loop2)=(gammae.*e1+i.*w.*e0(loop,loop2).*cos(o))...
./((e1.^2./e0(loop,loop2)).*gammae.*sin(o).^2+(i.*w.*e0(loop,loop2))./(
gammae.*k)+(e1.*cos(o))./k)).*A;
        C(loop,loop2)=(k.*gammae.^2.*e1.*sin(o).*cos(o)-
gammae.*e1.*sin(o))...
./ (gammae.*e0(loop,loop2).*e1.*cos(o)+i.*w.*e0(loop,loop2).^2+k.*gammae
.^2.*e1.^2.*sin(o).^2)).*A;
        B2(loop,loop2)=((-
C(loop,loop2).^2.*e1.*sin(o))./2+A.*C(loop,loop2).*cos(o)...
-
(B(loop,loop2).*C(loop,loop2).*e1.*cos(o))./e0(loop,loop2)-
(A.*B(loop,loop2).*sin(o))./e0(loop,loop2)...
+(B(loop,loop2).^2.*e1.*sin(o))./e0(loop,loop2).^2.0...
+((2.*i.*w.*e0(loop,loop2))./gammae+e1.*cos(o)).*(-
C(loop,loop2).^2./(2.*tan(o))-A.*C(loop,loop2))./e1...
-(-
(isat.*e0(loop,loop2).*B(loop,loop2).^2.*r(loop,loop2)).*(i.*w.*T1+1))./
(i.*w.*T1.*isat+isat+e0(loop,loop2).^2).^2.0...

```

```

+(e0(loop,loop2).*B(loop,loop2).^2.*r(loop,loop2))./(i.*w.*T1.*isat+isa
t+e0(loop,loop2).^2))./(2.*tc.*gammae.*e1.*sin(o)))./...

((e1.*sin(o))./e0(loop,loop2)+((2.*i.*w.*e0(loop,loop2))./gammae+e1.*co
s(o)).*...
      ((4.*i.*w.*tc-
(e0(loop,loop2).^2.*r(loop,loop2))./(i.*w.*T1.*isat+isat+e0(loop,loop2)
.^2)+r(loop,loop2)-1)...
      ./ (2.*tc.*gammae.*e1.*sin(o))));
end
end
atemp=ones(length(e1p),100);
for loop=1:1:length(e1p)
    atemp(loop,:)=atemp(loop,:)*Ap(loop);
end
figure(1)
plot(f',(sqrt(B'.*conj(B')).*(etemp')./atemp').^2.*fudge)
axis([-4e8,4e8,0,.05])
title('Modulation Transfer Function vs. Frequency Offset (1st
Harmonic)')
xlabel('Frequency Offset (Hz)')
ylabel('Modulation Transfer Ratio')
legend(strings,-1);
figure(2)
plot(f',(sqrt(B2'.*conj(B2')).*(etemp')./atemp').^2.*fudge)
axis([-4e8,4e8,0,5e-8])
title('Modulation Transfer Function vs. Frequency Offset (2nd
Harmonic)')
xlabel('Frequency Offset (Hz)')
ylabel('Modulation Transfer Ratio')
legend(strings,-1);

```

```

%Matlab Function for solving for e0
function e0=solve_e0(isat,tc,gammae,e1,o,P,T1)
start=1;
step=-.1;
stop=0;
for loop=1:1:10
    flag=1;
    while flag

s1=sign((start).^3/isat+(2.*tc.*gammae.*e1.*cos(o)./isat).*(start).^2+(
1-P.*T1).*(start)+(2.*tc.*gammae.*e1.*cos(o)));

s2=sign((start+step).^3/isat+(2.*tc.*gammae.*e1.*cos(o)./isat).*(start+
step).^2+(1-P.*T1).*(start+step)+(2.*tc.*gammae.*e1.*cos(o)));
        if (s1~=s2)
            flag=0;
            stop=start+step;
            step=step/10;
        else
            start=start+step;
            if start<stop
                disp('No Solution');
                return;
            end
        end
    end
end
end
e0=start;

```

## Appendix B – Matlab Code for Plotting Results for Fabry-Perot Injection Locking

```

%MatLab Code for Ploting Magnitude and Phase of 1st Harmonic
%for various injected powers

clear
op=linspace(-pi/2,pi/2,1001);

isatp=10.^(sin(op))/1000;
%isatp=linspace(10^1/1000,10^1/1000,1001);
dp=-3;
loop=1;
loop2=0;
for o=op
    loop2=loop2+1;
    isat=isatp(loop2);
    runsat=2;
    tc=4.4e-12;
    T1=1e-9;
    gammae=-1./(tc);
    P=runsat./T1;
    U=isat.*T1;
    w=1e6;
    e1=sqrt(10^dp/1000);
    eL1=sqrt(10^-4/1000);
    A=e1.*sqrt(.25);
    e0(loop,loop2)=solve_e0_2(isat,tc,gammae,e1,eL1,o,P,T1);
    eL0(loop,loop2)=(e0(loop,loop2).*eL1)./(e1.*cos(o));
    etemp(loop,loop2)=e1./e0(loop,loop2);
    r=(P.*T1)./(1+e0.^2./isat);
    f(loop,loop2)=-gammae.*(e1./e0(loop,loop2)).*sin(o);
    D=-
(e0(loop,loop2).^2.*r(loop,loop2))./(i.*w.*T1.*isat+isat+e0(loop,loop2)
.^2);
    B(loop,loop2)=(gammae.*e1+i.*w.*e0(loop,loop2).*cos(o))...
./((e1.^2./e0(loop,loop2)).*gammae.*sin(o).^2+(i.*w.*e0(loop,loop2))./
gammae+(e1.*cos(o))...
.*(i.*w-
(e0(loop,loop2).*r(loop,loop2))./(tc.*(i.*w.*T1.*isat+e0(loop,loop2).^2
....
+((1+r(loop,loop2)-2.*i.*w.*tc)./(1-r(loop,loop2)-
2.*i.*w.*tc)).*((e0(loop,loop2).*eL1)./(e1.*cos(o)).^2)+(r(loop,loop2)
)-1)./(2.*tc))));
end
f2=(sqrt(B'.*conj(B')).*(etemp')./A).^2;
plot(f(2:1000)',f2(2:1000))
axis([-1e9,3e9,0,.05])
title('Modulation Transfer Function vs. Frequency Offset (1st
Harmonic)')
xlabel('Frequency Offset (Hz)')
ylabel('Modulation Transfer Ratio')
grid;

```

```

%Matlab Function for solving for e0

function e0=solve_e0(isat,tc,gammae,e1,eL1,o,P,T1)
start=1;
step=-.1;
stop=0;
K=(1+eL1./(e1.*cos(o))).^2;
for loop=1:1:10
    flag=1;
    while flag

s1=sign(K.*(start).^3/isat+K.*(2.*tc.*gammae.*e1.*cos(o)./isat).*(start
).^2+(1-P.*T1).*(start)+(2.*tc.*gammae.*e1.*cos(o)));

s2=sign(K.*(start+step).^3/isat+K.*(2.*tc.*gammae.*e1.*cos(o)./isat).*(
start+step).^2+(1-P.*T1).*(start+step)+(2.*tc.*gammae.*e1.*cos(o)));
        if (s1~=s2)
            flag=0;
            stop=start+step;
            step=step/10;
        else
            start=start+step;
            if start<stop
                disp('No Solution');
                return;
            end
        end
    end
end
end
e0=start;

```

## Appendix C – Matlab Code for Plotting Phase Modulation due to Amplitude Modulation on Input

```

%MatLab Code for Ploting Phase Modulation of 1st Harmonic

clear
op=linspace(-pi/2,pi/2,1001);
isat=10^-1/1000;

runsat=2;
tc=5e-10;
T1=.5e-9;
gammae=-1./(tc);
P=runsat./T1;
U=isat.*T1;
wp=0;
e1=sqrt(10^-2);
A=.05.*e1;
C1=pi./100;
ah=10;
for loop=1:1:length(wp)
    loop2=0;
    for o=op
        loop2=loop2+1;
        e0=solve_e0(isat,tc,gammae,e1,o,P,T1);
        r=(P.*T1)./(1+e0.^2./isat);
        f(loop,loop2)=-gammae.*(e1./e0).*sin(o);
        C(loop,loop2)=(cos(o)./((r-1)./2-(r.*e0.^2)./(isat+e0.^2))-...
            sin(o)./((tc.*gammae.*e1.*sin(o))./e0-
            (r.*e0.^2.*ah)./(isat+e0.^2)))./...
            ((e1.*sin(o))./((r-1)./2-(r.*e0.^2)./(isat+e0.^2))-...
            (e1.*cos(o))./((tc.*gammae.*e1.*sin(o))./e0-
            (r.*e0.^2.*ah)./(isat+e0.^2))));
    end
end
plot(f',(sqrt(C'.*conj(C'))))
axis([-1.5e9,1.5e9,0,10])
xlabel('Frequency Offset (Hz)')
ylabel('Phase Modulation Transfer Ratio')

```

## Appendix D – Stamp Basic Code for the Microcontroller

```
' {$STAMP BS2sx}
' {$PBASIC 2.5}

sublooper VAR Nib
looper VAR Word
counter VAR Nib
thepoint VAR Word
theposa VAR Word
theposb VAR Word
temp VAR Word
temp2 VAR Word
thelimit VAR Byte

thelimit = 100

'Data Out
LOW 0
'Output CLK Out
LOW 1
'Load Out
LOW 2

'Filter Select
LOW 3
'Injection Select
LOW 4
'Phase Select
LOW 5

'Error Light
LOW 8

'Filter OK
LOW 9
'Filter OK
LOW 10
'Filter OK
LOW 11

'Data In
INPUT 12
'Input CLK Out
INPUT 6
'Input Busy
INPUT 13
'Load In
LOW 14

'Start Switch
INPUT 15

Main:
```

```

'Running Light
LOW 7

IF (IN15 = 0) THEN Main
HIGH 7
LOW 8
LOW 9
LOW 10
LOW 11

HIGH 3
LOW 4
LOW 5
counter=0
filterloop:
counter=counter+1
thepoint = 0
FOR looper = 0 TO 4095
  SHIFTOUT 0, 1, MSBFIRST, [looper\12]
  PULSOUT 2, 1
  PULSOUT 14, 1
  stillbusyla:
  IF (IN13 = 0) THEN stillbusyla
  temp = 65535
  FOR sublooper = 0 TO 4
    SHIFTTIN 12, 6, MSBPOST, [temp2\12]
    temp2.BIT11 = ~temp2.BIT11
    IF (temp < temp2) THEN doneavgla
    temp = temp2
  doneavgla:
  NEXT
  IF thepoint >= temp THEN isfinela
  thepoint = temp
  theposa = looper
  isfinela:
NEXT
thepoint = 0
FOR looper = 0 TO 4095
  SHIFTOUT 0, 1, MSBFIRST, [looper\12]
  PULSOUT 2, 1
  PULSOUT 14, 1
  stillbusylb:
  IF (IN13 = 0) THEN stillbusylb
  temp = 65535
  FOR sublooper = 0 TO 4
    SHIFTTIN 12, 6, MSBPOST, [temp2\12]
    temp2.BIT11 = ~temp2.BIT11
    IF (temp < temp2) THEN doneavglb
    temp = temp2
  doneavglb:
  NEXT
  IF thepoint >= temp THEN isfinelb
  thepoint = temp
  theposb = looper
  isfinelb:
NEXT
IF (counter<3) THEN continuel

```

```

HIGH 8
GOTO Main
continuel:

IF (ABS (theposa - theposb)) > thelimit THEN filterloop
looper = 0
startloop1:
  SHIFTOUT 0, 1, MSBFIRST, [looper\12]
  PULSOUT 2, 1
  PULSOUT 14, 1
  stillbusylc:
  IF (IN13 = 0) THEN stillbusylc
  temp = 65535
  FOR sublooper = 0 TO 4
    SHIFTOIN 12, 6, MSBPOST, [temp2\12]
    temp2.BIT11 = ~temp2.BIT11
    IF (temp < temp2) THEN doneavg1c
      temp = temp2
  doneavg1c:
  NEXT
  IF ((temp>((thepoint*3)/4)) AND ((looper-
thelimit)<((theposa+theposb)/2)) AND
((looper+thelimit)>((theposa+theposb)/2))) THEN endloop1
  IF (counter<3) THEN nofiltererror
  HIGH 8
  GOTO Main
  nofiltererror:
  IF (looper>((theposa+theposb)/2)+thelimit)) THEN
filterloop
  looper=looper+1
  GOTO startloop1
endloop1:
HIGH 9

LOW 3
HIGH 4
LOW 5
injectionloop:

thepoint = 0
FOR looper = 0 TO 4095
SHIFTOUT 0, 1, MSBFIRST, [looper\12]
PULSOUT 2, 1
PULSOUT 14, 1
stillbusy2a:
IF (IN13 = 0) THEN stillbusy2a
temp = 0
FOR sublooper = 0 TO 2
  SHIFTOIN 12, 6, MSBPOST, [temp2\12]
  temp2.BIT11 = ~temp2.BIT11
  IF (temp > temp2) THEN doneavg2a
    temp = temp2
doneavg2a:
NEXT
IF thepoint >= temp THEN isfinelb

```

```

        thepoint = temp
        isfine2a:
NEXT

looper=0
counter=0
startloop2:
SHIFTOUT 0, 1, MSBFIRST, [looper\12]
PULSOUT 2, 1
PULSOUT 14, 1
stillbusy2b:
IF (IN13 = 0) THEN stillbusy2b
    temp = 0
    FOR sublooper = 0 TO 2
        SHIFTLIN 12, 6, MSBPOST, [temp2\12]
        temp2.BIT11 = ~temp2.BIT11
        IF (temp > temp2) THEN doneavg2b
        temp = temp2
    doneavg2b:
    NEXT
dothis2a    IF ((temp>(3*(thepoint/4))) AND (counter=0)) THEN

dothis2c    IF ((temp<(thepoint/2)) AND (counter=1)) THEN dothis2b
            IF ((temp>(3*(thepoint/4))) AND (counter=2)) THEN

dothis2a:
theposa=looper
counter=counter+1
GOTO continue2
dothis2b:
counter=counter+1
GOTO continue2
dothis2c:
theposb=looper
counter=counter+1
continue2:
looper=looper+1
IF ((counter<3) AND (looper<4095)) THEN startloop2
IF (counter=3) THEN endloop2
HIGH 8
GOTO Main
endloop2:
looper=((theposa+theposb)/2)
SHIFTOUT 0, 1, MSBFIRST, [looper\12]
PULSOUT 2, 1
HIGH 10

GOTO Main

```

## References

- [1] J. M. Kahn, "1 Gbit/s PSK homodyne transmission system using phase-locked semiconductor lasers," *IEEE Photonics Technology Letters*, vol. 1, Oct 1989, pp. 340-342.
- [2] T. Okoshi, "Ultimate Performance of Heterodyne/Coherent Optical Fiber Communications", *Journal of Lightwave Technology*, Vol. 4, Oct 1986, pp.1556-1562.
- [3] Dietrich Marcuse, "Derivation of Analytical Expressions for the Bit-Error Probability in Lightwave Systems with Optical Amplifiers", *Journal of Lightwave Technology*, Vol. 8, No. 12, Dec 1990, pp. 1816-1823.
- [4] Y. M. Zhang, V. Borzenets, N. Dubash, T. Reynolds, Y. G. Wey, J. Bowers, "Cryogenic Performance of a High-Speed GaInAs/InP p-i-n Photodiode", *Journal of Lightwave Technology*, Vol. 15, No. 3, March 1997, pp. 529-533
- [5] Albert Leon-Garcia, Probability and Random Processes for Electrical Engineering (2nd Edition)
- [6] N. A. Olsson, "Lightwave Systems With Optical Amplifiers", *Journal of Lightwave Technology*, Vol. 7, No. 7, July 1989
- [7] Gerd Keiser, Optical Fiber Communications 3<sup>rd</sup> Edition, McGraw Hill (2000). p. 254-256
- [8] T. Okoshi, K. Emura, K. Kikuchi, R. Th. Kersten, "Computation of Bit-Error Rate of Various Heterodyne and Coherent-Type Optical Communication Schemes", *Journal of Optical Communications*, 1981, pp. 89-96

- [9] C. C. Davis, "Coherence Theory", Lasers and Electro-Optics, Cambridge University Press (1996). p. 607-609
- [10] C. C. Davis, "Coherent Detection", Lasers and Electro-Optics, Cambridge University Press (1996). p. 598-602
- [11] Anthony E. Siegman, "Laser Injection Locking", Lasers, (University Science Books, 1986), Chap. 11
- [12] Stephen R. Chinn, Don M. Boroson, Jeff C. Livas, "Sensitivity of Optically Preamplified DPSK Receivers with Fabry-Perot Filters", Journal of Lightwave Technology, Vol. 14, No. 3, March 1996, pp. 370-376
- [13] Emmanuel Desurvire, Erbium-Doped Fiber Amplifiers, John Wiley & Sons, Inc. (1994). p. 65-153
- [14] Shinji Yamashita, Takanori Okoshi, "Suppression of Beat Noise from Optical Amplifiers Using Coherent Receivers", Journal of Lightwave Technology, Vol. 12, No. 6, June 1994, pp. 1029-1035
- [15] M. A. Mahdi, S. Selvakennedy, P. Poopalan, H. Ahmad, "Stauration Parameters of Erbium Doped Fibre Amplifiers", IEEE International Conference on Semiconductor Electronics, 1998, pp. 134-137
- [16] T. Liu, K. Obermann, K. Petermann, F. Girardin, G. Guekos, "Effect of Saturation Caused by Amplified Spontaneous Emission on Semiconductor Optical Amplifier Performance", Electronics Letters, Vol. 33, No. 24, November 1997, pp. 2042-2043
- [17] New Focus, "45-GHz Photodetectors: Datasheet", 2006

- [18] Rongqing Hui, Alessandro D'Ottavi, Antonio Mecozzi, and Paolo Spano, "Injection Locking in Distributed Feedback Semiconductor Lasers", IEEE Journal of Quantum Electronics, Vol. 27, June 1991, pp. 1688-1695.
- [19] A. C. Bordonalli, C. Walton, and Alwyn J. Seeds, "High-Performance Locking of Wide Linewidth Semiconductor Lasers by Combined Use of Optical Injection Locking and Optical Phase-Lock Loop," Journal of Lightwave Technology vol. Feb.17, 1999, pp. 328-342.
- [20] K. Nakagawa, M. Teshima, M. Ohtsu, "Injection Locking of a Highly Coherent and High-Power Diode Laser at 1.5 $\mu$ m", Optics Letters, Vol. 16, No. 20, October 15, 1991, pp. 1590-1592
- [21] Olivier Lidoyne, Philippe Gallion, Didier Erasme, "Analysis of a Homodyne Receiver Using an Injection-Locked Semiconductor Laser", Journal of Lightwave Technology, Vol. 9, No. 5, May 1991
- [22] C. C. Davis, "Passive Optical Resonators", Lasers and Electro-Optics, Cambridge University Press (1996). p. 68-79
- [23] C. C. Davis, "Semiconductor Laser Structures", Lasers and Electro-Optics, Cambridge University Press (1996). p. 297-304
- [24] Anthony E. Siegman, "Laser Injection Locking", Lasers, (University Science Books, 1986), Chap. 29
- [25] T.N. Danilova, A.P. Danilova, A.N. Imenkov, N.M. Kolchanova, M.V. Stepanov, V.V. Sherstnev, Yu. P. Yakovlev, "InAsSb/InAsSbP Heterostructure Lasers with a Large Range of Current Tuning of the Lasing Frequency", Technical Physics Letters, Oct. 1999, vol.25, no.10, pp. 766-768

- [26] C. C. Davis, "Fabry-Perot Resonator Containing an Amplifying Medium", Lasers and Electro-Optics, Cambridge University Press (1996). p. 88-92
- [27] Moshe Nazarathy, Wayne V. Sorin, Douglas M. Baney, Steven A. Newton, "Spectral Analysis of Optical Mixing Measurements", Journal of Lightwave Technology, Vol. 7, No. 7, July 1989
- [28] L. Richter, H. Mandelberg, M. Kruger, P. McGrath, "Linewidth Determination from Self-Heterodyne Measurements with Subcoherence Delay Times", IEEE Journal of Quantum Electronics, Vol. QE-22, No. 11, November 1986
- [29] X. Jin, S. L. Chuang, "Relative Intensity Noise Characteristics of Injection-Locked Semiconductor Lasers", Applied Physics Letters, Vol. 77, No. 9, Aug. 28, 2000. pp. 1250-1252
- [30] G. Yabre, H. De Waardt, H. P. A. Van den Boom, G.-D. Khoe, "Noise Characteristics of Single-Mode Semiconductor Lasers Under External Light Injection", IEEE Journal of Quantum Electronics, Vol. 36, No. 3, March 2000, pp. 385-393
- [31] Gary M. Carter, Kao-Yang Huang, Joel Brotman, Robert Grober, Hirsch Mandelberg, "Frequency and Intensity Modulation Characteristics of GaAs Lasers in an External Cavity", IEEE Journal of Quantum Electronics, Vol. 29, No. 12, Dec. 1993, pp. 2910-2918
- [32] Kazovsky, L., "Impact of reflections on phase-diversity optical homodyne receivers", Electronics Letters, April 28, 1988; vol.24; no.9; pp. 522-524
- [33] Sircar, Cid, "Interview with Cid Sircar (Application Engineer)", Ortel, July 25, 2006

- [34] U. Gliese, T. N. Nielsen, M. Bruun, E. Lintz Christensen, K. E. Stubkjær, S. Lindgren, B. Broberg, "A Wideband Heterodyne Optical Phase-Locked Loop for Generation of 3-18 GHz Microwave Carriers", *IEEE Photonics Technology Letters*, Vol. 4, No. 8, Aug. 1992, pp. 936-938.
- [35] R. T. Ramos and A. J. Seeds, "Fast heterodyne optical phase-lock loop using double quantum well laser diodes," *Electron. Lett.*, vol. 28, no. 1, pp. 82-83, 1992.
- [36] K. J. Williams, L. Goldberg, R. D. Esman, M. Dagenais, J. F. Weller, "6-34GHz Offset Phase-Locking of Nd:YAG 1319nm Nonplanar Ring Lasers", *Elec. Letters*, Vol. 25, No. 18, pp. 1242-1243, 1989.
- [37] M. Kouroggi, C-H. Shin, M. Ohtsu, "A 134 MHz bandwidth homodyne optical phase-locked-loop of semiconductor laser diodes", *IEEE Photonics Technology Letters*, Vol. 3, March 1991, pp. 270-272.
- [38] L. G. Kazovsky, "Balanced Phase-Locked Loops for Optical Homodyne Receivers: Performance Analysis, Design Considerations, and Laser Linewidth Requirements", *Journal of Lightwave Technology*, Feb. 1986, pp. 182-195.
- [39] V. Annovazzi-Lodi, S. Donati, M. Manna, "Chaos and Locking in a Semiconductor Laser Due to External Injection", *IEEE Journal of Quantum Electronics*, Vol. 30, No. 7, July 1994, pp. 1537-1541.
- [40] Valerio Annovazzi-Lodi, Alessandro Sciré, Marc Sorel, Silvano Donati, "Dynamic Behavior and Locking of a Semiconductor Laser Subjected to External Injection", *IEEE Journal of Quantum Electronics*, Vol. 34, No. 12, July 1998, pp. 2350-2357.

- [41] S. C. Kan, K. Y. Lau, "Intrinsic Equivalent Circuit of Quantum-Well Lasers", IEEE Photonics Technology Letters, Vol. 4, No. 6, June 1992, pp. 528-530.
- [42] C. H. Henry, N. A. Olsson, and N. K. Dutta, "Locking range and stability of injection locked 1.54 um InGaAsP semiconductor lasers," IEEE J. Quantum Electron., vol. QE-21, pp. 1152-1156, 1985
- [43] F. Morgensen, H. Olesen, and G. Jacobsen, "Locking conditions and stability properties for a semiconductor laser with external light injection," IEEE J. Quantum Electron., vol. QE-21, pp. 784-793, 1985
- [44] R. Lang, "Injection locking properties of a semiconductor laser," IEEE J. Quantum Electronics, vol. QE-18, pp. 976-983, 1982
- [45] S. Kobayashi and T. Kimura, "Coherence of injection phase-locked AlGaAs semiconductor laser," Electron. Lett., vol. 16, no. 7, pp. 668-670, 1980.
- [46] O. Lidoyne, P. Gallion, C. Chabran, and G. Debarge, "Locking range, phase noise and power spectrum of an injection-locked semiconductor laser," Inst. Elec. Eng. Proc., vol. 137, pt. J, no. 3, pp. 147-154, 1990.
- [47] Pezeshki, J., "Generation of a CW Local Oscillator Signal Using a Stabilized Injection Locked Semiconductor Laser", unpublished
- [48] Pezeshki, J., Saylor, M., Mandelberg, H., Goldhar, J, " Amplitude modulation transfer in an injection-locked DFB semiconductor laser", IEEE Photonics Technology Letters, Nov. 2005, vol.17, no.11, pp. 2433-2435
- [49] Kazovsky, L. G., Kalogerakis, G., Shaw, W. T., "Homodyne Phase-Shift-Keying Systems: Past Challenges and Future Opportunities", Journal of Lightwave Technology, vol.24, Dec. 2006, pp. 4876-4884

- [50] Isabelle Petitbon, Philippe Gallion, Guy Debarge, Claude Chabran, "Locking Bandwidth and Relaxation Oscillations of an Injection-Locked Semiconductor Laser", IEEE Journal of Quantum Electronics, Vol. 24., No.2, Feb. 1988, pp. 148-154.